Fingerprints of a New Normal Urban Air Quality in the United States

Shobha Kondragunta[1,1], Zigang Wei[2,2], Brian McDonald[3,3], Daniel Goldberg[4,4], and Daniel Tong[5,5]

[1]National Oceanic and Atmospheric Administration (NOAA)
[2]IM Systems Group
[3]NOAA Chemical Sciences Laboratory
[4]George Washington University
[5]GMU

November 30, 2022

Abstract

Most countries around the world including the United States took actions to control COVID-19 spread that lead to an abrupt shift in human activity. On-road NOx emissions from light and heavy-duty vehicles decreased by 9% to 19% between February and March at the onset of the lockdown period in the middle of March in most of the US; between March and April, the on-road NOx emissions dropped further by 8% to 31% when lockdown measures were the most stringent. These precipitous drops in NOx emissions correlated well with tropospheric NO2 column amount observed by the Sentinel 5 Precursor TROPOspheric Monitoring Instrument (S5P TROPOMI). Furthermore, the changes in TROPOMI tropospheric NO2 across the continental U.S. between 2020 and 2019 correlated well with changes in on-road NOx emissions (r = 0.68) but correlated weakly with changes in emissions from the power plants (r = 0.35). At the height of lock-down related unemployment in the second quarter of 2020, the NO2 values decreased at the rate of 0.8 µmoles/m2 per unit percentage increase in the unemployment rate. Despite the lifting of lockdown measures, parts of the US continued to have ˜20% below normal on-road NOx emissions. To achieve this new normal urban air quality in the US, continuing remote work policies that do not impede economic growth may become one of the many options.

Fingerprints of a New Normal Urban Air Quality in the United States

S. Kondragunta[*1], Z. Wei[2], B. C. McDonald[3], D. L. Goldberg[4], D. Q. Tong[5]

[1]NOAA NESDIS Center for Satellite Applications and Research, 5825 University Research Court, College Park, MD

[2]IM Systems Group, 5825 University Research Court, College Park, MD

[3]NOAA Chemical Systems Laboratory, Boulder, CO

[4]Milken School of Public Health, George Washington University, Washington, DC

[5]Department of Atmospheric, Oceanic, and Earth Sciences, George Mason University, Fairfax, VA

[*] Corresponding author: Phone: 301-655-7311. Email: Shobha.Kondragunta@noaa.gov

Abstract

Most countries around the world including the United States took actions to control COVID-19 spread that included social distancing, limiting air and ground travel, closing schools, suspending sports leagues, closing factories etc., leading to an abrupt shift in human activity. On-road NO_x emissions from light and heavy duty vehicles decreased by 9% to 19% between February and March at the onset of lockdown in the middle of March in most of the US; between March and April, the on-road NO_x emissions dropped further by 8% to 31% when lockdown measures were the most stringent. These precipitous drops in NO_x emissions correlated well with tropospheric NO_2 column amount observed by Sentinel 5 Precursor TROPOspheric Monitoring Instrument (S5P TROPOMI). Further, the changes in TROPOMI tropospheric NO_2 across the continental U.S. between 2020 and 2019 correlated well with changes in on-road NO_x emissions ($r = 0.68$) but correlated weakly with changes in emissions from the power plants ($r = 0.35$). These findings confirm the known knowledge that power plants are no longer a major source of NO_2 in urban areas of the US. With increased unemployment rate in 2020 after the lockdown combined with telework policies across the nation for non-essential workers, the NO_2 values decreased at the rate of 0.8 μmoles/m^2 decrease per unit percentage increase in unemployment rate. Across the urban regions we found positive correlation between S5P TROPOMI NO_2 and Suomi NPP Visible Infrared Imaging Radiometer Suite (VIIRS) aerosol optical depths indicating common source sectors for NO_2 and aerosols/aerosol precursors.

Key Words: COVID-19, nitrogen dioxide, aerosol optical depth, TROPOMI, NOx emissions

Plain Language Summary

This study documents the different phases of lockdown and how traffic emissions changed accordingly across the US and in particular in five different cities, namely Los Angeles, San Francisco, San Joaquin Valley, New York City, and Atlanta. Analysis of data for these cities from measurements on the ground and satellite data indicate that a down turn in economy and telework policies reduced the number of cars and trucks on the road in March and April due to which air quality got better. This provided a window into the future as to how we can achieve improved air quality.

1. Introduction

As the 2019 novel Corona virus (COVID-19) spread from China to other parts of the world, various countries imposed lockdown measures one by one. Reports of improved air quality from

ground and satellite observations of aerosol optical depth and nitrogen dioxide soon followed in the media as documented by Kondragunta et al. (2020). The precipitous drops seen in the tropospheric vertical column nitrogen dioxide (NO_2, tropNO_2 here onwards) measured by the Sentinel 5P Tropospheric Monitoring Instrument (TROPOMI) were substantial, especially during the strict lockdown period for each country (Gkatzelis et al., 2020). Goldberg et al. (2020) reported that in the United States (US), tropNO_2 decreased by 9.2% to 45% in 26 cities during March 15 to April 30, 2020 compared to the same time period in 2019; these reported reductions account for the influence of the weather. Other researchers reported similar findings, mainly reductions of tropNO_2 attributed to reductions in traffic emissions both in the U.S. and across the globe in major urban areas of Europe, India, and China (Bauwens et al., 2020; Keller et al., 2020; Zheng et al., 2020; Vaderu et al., 2020; Straka et al., 2020; Nager et al., 2020). For example in Washington D.C., average distance traveled by people dropped by 60% between February and April when restrictions were fully in place (Straka et al., 2020). This sudden drop in tropNO2 in major metropolitan areas where transportation source sector for NO_x is strong is due to reduced traffic on top of an already observed general decreasing trend in NO_x emissions. According to Lamsal et al. (2015), tropNO_2 observed by the Ozone Monitoring Instrument showed a decreasing trend with an overall decrease of 28% between 2005 and 2013. These reductions are consistent with NO_x emissions reductions from major power plants in the US due to Clean Air Interstate Rule and Cross State Air Pollution Rule. The NO_x emissions continued to drop as more and more power plants switched to natural gas or began to rely on clean coal (de Gouw et al., 2014)

The significance of NO_2 is that it is a precursor for both ozone and particulate matter, primary components of photochemical smog. Whether it enhances or decreases ozone

production is dependent on a given region being NO_x saturated or volatile organic compound (VOC) saturated, the inherent non-linearity of ozone photochemistry (Kroll et al., 2020; Mazzuca et al., 2016). The two main sources of NO_2 in the US are energy sector and transportation sector according to the 2014 Community Emissions Data System (Hoesly et al., 2018). A study by Zheng et al. (2020) analyzed the reductions in trace gas and aerosol concentrations in China during the lockdown and found that the most significant drop in aerosols was for nitrate aerosol. For the time period corresponding to the lockdown in China, January 23 to February 22, 2020, mean nitrate aerosol concentration was 14.1 $\mu g/m^3$; for the same time period in 2019, concentration was 23.8 $\mu g/m^3$. This 41% reduction is corroborated by reductions in NO_2 observed by TROPOMI (Bauwens et al., 2020).

Though NO_2 is considered important due to its ozone and aerosol producing potential, it has harmful human health impacts when inhaled. Achakulwisut et al (2019) showed that 64% of four million pediatric asthma cases each year are due to exposure to NO_2. It should be noted though that NO_2 was used as a proxy for traffic-related pollution. The World Health Organization (WHO) standard for NO_2 is an annual average of 21 parts per billion and for the US, it is 53 parts per billion. The authors do note that that daily exposures to NO_2 can vary from annual averages and traffic pollution is usually a mixture of precursor gases, primary particulates, and photochemically formed ozone and aerosols. Nevertheless, when countries went into lockdown, the most noticeable indication of a drop in traffic related pollution is tropNO_2 in urban areas observed by TROPOMI, lending support to the assumption that NO_2 is a good proxy for traffic related pollution. The COVID-19 lockdown measures disproportionately impacted traffic more than industrial operations. We analyzed TROPOMI tropNO_2 and Suomi National Polar-orbiting Partnership Visible Infrared Imaging Radiometer Suite (Suomi NPP VIIRS) AOD data in

conjunction with on-road NO_x ($NO+NO_2$) emissions data, NO_x emissions from power plants, and unemployment rates where available. The goal of this study is to examine the trends in on-road and power plant emissions for five different locations (four urban areas and one rural area) to answer the questions: (1) are changes in NO_x emissions during the lockdown detectable in TROPOMI tropNO_2 data, (2) are the economic indicators consistent with emissions changes, and (3) are the trends reversing with the removal of lockdown measures in the major metro areas. These questions are answered with spatial and temporal analysis of ground-based observations and satellite data, relating indicators of human activity during and prior to COVID-19 lockdown with air quality, and examining if a new normal urban air quality can be achieved with novel policies.

2. Methods

2.1. Sentinel 5P TROPOMI NO2

The TROPOMI NO_2 algorithm is based on the Differential Optical Absorption Spectroscopy technique that involves fitting the spectra in the NO_2 absorption region between 405 nm and 465 nm using known laboratory-measured reference absorption spectra. The Sentinel 5P flies in formation with SNPP. Though some Sentinel 5P trace gas algorithm retrievals depend on VIIRS cloud mask, the NO_2 algorithm relies on cloud retrievals using its oxygen A-band absorption (van Geffen et al., 2019). The cloud fraction and cloud top pressure are used in air mass factor calculation for partially cloudy pixels. There is an indication that the cloud algorithm is likely conservatively masking out good NO_2 retrievals according to a validation study conducted by Judd et al. (2020). Though Judd et al (2020) used data with quality flag equals to unity, we used the quality flag value recommended by the NO_2 algorithm

theoretical basis document (van Geffen et al., 2019). Only data with quality flag > 0.75 were used as this quality flag setting ensures that cloudy retrievals or retrievals with snow/ice covered pixels are screened out. The TROPOMI Level 2 product file consists of pixel level (3.5 km x 5.6 km) NO_2 column amount for troposphere that we used in this study. The NO_2 algorithm retrieves total column NO_2 and separates the stratosphere from troposphere using chemical transport model predicted stratospheric NO_2 analysis fields (van Geffen et al., 2019). The expected accuracy of tropospheric NO_2 column for polluted regions with high NO_2 values is ~25% and independent validation efforts using ground based spectrometers such as Pandora have confirmed that tropNO2 is generally under estimated, especially in polluted regions and that significant sources of errors come from coarser resolution a priori profiles used in the retrieval algorithm (Chan et al., 2020). Comparisons of TROPOMI tropNO_2 column with Pandora ground station retrievals of tropospheric NO_2 in Helsinki showed that mean relative difference is −28.2% ± 4.8% (Ialongo et al., 2019). Similar comparisons between Pandora ground station retrievals and tropNO_2 in Canada for urban (Toronto) and rural (Egbert) stations show that tropNO_2 has a -23% to -25% bias for polluted regions and a 7% to 11% high bias in rural region. Sources of error in tropNO_2 include altitude dependent air mass factors, stratosphere-troposphere separation of NO_2, a priori NO_2 profile and shape, surface albedo climatology, and calibration errors as a function of view angle (van Geffen et al., 2019; Judd et al., 2020; Ialongo et al., 2019; Zhao et al., 2020; Chan et al., 2020). Judd et al. (2020) showed that the TROPOMI NO_2 validation carried out during the Long Island Sound Tropospheric Ozone Study (LISTOS) experiment showed that the TROPOMI tropNO_2 column retrievals have a bias of -33% and -19% versus Pandora and airborne spectrometer retrievals respectively. The biases improve to -19% and -7% when TROPOMI NO_2 algorithm is run with a priori profiles from a regional air quality model

169 indicating that retrievals are very sensitive to a priori profile. One aspect that is not fully
170 explored by Judd et al. (2020) is the influence of aerosols on air mass factor calculations.
171 Research on aerosol impact on air mass factors indicates that the impact of aerosols on NO_2
172 retrieval can vary depending on aerosol type (absorbing or scattering), amount, and vertical
173 location (aerosol mixed in with NO_2 in the boundary layer or is the layer detached from NO_2
174 layer) in the atmospheric column (Tack et al., 2019; Judd et al., 2019; Liu et al., 2020; Lin et al.,
175 2014).

176 For this analysis, the pixel level NO_2 data were rotated to orient the pixels in the
177 downwind direction and remapped to 5 km x 5 km fixed grids prior to computing mean values
178 around major cities for which on-road emissions data are available. Average NO_2 was computed
179 within 100 km in the downwind direction from the city center, 50 km upwind direction, and ± 50
180 km in the cross-wind direction. In computing daily mean values for a location of interest, we
181 used a criteria of having a minimum 25% of the pixels with high quality NO_2 retrieval in each
182 grid. The data for January to February 2020 is considered BAU), the data for 15 March to 30
183 April 2020 is considered the lockdown period, and the data for 1 May to November 2020 is
184 considered as representing the post lockdown time period. The Level 2 TROPOMI NO_2 data
185 were downloaded from the European Space Agency datahub
186 (https://s5phub.copernicus.eu/dhus/#/home).

187 The TROPOMI data is available only from mid-2018 to present. We removed the
188 seasonality in tropNO_2 data in two simple ways: by simply taking the difference between 2019
189 and 2020 for the same month so the sun-satellite geometries and weather conditions are similar
190 barring any unusual inter-annual variabilities, and by doing double differencing when changes

191 from one month to the other month needed to be analyzed. The double differencing method is
192 described in section 3.1.

193 ## 2.2. On-road NOx Emissions
194

195 The on-road emissions are obtained using the Fuel-based Inventory of Vehicle Emissions
196 (FIVE) where vehicular activity is estimated using taxable fuel sales for gasoline and diesel fuel
197 reported at a state-level and downscaled to the urban scale using light- and heavy-duty vehicle
198 traffic count data (McDonald et al., 2014). Once the fuel use is mapped, NO_x emissions are
199 estimated using fuel-based emission factors (in g/kg fuel) based on roadside measurements or
200 tunnel studies (Hassler et al., 2016; McDonald et al., 2012; McDonald et al., 2018). The emission
201 factors are calculated separately for light-duty gasoline vehicles and heavy-duty diesel trucks.
202 The FIVE methodology was developed to derive traffic emissions to study their impact on air
203 quality (Kim et al., 2016; McDonald et al., 2018), but in the case of 2020, the fuel-based
204 methods provide evidence for quantifying the impact of reduced human activity during the
205 lockdown period on air pollutant emissions (e.g., NO_x).

206 Here, we downscale on-road gasoline and diesel fuel sales following McDonald et al. (2014)
207 for our 2019 base year, which is treated as the BAU case. We have chosen to focus on four US
208 urban areas where real-time traffic counting data are publicly available, including the South
209 Coast air basin (Los Angeles county, Orange counties, and portions of Riverside and San
210 Bernardino counties), San Francisco Bay Area (Marin, Sonoma, Napa, Solano, Contra Costa,
211 Alameda, Santa Clara, San Mateo, and San Francisco counties), New York City (Richmond,
212 New York, Kings, Queens, and Bronx counties), and Atlanta metropolitan region (Cherokee,
213 Clayton, Cobb, Coweta, Dekalb, Douglas, Forsyth, Fulton, Gwinnett, Henry, Rockdale, and

Spalding counties). We also include one rural region for contrast, the San Joaquin Valley in California (Fresno, Kern, Kings, Madera, Merced, San Joaquin, Stanislaus, Tulare counties). For the BAU case, we account for typical seasonal and day-of-week activity patterns of light- and heavy-duty vehicles separately). For the COVID-19 case, we scale the January BAU emissions case with real-time light- and heavy-duty vehicle traffic counting data for the year 2020, which are described in Harkins et al. (2020, to be submitted). Light-duty vehicle counts are used to project on-road gasoline emissions and heavy-duty truck counts for on-road diesel emissions during the pandemic.

To estimate NO_x emissions, the FIVE NO_x emission factors have been updated to 2019 based on the regression analyses of roadway studies (Hassler et al., 2016; McDonald et al., 2012; McDonald et al., 2018), and we use a value of running exhaust emission factors of 1.7 ± 2 g NO_x/kg fuel and 12.4 ± 1.9 g NO_x/kg fuel for on-road gasoline and diesel engines, respectively. Cold-start emissions are scaled relative to the running exhaust emissions based on the EPA MOVES2014 model (EPA, 2015). We use the 2019 NO_x emission factor for both the BAU and COVID-19 adjusted cases. Thus, the differences in the BAU and COVID-19 cases in are only due to changes in traffic activity. We use the same emission factor for 2019 and 2020 because past studies have shown during the 2008 Great Recession the turnover of the vehicle fleet and corresponding reductions in emission factors are slower). Total on-road NO_x emissions are the sum of emission estimates for light-duty vehicles with heavy-duty trucks. The off-road mobile source emissions are not included in the dataset. In cities, on-road transportation accounts for as much as 75% of the NO_x emissions (Kim et al., 2016), and is a critical emissions sector to quantify.

Uncertainties in FIVE on-road emission estimates arise from non-taxable fuel sales associated with off-road machinery, and mismatches in where fuel is sold and where driving occurs, though diesel fuel sales reports are adjusted based on where long-haul trucking occurs (McDonald et al., 2014). However, the main source of uncertainty is the accuracy of fuel-based emissions factors used to calculate co-emitted air pollutant species (McDonald et al., 2018). In general, there has been a downward trend in on-road NO_x emissions over multiple decades (Hassler et al., 2016; McDonald et al., 2012), although there are questions about the rate of decrease in more recent years (Bishop and Haugen, 2018; Jiang et al., 2018).

2.3. Power Plant NO_x Emissions

The daily power plant NO_x emissions were obtained from the US Environmental Protection Agency (EPA) Continuous Emissions Monitoring System (https://www.epa.gov/airmarkets) and the energy generation/consumption statistics were obtained from the Energy Information Administration (eia.gov). Unlike the traffic emissions, power plant emissions did not change much during the lockdown. Power generation from fossil fuels dropped from 38,332 Gwh in March to 29,872 Gwh in April and rebounded to pre-pandemic levels by June. The total NO_x emissions in the US from power plants dropped from 54,531 tons in March to 44,016 tons in April, a 19% decrease. This may seem like a big drop in production but the absolute values are quite small. For example, NO_x emissions from power plants within the 75 km of Los Angeles emitted only 20 tons in March 2020. In contrast, on-road emissions from vehicles in the Los Angeles area alone emitted nearly 5,367 tons of NO_x. The power plant NO_x emissions in the US have decreased substantially over the last two decades; they dropped from 6.4 to 0.88 million short tons annually from 1990 to 2019. This is due to the shift in relying on fossil fuels to other alternate energy sources for power generation. For example, the use of coal as a source of

electricity generation went down from 51% in 2001 to 23% in 2019 while the natural gas as a source increased from 17% in 2001 to 38% in 2019. In our analysis, comparing and contrasting NO_x emissions from on-road traffic and power plants for the six locations of interest, we considered only the power plants still operating using coal as a source and are within 75 km radius of the center of the city location being analyzed.

2.4. Suomi National Polar-orbiting Partnership Visible Infrared Imaging Radiometer Suite (SNPP VIIRS)

NOAA currently has two VIIRS instruments in orbit - one on SNPP launched on 28 October, 2011 and one on NOAA-20 launched on 18 November, 2017. The two VIIRS instruments continuously observe the Earth with a 50-minute time difference and provide aerosol optical depth (AOD) retrievals for cloud/snow-free scenes during the sunlit portion of the day. The VIIRS instruments have 22 bands with 16 of the bands in the visible to long-wave infrared at moderate resolution (750m), five bands at imager resolution (375m) covering 0.64μm, 0.865μm, 1.6μm. 3.74μm, and 11.45μm, and one broad Day-Night-Band (DNB) band centered at 0.7μm. The NOAA AOD algorithm over ocean is based on Moderate Imaging Spectroradiometer (MODIS) heritage and over land, the algorithm derives AOD for both dark targets as well as bright surfaces (Levy et al., 2007; Laszlo and Liu, 2016; Zhang et al., 2016; Huang et al., 2017). For this study, we used SNPP VIIRS AOD because SNPP flies in formation with S5P TROPOMI with less than three minute difference in overpass time with a local equator crossing time of 1:30 PM. The SNPP VIIRS AOD product has been extensively validated by comparing it to Aerosol Robotic Network (AERONET) AODs and the VIIRS 550nm AOD is shown to have a global bias of -0.046±0.097 for AODs over land less than 0.1 and for AODs between 0.1 and 0.8, the bias is -0.194±0.322. In the U.S., for VIIRS AODs ranging between 0.1

and 0.8, the bias is -0.008±0.089 and for AODs greater than 0.8, the bias is about 0.068±0.552 (Zhang and Kondragunta, 2021). For the analysis of AOD data in this study, we remapped the high quality (Quality Flag equals 0) 750m resolution retrievals to 0.05^{o} x 0.05^{o} resolution with a criteria that for a grid to have a mean AOD value, there should be a minimum of 20% 750m pixels with high quality AODs.

2.5. Unemployment Rate

The civilian labor force and unemployment estimates for metropolitan areas were obtained through the Local Area Unemployment Statistics (LAUS) provided by the Bureau of Labor Statistics (bls.gov). The LAUS program is a federal-state cooperative effort in which monthly estimates of total employment and unemployment are prepared for over 7,500 areas including metropolitan areas. The seasonal adjustments are carried out by the Current Employment Statistics State and Area program (CES) with statistical technique SEATS, or Signal Extraction in ARIMA (Auto Regressive Integrated Moving Average) Time Series. These datasets are smoothed using a Reproducing Kernel Hilbert Space (RKHS) filter after seasonal adjustment. The details of the data collection, processing and release can be found at https://www.bls.gov/lau/laumthd.htm. The data for January to November 2020 are used in this study. To compare the NO_2 variation in the metropolitan areas, the TROPOMI tropNO_2 column amounts were averaged inside each metropolitan area. The 1:50,000 polygon shape files were used to test if a TROPOMI pixel is inside or outside a metropolitan area. The shape files are from United States Census Bureau (https://www.census.gov/geographies/mapping-files/time-series/geo/cartographic-boundary.html).

2.6. Matchup Criteria

The NO_2 data were matched to the on-road mobile emissions data for statistical and trend analysis with certain criteria. Prior to generating the matchups, rotated wind analysis was carried out on the original pixel level data. It is important to do this when sampling the satellite data because the NO_2 concentrations accumulate in the cities when wind speed is low and disperse away from the city when wind speed is high. The satellite data are observed once a day in the mid-afternoon whereas on-road mobile emissions represent daily values. To minimize sampling differences, it is common to rotate the satellite pixel-level data in the direction of the wind (Fioletov et al., 2015; Lorente et al., 2019; Goldberg et al., 2019; Zhao et al., 2020). We used the European Center for Medium range Weather Forecast (ECMWF) Re-Analysis (ERA5) 30-km resolution global wind fields (Hersbach et al., 2020). To do the wind rotation, each TROPOMI pixel was collocated to ERA5 with tri-linear interpolation method in both temporal and horizontal directions. The wind profiles were merged to the location of the TROPOMI pixel center. The east-west (U) and north-south (V) wind speed components were averaged through the vertical distribution within the bottom 100 hPa, approximated to be within the boundary layer. Then, each TROPOMI pixel was rotated and aligned with the average wind direction from the city center. The rotated pixels are gridded with 5 km x 5 km resolution to generate monthly mean values for correlation analysis with on-road NOx emissions.

Once the pixels are rotated, they are sampled for 100 km in the downwind direction, 50 km in the upwind direction, and cross-wind direction. This way, the elevated concentrations of NO_2 moving away from the city in the downwind direction are captured. Figure 1a shows an example of the TROPOMI NO_2 tropospheric column amount for California with Los Angeles as the focus. The NO_2 data shown are monthly mean values for January 2020 remapped to a fixed grid. The black rectangle shows the area of interest over Los Angeles that we want to compare with

on-road emissions. The ERA5 wind vectors are plotted on the NO_2 map to show wind direction. To do the wind rotation, daily NO_2 pixel level data are first remapped to a 5 km x 5 km fixed grid resolution. The grids are then rotated to align with the wind direction with downwind direction pointing North (Figure 1b). The daily rotated grid values of NO_2 in 5 km x 5 km are averaged over a month to generate a monthly mean. The monthly mean values can vary quite a bit depending on missing data due to screening for high quality data as well as cloud cover. In a given month, the number of pixels with valid retrievals for a particular city can vary from 2% to 100% depending on cloud and snow cover, and the mean value varies depending on the location of the missing values, if they are in the center of the city where NO_2 is usually high or on the edges of the city where NO_2 values can be low depending on wind speed and direction. In our analysis for this study, prior to computing monthly mean, the criteria we employed is that on a given day, there should be a minimum of 25% of the pixels in a region selected for matchups of satellite data should have valid retrievals. The 25% threshold is a reasonable compromise because any value higher than that will reduce the sample size (number of days included in the monthly mean).

3. Results

3.1. Deseasonalizing tropNO_2 data

As already shown by many research studies, the global tropNO_2 column amounts dropped in coincidence with partial or complete lockdowns during the height of the COVID-19 pandemic in different parts of the world and in the US. In order to remove the seasonality from the signal, researchers have adopted different approaches including the use of numerical models to simulate the seasonality (e.g., Goldberg et al., 2020; Silver et al., 2020; Liu et al., 2020). Seasonality has to be accounted for because in the northern hemisphere winter months, NO_2 amounts are higher

than in summer months due to which during the transition from winter to summer, NO_2 amounts are higher in February than in March. In our study, we used a double differencing technique to account for seasonality. Consistent with Goldberg et al. (2020), we used 1 January to 29 February 2020 as pre-lockdown time period and 15 March to 30 April as lockdown time period. The difference in mean tropNO_2 between lockdown and pre-lockdown is referred to as 2020ΔNO_2. For the same two corresponding time periods in 2019, the difference in mean tropNO2 is 2019ΔNO_2. Then, the difference of 2019ΔNO_2 and 2020ΔNO_2 was computed to tease out the changes in NO_2 due to reductions in emissions during the lockdown (ΔNO_2). It should be noted though that the double differencing only removes the seasonality and does not fully account for differences in meteorological events such as precipitation or anomalously cold or hot conditions in one year versus the other but on a monthly time scale they are minimized.

Figure 2a-b shows 2019ΔNO_2 and 2020ΔNO_2 which includes changes due to seasonality and any changes to emissions either from natural sources such as fires or anthropogenic urban/industrial sources. Figure 2c shows ΔNO_2 for the CONUS due to just changes in emissions between the pre-lockdown and lockdown time periods in 2020 with the seasonality removed. Comparing Figure 2a and 2b, one can deduce that reductions in tropNO_2 between pre-lockdown and lockdown is much stronger in 2020 compared to 2019. However, the double difference plot in Figure 2c shows how much of that reduction seen in 2020ΔNO_2 (Figure 2b) is due to changes in traffic emissions. The NO_2 changes are smaller in Figure 2c than in Figure 2b, both in magnitude as well as spatial extent of the reductions.

The lockdown measures in most states in the US began in the middle of March 2020. The first state to institute stay at home measures was California on 19 March and the last state to enforce was Missouri on 6 April. The cities/regions with worse traffic related ozone pollution

levels based on the monitoring data from 2016-2018 compiled by the American Lung Association and the duration for which they were in a lockdown is shown in Table 1. For regions that fall into different states (e.g., Washington-Baltimore-Arlington), the dates for the state that had the longest duration of lockdown are listed in the table. Most states were in a lockdown mode only for one to two months and given the varying nature of the lockdown in different parts of the country, we treated 15 March and 30 April as lockdown months. As shown in Figure 2a, 2019ΔNO_2 is positive in some areas and negative in some areas whereas in 2020 (Figure 2b), large negative values (reductions) are observed in most of the CONUS except in the Great Plains region and the Pacific North West. These reduced tropNO_2 amounts are attributed to reduced emissions due to lockdowns. Changes in the rural areas (either positive or negative) of the US could be due to changes to natural sources such as soil and lightning NO_x emissions.

3.2. On-road NO_x emissions and tropNO_2

Focusing on the regions of interest with on-road NOx emissions available for this study, we calculated reductions in tropNO_2 for Los Angeles, Atlanta, San Francisco, San Joaquin Valley, and New York City. The largest reductions in tropNO_2 were observed for New York City (-28%) and the lowest were observed for San Francisco (-21%). For Los Angeles, the straight difference between pre-lockdown and lockdown in 2020 shows reductions of ~81 µmoles/m^2 when in fact NOx emissions reductions from traffic only likely reduced tropNO_2 by 32 µmoles/m^2 which is about 21% as estimated by the double differencing technique (Table2).

Goldberg et al (2020) reported tropNO_2 reductions of 20.2%, 18%, and 39% for Atlanta, New York, and Los Angeles respectively and their analysis is also for March 15 to April 30, 2020 time period. Our analysis shows that tropNO_2 reductions for these three cities are 21%,

17%, and 22%. Though the methodology used to remove the seasonality is different, the reductions in tropNO$_2$ from our analysis and that of Goldberg et al. (2020) is similar with Los Angeles showing the biggest drop in tropNO$_2$ due to lockdown measures.

The goal of this study is, however, not to repeat what other researchers have already reported for the COVID-19 lockdown impacts on tropNO$_2$ using TROPOMI data. What we examined in this study is the trends in on-road and power plant emissions for five different locations (four urban areas and one rural area) to answer the questions: (1) are changes in NOx emissions during the lockdown detectable in TROPOMI tropNO$_2$ data, (2) are the economic indicators consistent with emissions changes, and (3) are the trends reversing with the removal of lockdown measures.

Figure 3 shows the time series of on-road mobile (cars and trucks combined) and power plant NO$_x$ emissions for five different cities/regions in the US (Los Angeles, Atlanta, New York, San Joaquin Valley, and San Francisco) from January to November 2020 except for New York City for which the time series ends on 31 August due to the non-availability of traffic data. For Los Angeles, the daily NO$_x$ emissions are near 200 tons/day prior to lockdown with values slightly lower on weekends (~150 tons/day). The Los Angeles basin is home to 17 million people with 11.3 million cars; cars, trucks, and other off-road machinery contributing to 80% of the observed NO$_x$ in a typical year according to the 2019 emissions report by South Coast Air Quality Monitoring Division (http://www.aqmd.gov/docs/default-source/annual-reports/2019-annual-report.pdf?sfvrsn=9). Due to the lockdown and stay at home orders, people stopped driving and the NO$_x$ emissions quickly began dropping on 19 March 2020; the NOx emissions begin to increase on 16 April 2020, even before the lockdown was lifted on 4 May. The lowest weekday NO$_x$ emissions, 141.3 tons/day, occurred on 6 April. Even though the NOx emissions begin to

recover in the post lockdown time period, they are still lower than the pre-lockdown values. Compared to on-road emissions, power plant emissions are negligible for the Los Angeles area. Power plants in the vicinity of Los Angeles (~75 km radius) emit only ~0.8 tons per day on average compared to 200 tons per day emitted by on-road vehicles during the pre-lockdown on weekdays. On weekends, on-road emissions are lower (~150 to 175 tons/per day depending on whether it is a Saturday or Sunday) due to lower truck traffic (Marr and Harley, 2002), whereas power plant emissions do not have any weekday/weekend differences.

The NO_x emissions for the New York area encompass an area covering about 1,213 square kilometers. The city is home to 8.34 million people but there are only 1.9 million vehicles (230 cars per 1000 people) because of the reliance on public transportation, a factor of 3 lower than for Los Angeles basin which has 660 cars per 1000 people. Similar to Los Angeles, the NO_x emissions dropped in New York on 21 March when the lockdown measures began. The pre-lockdown levels of NOx emissions are on average ~125 tons/day. It should be noted that New York City is in the downwind region of NOx emissions from New Jersey and Pennsylvania and the recipient of regionally transported pollution (Tong et al., 2008). Unlike the Los Angeles area, the power plant emissions are higher but showed no trend similar to on-road emissions. It is noteworthy that there is a jump in power plant emissions towards the end of June which coincides with the opening of retails on 22 June in New York; the power plant emissions in the New York City are higher in the summer than in winter, associated with increased demand for air conditioning.

The NO_x emissions for the metro Atlanta area are similar to New York City but with a weak weekday/weekend cycle. The region encompassing Cherokee, Clayton, Cobb, Coweta, Dekalb, Douglas, Forsyth, Fulton, Gwinett, Henry, Rockdale, and Spalding counties is about 3,695

446 square kilometers and is home to nearly five million people. The pre-lockdown levels of NOx
447 emissions are on average ~125 tons/day. The metro Atlanta region is three times larger than the
448 area covered for the New York City region but the NOx emissions are similar in magnitude. The
449 state of Georgia where Atlanta is located never went into any prolonged lockdown. Though the
450 mayor of Atlanta ordered people not to gather in large groups beginning 15 March and the
451 Governor of Georgia ordered bars and clubs to close on 24 March, schools were not closed until
452 1 April; shelter in place was implemented on 8 April but was lifted immediately with no real
453 lockdown until 1 May through 23 May. Consistent with these policies, the on-road NO_x
454 emissions were lowest on 23 March (88.5 tons/day) and 26 May (74.5 tons/day) and returned to
455 pre-lockdown levels at the start of 1 June. The lowest on-road NOx emission value, 74.5 tons,
456 was observed on 26 May, towards the end of the shelter in place orders. By 1 June, NO_x
457 emissions values returned to normal, pre-lockdown levels in Atlanta.

458 For the pre-lockdown time period, the weekday/weekend difference in NO_x emissions is
459 stronger in New York City than Los Angles and Atlanta areas, due to commuter travel. Mean
460 difference in NO_x emissions between weekdays and Sundays (emissions are the lowest on
461 Sundays of each week) prior to the pandemic related lockdown in the Los Angeles, New York,
462 and Atlanta are 54.4 tons/day (26%), 65.4 tons/day (51%), and 41.1 tons/day (33%) respectively.

463 The San Joaquin valley is a rural area with low on-road and power plant emissions and the
464 data are expected to have a contrast to the urban/industrial locations such as Los Angeles and
465 New York City. The San Joaquin Valley NO_x emissions remained consistent at ~55 tons/day
466 throughout the year with a very weak weekday/weekend cycle. Similar to Los Angeles area, the
467 power plant emissions are insignificant. For the San Francisco Bay area, the on-road NO_x
468 emissions are higher than the San Joaquin Valley region but lower than the Los Angeles area.

The daily average NO_x emissions prior to the lockdown were ~90 tons/day and there was a small drop in emissions (-33.2 tons/day) on 6 April with a trend to return to normal by mid-April. The post lockdown NOx emissions are lower than pre lockdown values for San Francisco as well.

3.3. Correlation between on-road NO_x emissions and tropNO_2

Given the knowledge of changes in on-road emissions in five locations due to lockdown, we wanted to examine if tropNO_2 shows similar behavior by exhibiting a linear relationship and demonstrate that the time period for which lowest NO_x emissions were observed in traffic data also corresponds to the lowest observed tropNO_2 data. Additionally, we wanted to check if the post lockdown recovery in traffic emissions is reflected in tropNO_2 data. We first examined the direct relationship between daily tropNO_2 and daily on-road NO_x emissions for the five locations but only the analysis for Los Angeles is shown in Figure 4. The tropNO_2 and NO_x emissions for January and February 2020, representing the pre-lockdown phase, and for March through November 2020 are shown in Figure 4a and Figure 4b respectively. Again, the daily NO_x emissions data are for the Los Angeles basin. The coincident observations of tropNO_2 amount sampled in the predominant direction of wind are linearly correlated with on-road emissions but the correlation is weak (r=0.39). The traffic emissions fall into three clusters corresponding to emissions on Sundays (~150 tons/day), Saturdays (~180 tons/day), and weekdays (~199 tons/day) with minimal variability in each cluster whereas tropNO_2 amount varied between 50 and 225 µmoles/m^2.

The variability in tropNO_2 can be present due to different reasons. First, the day to day variability in cloud cover can lead to gaps in data. We used the recommended quality flag threshold of 0.75 to screen out the data that has potential contamination from clouds but this

strict screening reduces the number of retrievals for a given location. Second, there is also variability in the background NO_2 contribution to the tropospheric NO_2 column due to which column NO_2 does not correlate well with NO_x emissions from sources on the ground. We analyzed the background NO_2 signal in the tropospheric column amount for TROPOMI for 2019 and 2020 using Silvern et al. (2019) method and found it to be higher in the winter due to longer lifetime (lower temperature, weak photolysis, stronger wind dispersion, and less wet scavenging) and lower in the summer with monthly mean values ranging between 15 and 20 μmoles/m^2. Sources of background NO_2 are soil emissions of NO_x which are amplified after precipitation events, lightning produced NO_x, and chemical decomposition of peroxyacetyl and alkyl nitrates. When transport of NO_2 from rural areas to urban centers occur, this can enhance the tropNO_2 values that may not correlate well with NO_x emissions from sources on the ground. Third, wind speed and direction influences the mean tropospheric NO_2 computed for the Los Angeles basin because if the wind speed is high, NO_2 is dispersed and transported away from the city and when the wind speed is low, NO_2 is accumulated over the city. Any variability associated with background NO_2 is detected by TROPOMI and accounted for in the column NO_2 amount that has no relation to the NO_x emissions from the on-road sources on the ground. We did account for the effects of wind in our matchups by sampling the data in the downwind direction but higher wind speeds dilute the NO_2 concentrations observed by TROPOMI. The outliers that indicate tropNO_2 values are between 20 and 30 μmoles/m^2 even when on-road emissions are high indicate TROPOMI retrievals that are either sampled after pollutants are washed out of the atmosphere due to rain or on days when wind speeds are unusually high or are noisy and have errors associated with air mass factors and a priori profile. Parker et al. (2020) report that the Los Angeles basin was unusually wet in 2020, especially during the late March and early April

2020. Other researchers who correlated daily surface observations of NO_2 and TROPOMI $tropNO_2$ for 35 different stations in Europe reported similar findings and they found that correlation improved after averaging the data to monthly time scales (Ialongo et al., 2020; Cersosimo et al., 2020).

The comparison for the lockdown and post lockdown time period of March through November is shown in Figure 4b; the correlation remains the same (r = 0.39) but the one interesting feature is that the $tropNO_2$ and on-road emissions are very small compared to the pre-lockdown scenario. Daily NOx emissions on many days are between 100 and 150 tons after 14 March; prior to that in the first 15 days of March, the region was not under stay at home orders. The $tropNO_2$ never goes above 200 μmoles/m^2 for this time period. Compared to pre-lockdown period, the on-road NO_x emissions and $tropNO_2$ values shifted to lower values within each cluster (shown in blue for weekdays, green for Saturdays, and red for Sundays). During the lockdown phase, one would anticipate that there would not be any difference between weekday and weekend emissions but the difference is stark and is reflected in $tropNO_2$ data as well.

In order to correlate the changes in on-road NOx emissions to changes in $tropNO_2$ between 2019 and 2020 for each of the five regions in this study, we averaged daily NOx emissions values and $tropNO_2$ values for each month (January to November) and created an average value of all the five regions combined for each month. Figure 5a shows the monthly mean trend plot ΔNO_x and $\Delta tropNO_2$ for January to November where we see on-road emissions and tropNO2 drop steadily and hit the lowest values in March and April, consistent with lockdown measures. The recovery begins in May and continues to November for on-road emissions but not completely to the pre-lockdown levels. However, the $\Delta tropNO_2$ trend plot shows recovery up to August and then begins to show a decline from September to November. This decline in

538 tropNO_2 is coming from Los Angeles and San Francisco. The reason for this drop is currently
539 unclear and warrants further investigation but some initial analysis presented in Section 3.4
540 suggests there was likely an influence of biomass burning emissions on the Los Angeles area in
541 September 2020. Figure 5b shows the correlation of on-road NOx emissions changes (ΔNO_x)
542 between 2020 and 2019 with the difference in tropNO_2 amounts between 2020 and 2019
543 (ΔtropNO2). The NO_x emissions were lower in 2020 compared to 2019 for all the months and
544 all the cities. The positive linear correlation (r = 0.68) suggests that tropNO_2 observations
545 captured the changes in on-road emissions and can be used to study the changes in NOx
546 emissions due to traffic elsewhere in the US where we do not have observations from the ground.

547 Even though traffic emissions are the dominant source for NOx, there are power plants in the
548 vicinity of the cities emitting NOx on a continuous basis and unlike traffic emissions they do not
549 exhibit a weekday/weekend cycle. Figure 6 shows a map of tropospheric NO_2 for Quarter 2
550 2020 (April/May/June) with on-road emissions and power plant emission for each of the five
551 cities as stacks. The locations of power plants in other parts of the country are circled in pink
552 color, indicating that these power plants emit greater than 1500 tons in a given quarter; power
553 plants with lower monthly NOx emissions < 1500 tons are not highlighted on the maps. It is
554 difficult to isolate the NO_2 plumes from power plants in urban areas in the TROPOMI NO_2 map
555 as the NO_x emitted from the power plants mixes and becomes indistinguishable from on-road
556 emissions. Consistent with this analysis, changes in NO_x emissions between 2020 and 2019 for
557 power plants within 75 km of each of the five cities (New York, Atlanta, San Francisco, Los
558 Angeles, and San Joaquin Valley) correlated weakly with changes in tropNO_2 (Pearson
559 correlation coefficient = 0.35); power plant NO_x emissions can explain only 12% of the
560 variability seen in tropNO_2 (Figure 7). The changes in power plant emissions were higher in

2020 compared to 2019 for some plants and lower for some but mostly varied between ±20 tons/day whereas the on-road emissions reduced by about ~80 tons/day.

3.4. NO_x photochemistry

The premise for the impact of NO_x emissions reductions on improved air quality due to reduced human activity during the lockdown period depends on how the photochemical processes changed compared to the BAU scenario. It is known that in the Los Angeles area, reductions of NO_x emissions on the weekend due to reduced traffic compared to weekdays has led to an increase in ozone due to less NO_x available to remove ozone via titration (Baider et al., 2014). Parker et al. (2020) report that during the April to June 2020, when NO_x emissions were reduced substantially due to a 50% drop in traffic, there was a spatial modification of ozone production but not necessarily a drop, suggesting larger and more targeted NO_x reductions are needed in the Los Angeles area in order to consistently reduce ozone. While most of the NOx in the Los Angeles area comes from cars and trucks, only 25% of VOC emissions come from cars and trucks; sources of VOCs are mostly area and biogenic sources (Parker et al., 2020). McDonald et al. (2018) and Qin et al (2021) suggest the importance of volatile chemical products as sources of anthropogenic VOCs in the Los Angeles impacting both ozone and secondary organic aerosol. Most analysis using the satellite data are focusing on TROPOMI NO_2 and attributing the reductions of NO_x emissions to improved air quality; the reductions in VOC emissions are largely unknown, especially of non-vehicular sources. The aerosol formation (nitrate and organic aerosols) is driven by NO_x, VOCs, and ammonia emissions and if the photochemical processes are in NO_x limited or VOC limited regime. One complicated factor for aerosols is the transport of smoke aerosols if fires are burning upwind of the city. We established some baseline photochemical regime by calculating weekly correlation between

AOD and NO_2 and obtaining the slope for each week over one year in 2019 to document the changes in slope as a function of time during the year (Figure 8a-c); Figure 8a-b show how slopes are derived using the scatter plot between VIIRS AOD and TROPOMI tropNO2 for one week in September 2019 and in 2020 as an example. For 2019, when the fire season was not a major contributing factor, the slopes are small in the winter months and slowly increase towards the summer. This is consistent with the knowledge that ammonium nitrate formation peaks in the summer due to the availability of ammonia from increased agricultural activity and higher volatility associated with higher temperatures (Schiferl et al., 2014).

The black curve in the figure is a polynomial fit to the 2019 AOD-tropNO_2 slope data and represents the increase in the rate of nitrate aerosol formation from winter to summer, and decrease from summer to winter. The AOD to tropNO_2 slopes for the year 2020 are shown as red dots and any significant sudden increase in the slope is interpreted as the influx of transported aerosol into the domain. The weekly scatter plots of AOD and AOD-tropNO_2 for September 2019 and 2020 in Figure 8a-b show that the tropNO_2 values in both years ranged between 30 and 120 µmoles/m^2 whereas AOD values in 2020 were much higher (between 0.2 and 0.9) compared to values in 2019 that were only between 0.1 and 0.2. The AOD values typically range between 0 and 1, with higher AODs typically observed in the presence of biomass burning smoke or dust storms. The values in 2019 are akin to photochemically produced aerosols whereas the high values in 2020 indicate aerosols due to photochemically produced aerosols plus any transported aerosol from locations upwind of Los Angeles.

3.5. Economic activity indicators and tropNO_2

607 Because of the lockdown measures and work from home policies for majority of the
608 workplaces in the US, the service industry has taken a hit and the unemployment rate has risen.
609 The US unemployment rate increased from about 4.4% in March to 14.7% in April during the
610 first phase of lockdown. The unemployment rate nationwide improved as the year went by but
611 certain parts of the country continued to be under very high unemployment rate throughout 2020
612 (Figure 9). Amongst the employed, 28% of employees continue to work from home as of
613 November indicating that below normal NO_x emissions data are to be expected. The correlation
614 between unemployment rate and tropNO_2 for metropolitan areas with pre-pandemic civilian
615 labor force greater than two million is negative for the second and third quarters (the regression
616 line shown in Figure 9 is for second quarter data). The unemployment rate combined with
617 telework policies have contributed to reduced NO_x emissions and thus the lower tropNO_2 values
618 across the US. This is similar to the positive correlation between Gross Domestic Product (GDP)
619 and tropNO_2 reported by Keller et al. (2020). Cities such as Phoenix, AZ, Minneapolis, MN,
620 Dallas and Houston, TX, and Chicago, IL show no change or slight increase in tropNO_2 in 2020
621 compared to 2019 though unemployment rate in 2020 is much higher compared to 2019.

622 ## 4. Discussion
623

624 The TROPOMI tropNO_2 data captures the day to day variability but due to cloud cover and
625 uncertainties associated with assumptions such as a priori profile and lower sensitivity to near
626 surface NO_2, on certain days the retrievals do not adequately represent the changes in near
627 surface NO_2. Our analysis shows that the data reflect the NO_2 variability very well on monthly
628 scales and even on weekly scales, to the extent that even weekday/weekend cycles are
629 noticeable. When using the TROPOMI tropNO_2 data, we wanted to establish that it not only

630 shows the reductions/drop in tropNO_2 due to reductions in on-road emissions but that the trend
631 during post-lockdown recovery can be detected as well. Therefore we examined the trends in
632 on-road and power plant emissions for five different locations (four urban areas and one rural
633 area) to answer the questions: (1) are changes in NOx emissions during the lockdown detectable
634 in TROPOMI tropNO_2 data, (2) are the economic indicators consistent with emissions changes,
635 and (3) are the trends reversing with the removal of lockdown measures in the major metro areas.
636 These locations have diversity from a geographical perspective, are driven by different
637 economies, and experience different meteorology and climate. The inventory from ground
638 monitors for locations nationwide and its analysis is the subject of a different publication. The
639 focus in this paper is to corroborate trends seen in satellite data with ground observations.

640 The spatial and temporal analysis, relating indicators of human activity during and prior to
641 COVID-19 lockdown with air quality shows that while power plant emissions changes were not
642 drastic compared to on-road emissions, the on-road emissions in the four urban and one rural
643 location dropped coinciding with lockdown start date and duration. The changes in on-road NOx
644 emissions correlated with tropNO_2 changes for these five locations, giving confidence to use
645 tropNO_2 data in other parts of the CONUS to draw conclusions about relating changes in
646 tropNO_2 to economic activity changes. We found that the weekday-weekend differences were
647 pronounced in on-road emissions and tropNO_2 data with the lowest values of on-road NOx were
648 all on weekends even during the pandemic related lockdown periods. The unemployment rate
649 and its increase during the lockdown and post lockdown period appears to also be a good proxy
650 for economic activity and correlated well with decrease in tropNO_2 changes. At the height of the
651 pandemic related lockdown in second quarter 2020, the unemployment rate increase was as high
652 as 17% in populated metropolitan areas and even at the end of the third quarter in 2020, the

653 unemployment increase is ~10%. The first quarter unemployment showed no relationship to
654 tropNO_2 as expected because it was constant at ~5% and did not vary.

655 The satellite data must be analyzed by considering various quality flags and understanding
656 the limitations of the algorithm. It is likely that by using the quality flag > 0.75, we were
657 conservative in the use of TROPOMI data but the extremely low daily tropNO_2 values on certain
658 days even when on-road NO_x emissions were high is indicative that the data are more
659 interpretable when averaged to weekly or monthly time scales. For tropNO_2 retrievals that have
660 quality flags between 0.5 and 0.75, suggesting cloud contamination, we can look at coincident
661 high resolution (750m) VIIRS cloud mask product to analyze TROPOMI flags for cloud
662 contamination. This analysis will help us improve our analysis using the daily tropNO_2 retrievals
663 by either including more retrievals or removing some retrievals from the matching with on-road
664 emissions data.

665 ## 5. Conclusions

666
667 It has already been established by numerous research studies that reduced traffic (on-
668 road) and industrial emissions led to improved air quality during the lockdown measures
669 implemented by various countries across the globe. However, most studies used mobility data as
670 a proxy for reduced human activity to interpret satellite observations of tropNO_2 but did not
671 directly relate the reduced on-road emissions with reduced air quality observations. Here, for
672 the first time we directly correlate on-road NO_x emissions data to TROPOMI tropNO_2 in four
673 metropolitan and one rural areas in the US. For this, we used TROPOMI tropNO_2, VIIRS AOD,
674 on-road NOx emissions, and unemployment rates to develop a comprehensive analysis for 2019
675 and 2020. Where needed, we conducted rotated wind analyses to correctly sample and match the

676 on-road NOx emissions with tropNO_2 data, developed a novel way of deseasonalizing tropNO_2 -
677 data, and used changes in unemployment rate data as an indicator for economic activity.

678 Our analysis of reductions in on-road NO_x emissions from light and heavy duty vehicles
679 derived from fuel sales data showed a reduction from 9% to 19% between February and March at
680 the onset of lockdown in the middle of March in most of the US and between March and April,
681 the on-road NO_x emissions dropped further by 8% to 31% when lockdown measures were the
682 most stringent. These precipitous drops in NO_x emissions correlated well with tropNO_2.
683 Further, the changes in tropNO_2 across the continental U.S. between 2020 and 2019 correlated
684 well with changes in on-road NO_x emissions (Pearson correlation coefficient of 0.68) but
685 correlated weakly with changes in emissions from the power plants (Pearson correlation
686 coefficient of 0.35). These findings confirm the known knowledge that power plants are no
687 longer a major source of NO_2 in urban areas of the United States. As the US entered into a post-
688 pandemic phase between May and November 2020, the increased mobility resulted in increased
689 NO_x emissions nearly to the pre-lockdown phase but not entirely back to 100%. These changes
690 are reflected in the tropNO_2 data except that for Los Angeles and San Francisco, the tropNO_2
691 diverged from on-road NO_x emissions that needs further inquiry. The negative correlation
692 between changes in tropNO_2 in 2020 compared to 2019 and increased unemployment rate
693 indicates that with increased unemployment rate combined with telework policies across the
694 nation for non-essential workers, the NO_2 values decreased at the rate of 0.8 μmoles/m^2 decrease
695 per unit percentage increase in unemployment rate.

696 Across the CONUS we found positive spatial correlation between S5P TROPOMI NO_2 and
697 SNPP VIIRS AOD measurements in these urban regions indicating common source sectors for
698 NO_2 and aerosols/aerosol precursors. Once the data are averaged into weekly means and

699 temporally correlated and weeks when transported smoke mixes in with locally produced
700 emissions are removed, there is a negative correlation between AOD and tropNO_2 indicating that
701 photochemical conversion of NO_2 to nitrate aerosol is being captured in this analysis. This
702 methodology of screening for fire events influencing aerosol concentrations over urban/industrial
703 regions also helps with analyzing changes in aerosols due to emissions reductions. This is the
704 subject of a different manuscript that is currently in preparation. The COVID-19 pandemic
705 experience has provided the scientific community an opportunity to identify scenarios that can
706 lead to a new normal urban air quality and if the new normal can be sustained with novel policies
707 such as increased telework policies and a shift towards driving electric cars.

708
709

710 **Acknowledgements.** This work is part of a NOAA wide COVID-19 project funded by the
711 Joint Polar Satellite System (JPSS) and the office of Oceanic and Atmospheric Research (OAR)
712 to investigate the impact of lockdown on aerosols and trace gases including greenhouse gases.
713 The authors thank Mitch Goldberg (Chief Scientist of NOAA National Environmental Satellite
714 Data and Information Services), Greg Frost (Program Manager, NOAA Climate Program
715 Office), and Satya Kalluri (Science Advisor to the JPSS program) for securing funds for this
716 work. The authors thank the European Space Agency for the provision of the Sentinel 5
717 Precursor Tropospheric Monitoring Instrument data. The authors also thank members of NOAA
718 NESDIS JPSS aerosol calibration and validation team for the routine validation of Suomi
719 National Polar-orbiting Partnership Visible Infrared Imaging Radiometer Suite aerosol optical
720 depth product (Istvan Laszlo, Hongqing Liu, and Hai Zhang) used in our analysis. Brian
721 McDonald acknowledges the support from NOAA NRDD Project (#19533) - “COVID-19: Near
722 Real-time Emissions Adjustment for Air Quality Forecasting and Long-Term Impact

Analyses." Daniel Tong acknowledges the partial support of NOAA Weather Program Office (NA19OAR4590082), and Daniel Goldberg acknowledges the support of NASA RRNES grant #: 80NSSC20K1122.

Author Contributions. SK conceived the scope of the scientific study and formulated the analysis and wrote the manuscript. ZW conducted the scientific analyses including the generation of the figures used in the manuscript. BM processed and provided the on-road NO_x emissions data and wrote Section 2.2. DLG and DT conducted analysis that helped interpret the features observed in TROPOMI tropospheric NO_2 data shown in Figures 4 and 5 and reviewed the manuscript.

Disclaimer. The scientific results and conclusions, as well as any views or opinions expressed herein, are those of the author(s) and do not necessarily reflect those of NOAA or the Department of Commerce.

Data Statement. The publicly available SNPP VIIRS AOD data can be obtained from NOAA CLASS (https://www.avl.class.noaa.gov) and the gridded Level 3 AOD data can be obtained from ftp://ftp.star.nesdis.noaa.gov/pub/smcd/VIIRS_Aerosol/npp.viirs.aerosol.data/epsaot550. The Sentinel 5P TROPOMI NO2 data can be obtained from https://scihub.copernicus.eu/. The on-road NOx emissions data are currently not publicly available as the team is still conducting the analysis for publication purpose.

746

747

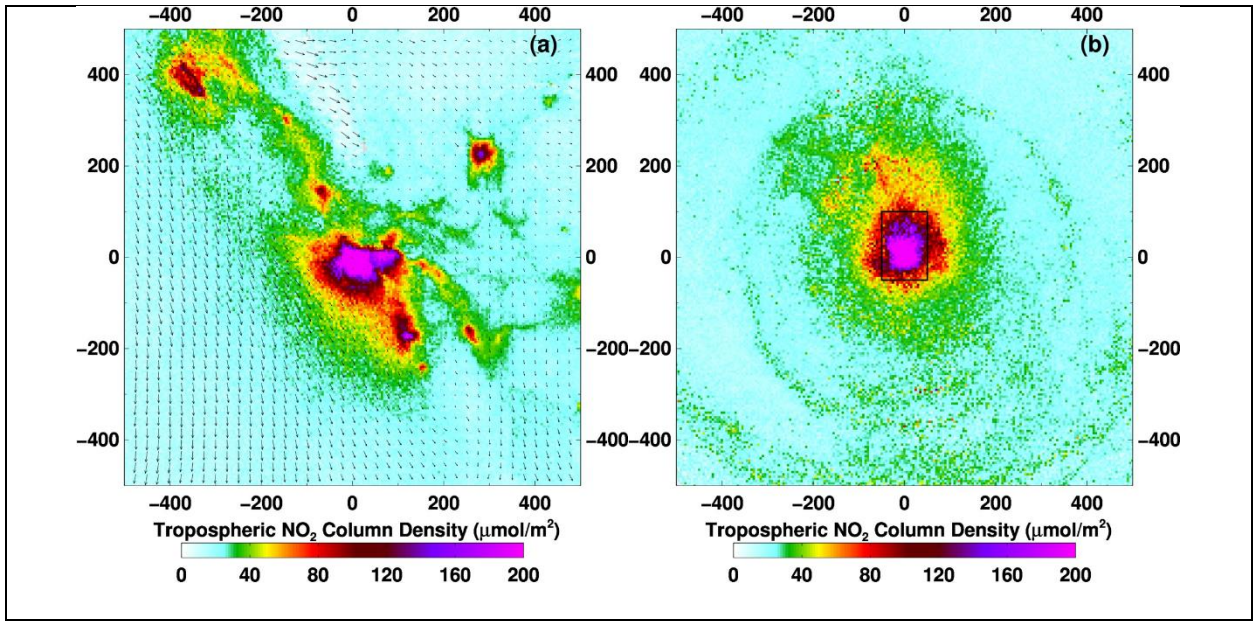

748

749

750

751

752

Figure 1: Sentinel 5P TROPOMI monthly mean NO_2 for January 2020 for California. (a) Original pixel level data remapped to 5 km x 5 km resolution and averaged for the month. The monthly mean ERA5 wind vectors are overlaid on the NO_2 map to indicate the wind direction. (b) Original pixel level NO_2 data remapped to 5 km x 5 km grids and the grids rotated in the direction of the wind using ERA5 wind fields. The downwind direction is shown pointing North. For the monthly mean to be computed, we used a criteria that at least 25% of the days in a month should have retrievals.

753

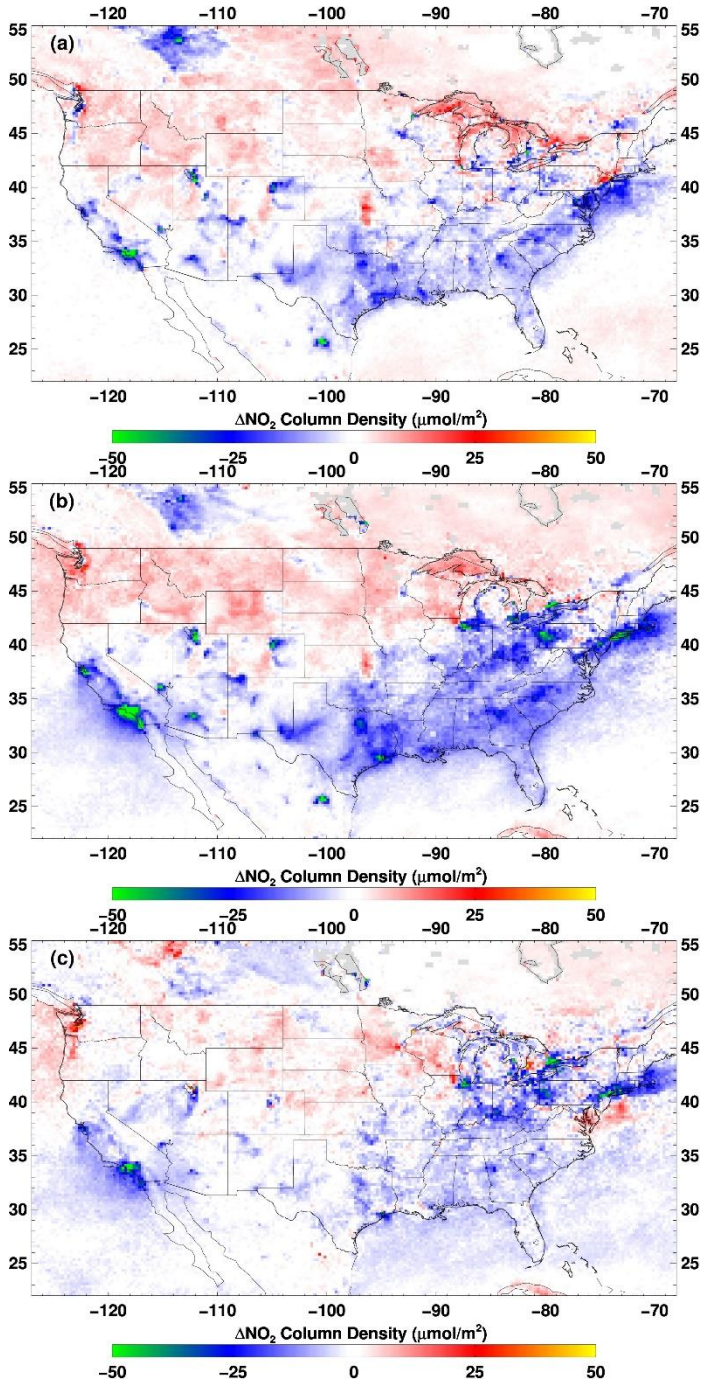

Figure 2: Tropospheric NO_2 changes between pre-lockdown time period (January to February) and lockdown period (15 March to 30 April) for (a) 2019ΔNO_2, (b) 2020ΔNO_2, and (c) the difference between 2020ΔNO_2 and 2019ΔNO_2. The double differencing is expected to remove the seasonal differences and provide a realistic estimate of change in tropNO_2 due to emissions changes.

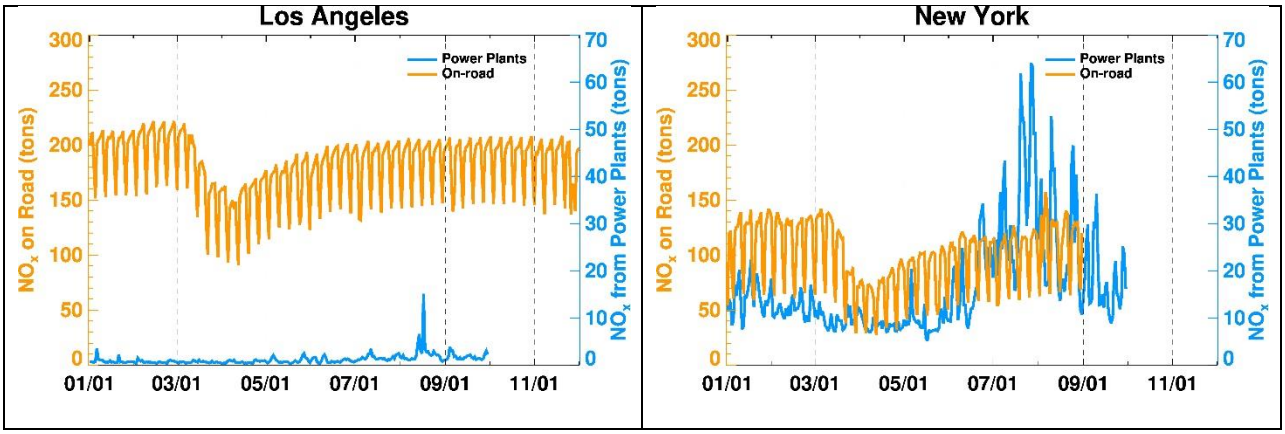
Los Angeles
New York
Power Plants
On-road
NO_x on Road (tons)
NO_x from Power Plants (tons)
300
250
200
150
100
50
0
70
60
50
40
30
20
10
0
01/01
03/01
05/01
07/01
09/01
11/01

754

755

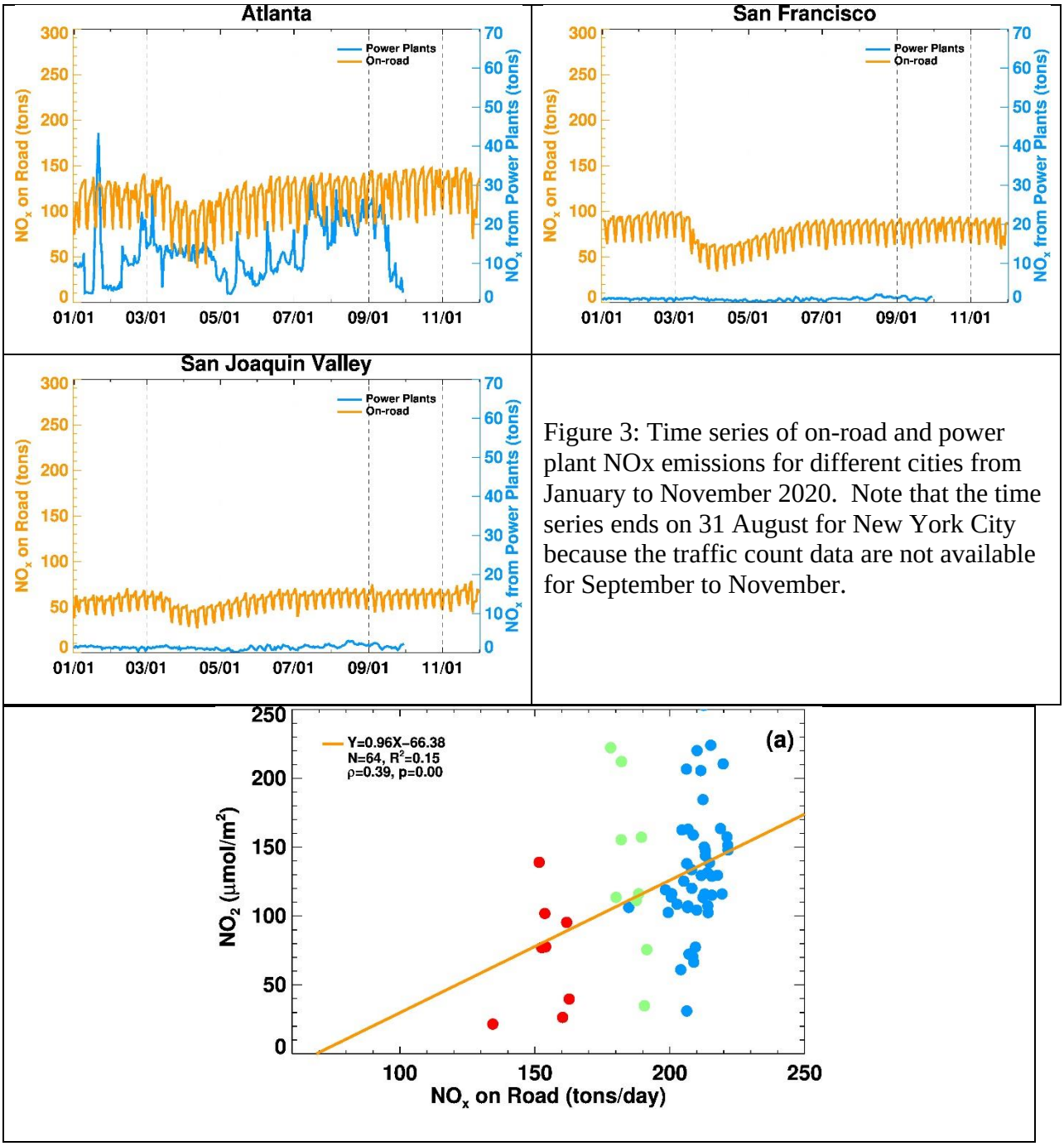

Figure 3: Time series of on-road and power plant NOx emissions for different cities from January to November 2020. Note that the time series ends on 31 August for New York City because the traffic count data are not available for September to November.

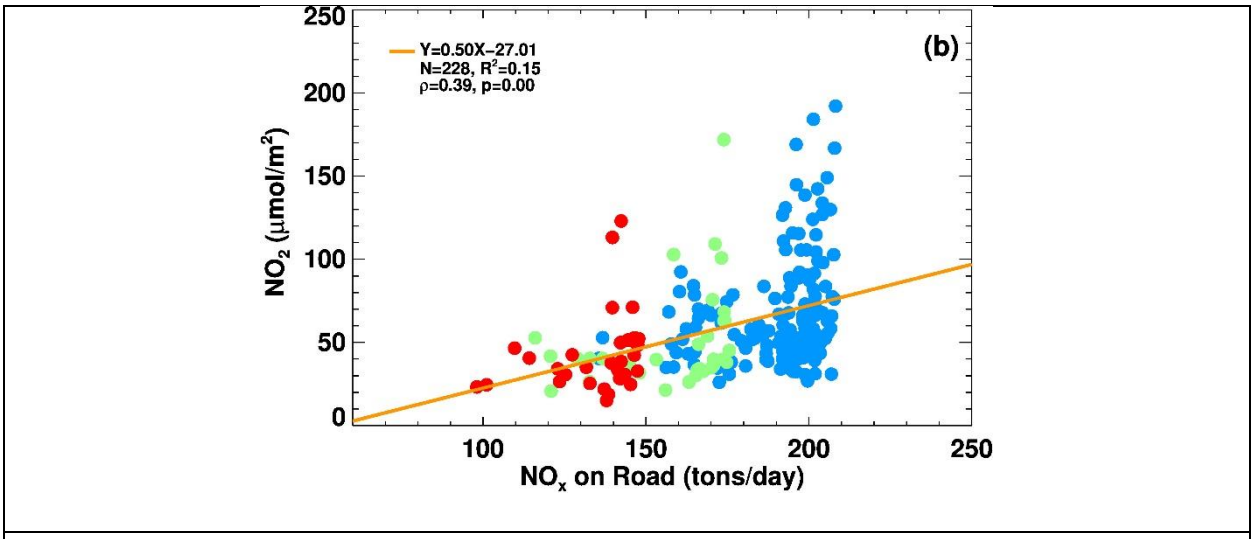

Figure 4: Correlation between tropNO_2 and on-road NO_x emissions for Los Angeles, CA. (a) For pre-lockdown (January and February) and (b) For lockdown and post lockdown time period (March through end of November). Red color is for data gathered on Sundays, green color is for data gathered on Saturdays, and blue color is for data gathered on weekdays.

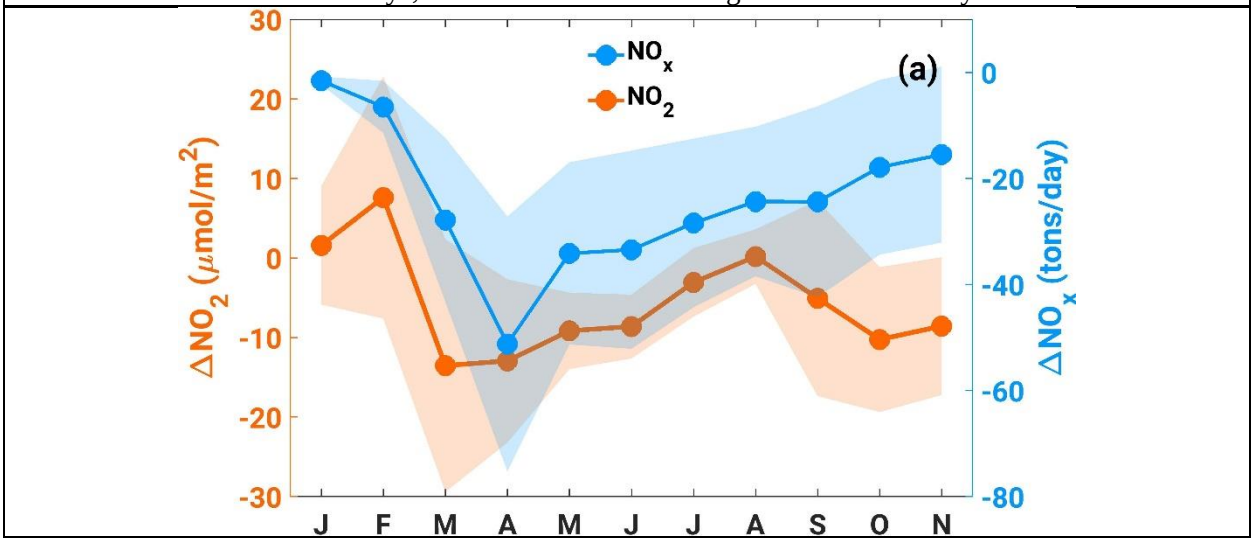

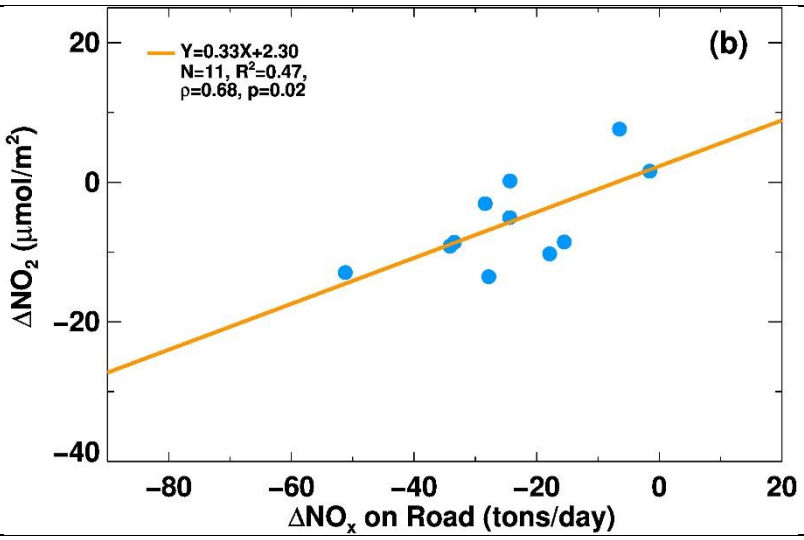

Figure 5: Trends in changes in on-road monthly mean NOx emissions (tons/day) and tropNO_2 (µmoles/m^2) between 2019 and 2020. (a) Average monthly mean differences for five cities (New York, Atlanta, Los Angeles, San Francisco, and San Joaquin Valley) across the United States from January to November. (b) Correlation between changes in on-road monthly mean NOx emissions and changes in tropNO_2 for the same five cities.

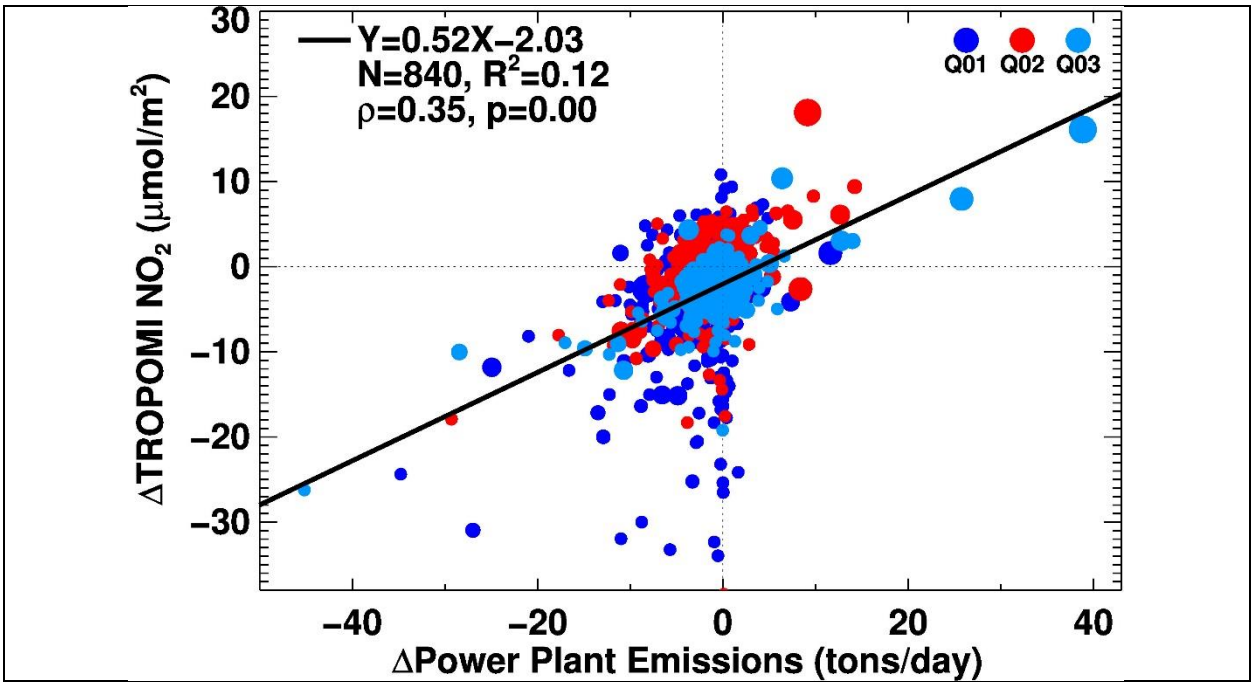

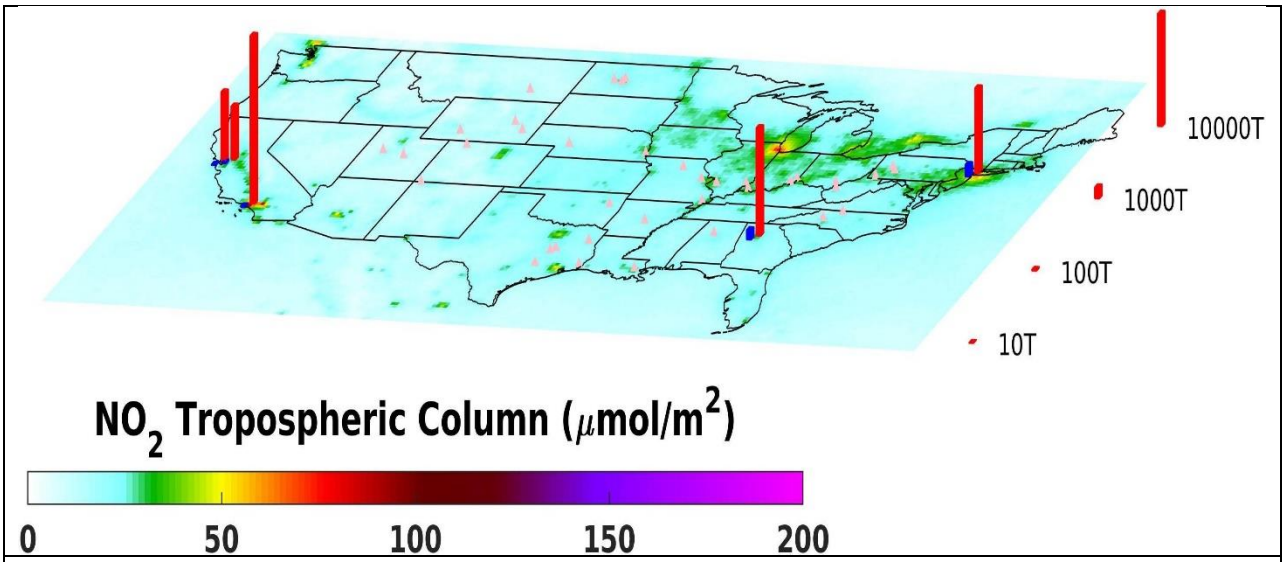

Figure 6: tropNO2 map for second quarter 2020 with the five locations where on-road NO_x emissions data were collected by NOAA. The red columns show total NOx emissions and the blue columns show NOx emissions from power plants nearby these five cities (New York, Atlanta, Los Angeles, San Francisco, and San Joaquin Valley). Power plants with monthly mean NOx emissions greater than 500 tons are also shown in the map as pink dots.

774

775

776

777

Figure 7: Correlation of tropNO_2 changes between 2020 and 2019 with changes in power plant monthly mean NO_x emissions. Daily total NO_x emissions were added and divided by the number of days in a month to get average values in units of tons/day.

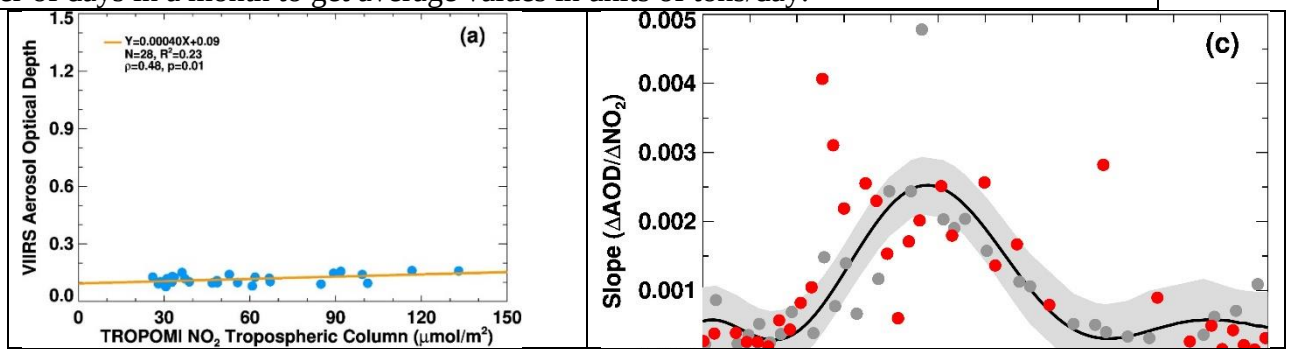

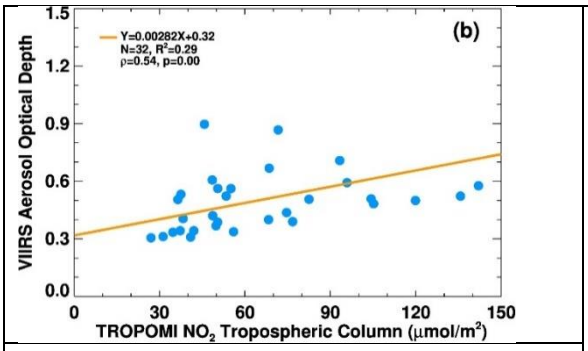

Figure 8: (a) Example correlation of VIIRS AOD and TROPOMI tropNO_2 during one week, September 15-21, 2019, (b) Same for September 13-19, 2020, (c) Time series of weekly slope (AOD/NO_2) with data for 2019 in gray color and data for 2020 in red color for Los Angeles, California. The black solid line is the fit to 2019 data indicating the photochemical processes of the impact of NOx on secondary aerosol formation. Any data points that depart from the fit line are treated as the time period when transported aerosols (e.g., smoke) influenced the air mass over Los Angeles.

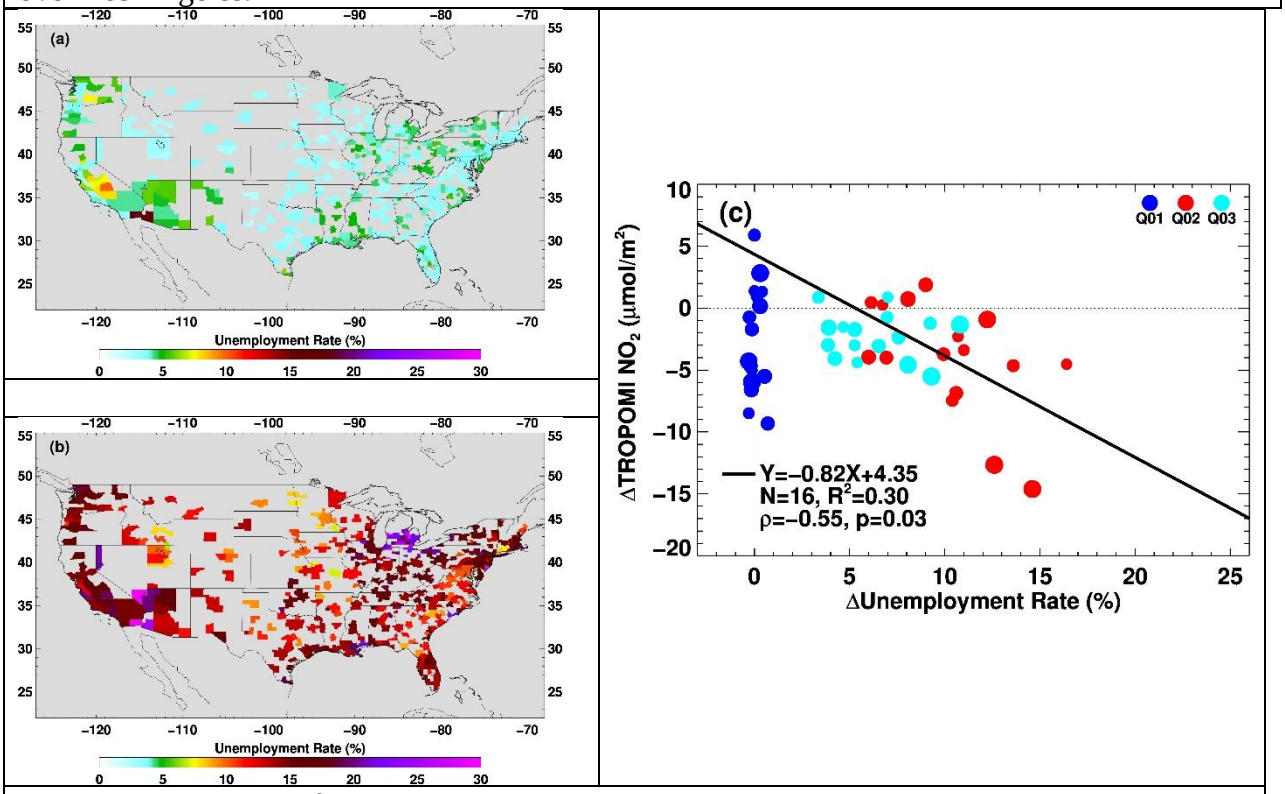

Figure 9: The impact of COVID-19 lockdown on unemployment rate in metropolitan areas and tropNO_2. (a) Unemployment rate in April 2019, (b) Unemployment rate in April 2020, and (c) Correlation between increase in unemployment between 2020 and 2019 and tropNO_2 changes. Only data for metropolitan areas where civilian labor force in 2019 was greater than two million

are shown in the correlation plot. In the first quarter (Q01) unemployment changes are close to zero as pandemic impact did not begin until late March. Strong negative correlation is observed for the second (Q02) and third (Q03) quarters. The solid black line is the fit to the second quarter data.

Table 1: Ranking of cities for ozone pollution and their lockdown time periods

City/Region	Ozone Pollution Ranking	Lockdown Start Date	Lockdown End Date
Los Angeles-Long Beach, CA	1	19-Mar	4-May
Visalia, CA	2	19-Mar	4-May
Bakersfield, CA	3	19-Mar	4-May
Fresno-Madera-Hanford, CA	4	19-Mar	4-May
Sacramento-Roseville, CA	5	19-Mar	4-May
San Diego-Chula Vista-Carlsbad, CA	6	19-Mar	4-May
Phoenix-Mesa, AZ	7	30-Mar	30-Apr
San Jose-San Francisco-Oakland, CA	8	19-Mar	4-May
Las Vegas-Henderson, NV	9	1-Apr	30-Apr
Denver-Aurora, CO	10	26-Mar	26-Apr
Salt Lake City-Provo-Orem, UT	11	30-Mar	13-Apr
New York-Newark, NY-NY-CT-PA*	12	22-Mar	15-May
Redding-Red Bluff, CA	13	19-Mar	4-May
Houston-The Woodlands, TX	14	2-Apr	20-Apr
El Centro, CA	15	19-Mar	4-May
Chicago-Naperville, IL-IN-WI*	16	23-Mar	1-May
El Paso-Las Cruces, TX-NM	17	2-Apr	15-May
Chico, CA	18	19-Mar	4-May
Fort Collins, CO	19	26-Mar	26-Apr
Washington-Baltimore-Arlington, DC-MD-VA-WV-PA*	20	30-Mar	15-May
Dallas-Fort Worth, TX-OK	21	2-Apr	20-Apr
Sheboygan, WI	22	24-Apr	26-May
Philadelphia-Reading-Camden, PA-NJ-DE-MD*	23	30-Mar	15-May
Milwaukee-Racine-Waukesha, WI	24	24-Apr	26-May
Hartford-East Hartford, CT	25	23-Mar	20-May

*Dates reflect the time period that is the longest for any given state in the region

872

873

Table 2: Reductions in on-road NOx emissions and tropNO2 between 15 March to 30 April and 1 January to 29 February

City	2019ΔNOx (%)	2020ΔNOx (%)	Seasonality Removed On-road NOx Emissions Changes (%) 2020ΔNOx - 2019ΔNOx)	2019ΔNO2 (%)	2020ΔNO2 (%)	Seasonality Removed TropNO2 Reductions (%) ($2020\Delta tropNO_2$ - $2019\Delta tropNO_2$)
Atlanta	10.41	-17.70	-28.11	-22.67	-44.14	-21.47
San Francisco	10.54	-33.95	-44.49	-23.79	-48.18	-24.39
San Joaquin Valley	14.27	-18.39	-32.66	-27.30	-44.62	-17.32
New York City	11.04	-36.87	-47,91	-6.07	-34.05	-27.98
Los Angeles	10.57	-25.10	-35.67	-37.90	-59.68	-21.78

874

875

876

877

878

879

880

881

882

883

884

885

886

887

888

889

890

891

References

Achakulwisut, P., Brauer, M., Hystad, P., Anenberg, S. C. (2019). Global, national, and urban burdens of paediatric asthma incidence attributable to ambient NO_2 pollution: estimates from global datasets. *Lancet Planet Health*. 1-4, DOI: 10.1016/S2542-5196(19)30046-4

Baidar, S., Hardesty, R. M., Kim, S.-W., Langford, A. O., Oetjen, H., Senff, C. J., et al. (2015).Weakening of the weekend ozone effect over California's South Coast Air Basin: Weekend ozone effect over California. *Geophysical Research Letters*, *42*, 9457–9464. doi: 10.1002/2015GL066419

Bauwens, M., Compernolle, S., Stavrakou, T., Muller, J.-F., van Gent, J., Eskes, H., Levelt, P. F., Van der A. R., Veefkind, P., Vlietinck, J., Yu, H., Zehner, C. (2020). *Geophysical Research Letters*. doi: 10.1029/2020GL087978

Bishop, G. A., and Stedman, D. H. (2014), The recession of 2008 and its impact on light-duty vehicle emissions in three western United States cities, *Environ Sci Technol*, *48*, 14822-14827, doi:10.1021/es5043518.

Bishop, G. A., and Haugen, M. J. (2018), The story of ever diminishing vehicle tailpipe emissions as observed in the Chicago, Illinois area, *Environ Sci Technol*, doi:10.1021/acs.est.8b00926.

Cersosimo, A., Serio, C., Masiello, G. (2020). TROPOMI NO_2 Tropospheric Column Data: Regridding to 1 km Grid-Resolution and Assessment of their Consistency with In Situ Surface Observations. *Remote Sens.*, *12*, 2212. https://doi.org/10.3390/rs12142212

Chan, K. L., M. Wiegner, J. van Geffen, I. De Smedt, C. Alberti, Z. Cheng, S. Ye, and M. Wenig, MAX-DOAS measurements of tropospheric NO2 and HCHO in Munich and the comparison to OMI and TROPOMI satellite observations (2020). *Atmos. Meas. Tech.*, *13*, 4499–4520. https://doi.org/10.5194/amt-13-4499-2020

de Gouw, J.A., Parrish, D.D., Frost, G.J. and Trainer, M. (2014), Reduced emissions of CO_2, NOx, and SO_2 from U.S. power plants owing to switch from coal to natural gas with combined cycle technology. Earth's Future, 2: 75-82. https://doi.org/10.1002/2013EF000196

EPA (2015), MOVES2014a (Motor Vehicle Emission Simulator), Office of Transportation and Air Quality, U.S. Environmental Protection Agency.

Fioletov, V. E., McLinden, C. A., Krotkov, N., Li, C. (2015). Lifetimes and emissions of SO2 from point sources estimated from OMI. *Geophys. Res. Lett.*, *42*, 1969–1976, doi: 10.1002/2015GL063148.

935 Gkatzelis, G.I., J.B. Gilman, S.S. Brown, H. Eskes, A.R. Gomes, A.C. Lange, B.C. McDonald, J.
936 Peischl, A. Petzold, C. Thompson, A. Kiendler-Scharr (accepted). The Global Impacts of
937 COVID-19 Lockdowns on Urban Air Pollution: A Review. *Elementa: Science of Anthropocene*.
938
939 Goldberg, D. L., Anenberg, S. C., Griffin, D., McLinden, C. A., Lu, Z., & Streets, D.
940 G. (2020). Disentangling the impact of the COVID-19 lockdowns on urban NO_2 from natural
941 variability. *Geophysical Research Letters*, 47,
942 e2020GL089269. https://doi.org/10.1029/2020GL089269
943
944 Goldberg, D. L., Lu, Z., Streets, D. G., de Foy, B., Griffin, D., McLinden, C. A., Lamsal, L. N.,
945 Krotkov, N. A., Eskes, H. Enhanced capabilities of TROPOMI NO_2: Estimating NO_X from
946 North American 2 cities and power plants. (2019). *Environ. Sci. Technol.*, 53, 21, 12594–12601
947 https://doi.org/10.1021/acs.est.9b04488
948
949 Hassler, B., B. C. McDonald, G. J. Frost, A. Borbon, D. C. Carslaw, K. Civerolo, C. Granier, P.
950 S. Monks, S. Monks, D. D. Parrish, I. B. Pollack, K. H. Rosenlof, T. B. Ryerson, E. von
951 Schneidemesser, and M. Trainer (2016), Analysis of long-term observations of NOx and CO in
952 megacities and application to constraining emissions inventories, *Geophys Res Lett*, *43*, 9920-
953 9930, doi:10.1002/2016gl069894.
954
955 Hersbach, H, Bell, B, Berrisford, P, et al. The ERA5 global reanalysis. *Q J R Meteorol*
956 *Soc*. 2020; 146: 1999– 2049. https://doi.org/10.1002/qj.3803
957
958 Hoesly, R. M., Smith, S. J., Feng, L., Klimont, Z., Janssens-Maenhout, G., Pitkanen, T., Seibert,
959 J. J., Vu, L., Andres, R. J., Bolt, R. M., Bond, T. C., Dawidowski, L., Kholod, N., Kurokawa, J.-
960 I., Li, M., Liu, L., Lu, Z., Moura, M. C. P., O'Rourke, P. R., and Zhang, Q. (2018). Historical
961 (1750–2014) anthropogenic emissions of reactive gases and aerosols from the Community
962 Emissions Data System (CEDS). *Geosci. Model Dev.*, 11, 369–408.
963 https://doi.org/10.5194/gmd-11-369-2018
964 Huang, M., et al. (2014), Changes in nitrogen oxides emissions in California during 2005–2010
965 indicated from top-down and bottom-up emission estimates, *J. Geophys. Res.*
966 *Atmos.*, 119, 12,928– 12,952, doi:10.1002/2014JD022268.
967 Iolango, I., Virta, H., Eskes, H., Hovila, J., Douros, J. (2020). Comparison of
968 TROPOMI/Sentinel 5 Precursor NO_2 observations with ground-based measurements in Helsinki,
969 *Atmos. Meas. Tech.*, *13*, 205–218, https://doi.org/10.5194/amt-2019-329
970 Jiang, Z., B. C. McDonald, H. Worden, J. R. Worden, K. Miyazaki, Z. Qu, D. K. Henze, D. B. A.
971 Jones, A. F. Arellano, E. V. Fischer, L. Y. Zhu, and K. F. Boersma (2018), Unexpected
972 slowdown of US pollutant emission reduction in the past decade, *P Natl Acad Sci USA*, *115*,
973 5099-5104, doi:10.1073/pnas.1801191115.
974

Judd, L. M., J. A. All-Saadi, S. J. Janz, M. G. Kowalewski, R. B. Pierce, J. J. Szykman, L. C. Valin, R. Swap, A. Cede, M. Mueller, M. Tiefengarber, N. Abuhassan, D. Williams, Evaluating the impact of spatial resolution on tropospheric NO_2 column comparisons within urban areas using high-resolution airborne data, https://doi.org/10.5194/amt-2019-161

Judd, L. M., Al-Saadi, J. A., Szykman, J. J., Valin, L. C., Janz, S. J., Kowalewski, M. G., Eskes, H. J., Veefkind, J. P., Cede, A., Mueller, M., Gebetsberger, M., Swap, R., Pierce, R. B., Nowlan, C. R., Abad, G. G., Nehrir, A., and Williams, D. (2020). Evaluating Sentinel-5P TROPOMI tropospheric NO_2 column densities with airborne and Pandora spectrometers near New York City and Long Island Sound, Atmos. Meas. Tech., 13, 6113–6140, https://doi.org/10.5194/amt-13-6113-2020

Keller, C. A., Evans, M. J., Knowland, K. E., Hasenkopf, C. A., Modekurty, S., Lucchesi, R. A., Oda, T., Franca, B. B., Mandarino, F. C., Díaz Suárez, M. V., Ryan, R. G., Fakes, L. H., and Pawson, S. (2020). Global Impact of COVID-19 Restrictions on the Surface Concentrations of Nitrogen Dioxide and Ozone, Atmos. Chem. Phys. Discuss. [preprint], https://doi.org/10.5194/acp-2020-685, in review.

Kim, S.-W., McDonald, B. C., Baidar, S., Brown, S. S., Dube, B., Ferrare, R. A., Frost, G. J., Harley, R. A., Holloway, J. S., Lee, H.-J., et al. (2016), Modeling the weekly cycle of NO_x and CO emissions and their impacts on O_3 in the Los Angeles-South Coast Air Basin during the CalNex 2010 field campaign, *J. Geophys. Res. Atmos.*, 121, 1340– 1360, doi:10.1002/2015JD024292.

Kondragunta, S., D. Crisp, and C. Zehner (2020), Disseminating scientific results in the age of rapid communication, *Eos, 101*, https://doi.org/10.1029/2020EO150710. Published on 20 October 2020.

Kroll, J.H., Heald, C.L., Cappa, C.D. *et al.* The complex chemical effects of COVID-19 shutdowns on air quality. *Nat. Chem.* **12,** 777–779 (2020). https://doi.org/10.1038/s41557-020-0535-z

Lamsal, N. L., Duncan, B.N., Yoshida, Y., Krotkov, N. A., Pickering, K. E., Streets, D. (2015). U.S. NO_2 trends (2005–2013): EPA Air Quality System (AQS) data versus improved observations from the Ozone Monitoring Instrument (OMI), *Atmospheric Environment*, *100*, 130-143.

Laszlo, I. and Liu, H., 2016. EPS Aerosol Optical Depth (AOD) Algorithm Theoretical Basis Document, version 3.0.1, June 28, 2016, NOAA NESDIS.

Levy, R.C., Remer, L.A., Mattoo, S., Vermote, E.F., and Kaufman, Y.J. (2007). Second-generation operational algorithm: retrieval of aerosol properties over land from inversion of

Moderate Resolution Imaging Spectroradiometer spectral reflectance. *J Geophys Res.*, *112*. doi:10.1029/2006JD007811

Lin, J.-T., Martin, R. V., Boersma, K. F., Sneep, M., Stammes, P., Spurr, R., Wang, P., Van Roozendael, M., Clémer, K., and Irie, H. (2014). Retrieving tropospheric nitrogen dioxide from the Ozone Monitoring Instrument: effects of aerosols, surface reflectance anisotropy, and vertical profile of nitrogen dioxide, *Atmos. Chem. Phys.*, *14*, 1441–1461. https://doi.org/10.5194/acp-14-1441-2014

Liu, F., Page, A., Strode, S. A., Yoshida, Y., Choi, S., Zheng, B., Lamsal, L., Li, C., Krotkov, N. A., Eskes, H., van der, R., Veefkind, P., Levelt, P. F., Hauser, O. P., Joiner, J. (2020). Abrupt decline in tropospheric nitrogen dioxide over China after the outbreak of COVID-19, *Science Advances*, *6*, 28, eabc2992. DOI: 10.1126/sciadv.abc2992

Liu, M., J. Lin, H. Kong, K. F. Boersma, H. Eskes, Y. Kanaya, Q. Hes, X. Tian, K. Qin, P. Xie, R. Spurr, R. Ni, Y. Yan, H. Weng, J. Wang (2020). A new TROPOMI product for tropospheric NO_2 columns over East Asia with explicit aerosol corrections. *Atmos. Meas. Tech.*, *13*, 4247–4259. https://doi.org/10.5194/amt-13-4247-2020

Lorente, A., Boersma, K.F., Eskes, H.J. *et al.* Quantification of nitrogen oxides emissions from build-up of pollution over Paris with TROPOMI. *Sci Rep* **9,** 20033 (2019). https://doi.org/10.1038/s41598-019-56428-5

Mazuuca, G. M., X. Ren, C. P. Loughner, M. Estes, J. H. Crawford, K. E. Pickering, A. J. Weinheimer, and R. R. Dickerson, Ozone production and its sensitivity to NOx and VOCs: results from the DISCOVER-AQ field experiment, Houston 2013. 2016. *Atmos. Chem. Phys.*, *16*, 14463–14474. doi: 10.5194/acp-16-14463-2016

McDonald, B. C., S. A. McKeen, Y. Y. Cui, R. Ahmadov, S. W. Kim, G. J. Frost, I. B. Pollack, T. B. Ryerson, J. S. Holloway, M. Graus, C. Warneke, J. B. Gilman, J. A. de Gouw, J. Kaiser, F. N. Keutsch, T. F. Hanisco, G. M. Wolfe, and M. Trainer (2018), Modeling ozone in the Eastern U.S. using a fuel-based mobile source emissions inventory, *Environ Sci Technol*, *52*, 7360-7370, doi:10.1021/acs.est.8b00778.

McDonald, B. C., T. R. Dallmann, E. W. Martin, and R. A. Harley (2012), Long-term trends in nitrogen oxide emissions from motor vehicles at national, state, and air basin scales, *J Geophys Res-Atmos*, *117*, D00V18, doi:10.1029/2012jd018304.

McDonald, B. C., Z. C. McBride, E. W. Martin, and R. A. Harley (2014), High-resolution mapping of motor vehicle carbon dioxide emissions, *J Geophys Res-Atmos*, *119*, 5283-5298, doi:10.1002/2013jd021219.

McDonald, B. C., Dallmann, T. R., Martin, E. W., and Harley, R. A. (2012), Long-term trends in nitrogen oxide emissions from motor vehicles at national, state, and air basin scales, *J. Geophys. Res.*, 117, D00V18, doi: 10.1029/2012JD018304

McDonald, B. C., et al. (2018). Volatile chemical products emerging as largest petrochemical source of urban organic emissions. *Science 359*, 760-764.

Naeger, A.R. and Murphy, K. (2020). Impact of COVID-19 Containment Measures on Air Pollution in California. *Aerosol Air Qual. Res.* https://doi.org/10.4209/aaqr.2020.05.0227

Parker, H. A., Hasheminassab, S., Crounse, J. D., Roehl, C. M., & Wennberg, P. O. (2020). Impacts of traffic reductions associated with COVID-19 on Southern California air quality. Geophysical Research Letters, 47, e2020GL090164. https://doi.org/10.1029/2020GL090164

Qin, M., Murphy, B.N., Isaacs, K.K. *et al.* (2021). Criteria pollutant impacts of volatile chemical products informed by near-field modelling. *Nat Sustain 4***,** 129–137. https://doi.org/10.1038/s41893-020-00614-1

Silver, B., X. He, S. Arnold, D. V. Spracklen, The impact of COVID-19 control measures on air quality in China. (2020). *Environ. Res. Lett. 15*, 084021. https://doi.org/10.1088/1748-9326/aba3a2

Schiferl, L. D., C. L. Heald, J. B. Nowak, J. S. Holloway, J. A. Neuman, R. Bahreini, I. B. Pollack, T. B. Ryerson, C. Wiedinmyer, and J. G. Murphy (2014), An investigation of ammonia and inorganic particulate matter in California during the CalNex campaign, J. Geophys. Res. Atmos., 119, 1883–1902, doi:10.1002/2013JD020765

Silvern, R. F., D. J. Jacob, L. J. Mickley, M. P. Sulprizio, K. R. Travis, E. A. Marais, R. C. Cohen, J. L. Laughner, S. Choi, J. Joiner, and L. N. Lamsal, Using satellite observations of tropospheric NO_2 columns to infer long-term trends in US NOx emissions: the importance of accounting for the free tropospheric NO_2 background. (2019). *Atmos. Chem. Phys.*, *19*, 8863–8878. https://doi.org/10.5194/acp-19-8863-2019

Tack, F., A. Merlaud, A. C. Meir, T. Vlemmix, T. Ruhtz, M-D. Iordache, X. Ge, :/ vam der War. D/ Schuettemeyer, M. Ardelean, A. Calcan, D. Constantin, A. Schonhardt, K. Meuleman, A. Richter, and M. V. Roozendae, Intercomparison of four airborne imaging DOAS systems for tropospheric NO_2 mapping – the AROMAPEX campaign. (2019). *Atmos. Meas. Tech.*,*12*, 211–236. https://doi.org/10.5194/amt-12-211

Today in energy, https://www.eia.gov/todayinenergy/detail.php?id=37752, December 11, 2018

Tong, D., L. Pan, W. Chen, L. Lamsal, P. Lee, Y. Tang, H. Kim, S. Kondragunta, I. Stajner, Impact of the 2008 Global Recession on air quality over the United States: Implications for surface ozone levels from changes in NOx emissions. (2016). *Geophys. Res. Lett.*, *10*.1002/2016GL069885

Tong, D.Q., L. Lamsal, L. Pan, C. Ding, H. Kim, P. Lee, T. Chai, and K.E. Pickering, and I. Stajner, Long-term NOx trends over large cities in the United States during the 2008 Recession: Intercomparison of satellite retrievals, ground observations, and emission inventories. (2015). *Atmospheric Environment*, *107*, 70-84. doi:10.1016/j.atmosenv.2015.01.035

van Geffen, J., H. J. Eskes, K. F. Boresma, J. D. Maasakkers, and J. P. Veefkind, TROPOMI ATBD of the total and tropospheric NO_2 data products, S5P-KNMI-L2-0005-RP, v1.4.0, 2019

Zhang, Q., Y. Pan, Y. He, W. W. Walters, Q. Ni, X. Liu, G. Xu, J. Shao, C. Jiang, Substantial nitrogen oxides emission reduction from China due to COVID-19 and its impact on surface ozone and aerosol pollution. (2021). *Science of The Total Environment, 753*.

Zhao, X., D. Griffin, V. Fioletov, C. McLinden, A. Cede, M. Tiefengraber, M. Muller, K. Bognar, K. Strong, F. Boersma, H. Eskes, J. Davies, A. Ogyu, and S. C. Lee. (2020). Assessment of the quality of TROPOMI high-spatial-resolution NO_2 data products in the Greater Toronto Area, *Atmos. Meas. Tech., 13*, 2131–2159. https://doi.org/10.5194/amt-13-2131-2020

Zhang, H., & Kondragunta, S. (2021). Daily and Hourly Surface PM2.5 Estimation from Satellite AOD. *Earth and Space Science*, 8, e2020EA001599. https://doi.org/10.1029/2020EA001599

Zheng, H., S. Kong, N. Chen, Y. Yan, D. Liu, B. Zhu, K. Xu, W. Cao, Q. Ding, B. Lan, Z. Zhang, M. Zheng, Z. Fan, Y. Cheng, S. Zheng, L. Yao, Y. Bai, T. Zhao, S. Qi. (2020). Significant changes in the chemical compositions and sources of PM2.5 in Wuhan since the city lockdown as COVID-19, Science of the Total Environment, 739.

COVID-19 Induced Fingerprints of a New Normal Urban Air Quality in the United States

S. Kondragunta*[1], Z. Wei[2], B. C. McDonald[3], D. L. Goldberg[4], D. Q. Tong[5]

[1]NOAA NESDIS Center for Satellite Applications and Research, 5825 University Research Court, College Park, MD

[2]IM Systems Group, 5825 University Research Court, College Park, MD

[3]NOAA Chemical Systems Laboratory, Boulder, CO

[4]Milken School of Public Health, George Washington University, Washington, DC

[5]Department of Atmospheric, Oceanic, and Earth Sciences, George Mason University, Fairfax, VA

* Corresponding author: Phone: 301-655-7311. Email: Shobha.Kondragunta@noaa.gov

Abstract

Most countries around the world including the United States took actions to control COVID-19 spread that lead to an abrupt shift in human activity. On-road NO_x emissions from light and heavy-duty vehicles decreased by 9% to 19% between February and March at the onset of the lockdown period in the middle of March in most of the US; between March and April, the on-road NO_x emissions dropped further by 8% to 31% when lockdown measures were the most stringent. These precipitous drops in NO_x emissions correlated well with tropospheric NO_2 column amount observed by the Sentinel 5 Precursor TROPOspheric Monitoring Instrument (S5P TROPOMI). Furthermore, the changes in TROPOMI tropospheric NO_2 across the continental U.S. between 2020 and 2019 correlated well with changes in on-road NO_x emissions ($r = 0.68$) but correlated weakly with changes in emissions from the power plants ($r = 0.35$). At the height of lock-down related unemployment in the second quarter of 2020, the NO_2 values decreased at the rate of 0.8 μmoles/m^2 per unit percentage increase in the unemployment rate. Despite the lifting of lockdown measures, parts of the US continued to have ~20% below normal on-road NOx emissions. To achieve this new normal urban air quality in the US, continuing remote work policies that do not impede economic growth may become one of the many options

Key Words: COVID-19, nitrogen dioxide, aerosol optical depth, TROPOMI, NOx emissions, air quality, power plants

Plain Language Summary

This study documents the different phases of COVID-19 lockdown in 2020 and how traffic emissions changed accordingly across the US, particularly in five different cities, namely Los Angeles, San Francisco, San Joaquin Valley, New York City, and Atlanta. Analysis of data for these cities from measurements on the ground and satellites indicate that a down turn in the economy and telework policies reduced the number of cars and trucks on the road in March and April due to which air quality got better. The recovery of traffic emissions after the lockdowns were lifted was slow and below normal emissions were observed into the end of 2020. While the cities in the east reached near normal levels, the west coast showed below normal traffic emissions. The air quality in 2020 provided a window into the future as to how improvements can be achieved.

1. Introduction

As the 2019 novel Corona virus (COVID-19) spread from China to other parts of the world, various countries imposed lockdown measures one by one. Reports of improved air quality from ground and satellite observations of aerosol optical depth (AOD) and nitrogen dioxide (NO_2) soon followed in the media as documented by Kondragunta et al. (2020). The precipitous drops seen in the tropospheric vertical column NO_2, ($tropNO_2$ here onwards) measured by the Sentinel 5P Tropospheric Monitoring Instrument (TROPOMI) were substantial, especially during the strict lockdown period for each country (Gkatzelis et al., 2020). Goldberg et al. (2020) reported that in the United States (US), $tropNO_2$ decreased by 9.2% to 45% in 26 cities from March 15 to April 30, 2020 compared to the same period in 2019; these reported reductions account for the influence of the weather. Other researchers reported similar findings, mainly reductions of $tropNO_2$ attributed to reductions in traffic emissions both in the US. and across the globe in major urban areas of Europe, India, and China (Bauwens et al., 2020; Keller et al., 2020; Zheng et al., 2020; Vaderu et al., 2020; Straka et al., 2021; Nager et al., 2020). For example in Washington D.C., average distance traveled by people dropped by 60% between February and April when restrictions were fully in place (Straka et al., 2021). This sudden drop in $tropNO_2$ in major metropolitan areas where the transportation source sector for NO_x ($NO+NO_2$) is strong is due to reduced traffic on top of an already observed general decreasing trend in NO_x emissions. According to Lamsal et al. (2015), $tropNO_2$ observed by the Ozone Monitoring Instrument showed a decreasing trend with an overall decrease of 28% between 2005 and 2013. These reductions are consistent with NO_x emissions reductions from major power plants in the US due to the Clean Air Interstate Rule and Cross State Air Pollution Rule. The NO_x emissions

continued to drop as more and more power plants switched to natural gas or began to rely on clean coal (de Gouw et al., 2014)

Nitrogen dioxide is released during combustion of fossil fuels and is a precursor for both ozone and particulate matter, primary components of photochemical smog. Whether it enhances or decreases ozone production is dependent on a given region being NO_x saturated or volatile organic compound (VOC) saturated, due to the inherent non-linearity of ozone photochemistry (Kroll et al., 2020; Mazzuca et al., 2016). The two main sources of NO_2 in the US are the energy sector and the transportation sector according to the 2014 Community Emissions Data System (Hoesly et al., 2018). A study by Zheng et al. (2020) analyzed the reductions in trace gas and aerosol concentrations in China during the lockdown and found that the most significant drop in aerosols was for nitrate aerosol. For the period corresponding to the lockdown in China, January 23 to February 22, 2020, mean nitrate aerosol concentration was 14.1 $\mu g/m^3$; for the same period in 2019, the concentration was 23.8 $\mu g/m^3$. This 41% reduction is corroborated by reductions in NO_2 observed by TROPOMI (Bauwens et al., 2020).

Though NO_2 is considered important due to its ozone and aerosol producing potential, it has harmful human health impacts when inhaled. Achakulwisut et al (2019) showed that 64% of four million pediatric asthma cases each year are due to exposure to NO_2. It should be noted though that NO_2 was used as a proxy for traffic-related pollution. The World Health Organization (WHO) standard for NO_2 is an annual average of 21 parts per billion and for the US, it is 53 parts per billion. The authors do note that that daily exposures to NO_2 can vary from annual averages and traffic pollution is usually a mixture of precursor gases, primary particulates, and photochemically formed ozone and aerosols. Nevertheless, when countries went into lockdown, the most noticeable indication of a drop in traffic related pollution is tropNO_2 in urban areas

observed by TROPOMI, lending support to the assumption that NO_2 is a good proxy for traffic related pollution. The COVID-19 lockdown measures disproportionately impacted traffic more than industrial operations.

We analyzed TROPOMI tropNO_2 and Suomi National Polar-orbiting Partnership Visible Infrared Imaging Radiometer Suite (Suomi NPP VIIRS) AOD data in conjunction with on-road NO_x emissions data, NO_x emissions from power plants, and unemployment rates where available. The goal of this study is to examine the trends in on-road and power plant emissions for five different locations (four urban areas and one rural area) to answer the questions: (1) are changes in NO_x emissions during the lockdown detectable in TROPOMI tropNO_2 data, (2) are the economic indicators consistent with emissions changes, and (3) did the trends reverse with the lifting of lockdown measures in the major metro areas. These questions are answered with spatial and temporal analysis of ground-based observations and satellite data, relating indicators of human activity during and prior to COVID-19 lockdown with air quality, and examining if a new normal urban air quality can be achieved with novel policies.

2. Methods

2.1. Sentinel 5P TROPOMI NO2

The TROPOMI NO_2 algorithm is based on the Differential Optical Absorption Spectroscopy technique that involves fitting the spectra in the NO_2 absorption region between 405 nm and 465 nm using known laboratory-measured reference absorption spectra. The Sentinel 5P flies in formation with SNPP. Though some Sentinel 5P trace gas algorithm retrievals depend on the VIIRS cloud mask, the NO_2 algorithm relies on cloud retrievals using its oxygen A-band absorption (van Geffen et al., 2019). The cloud fraction and effective pressure

142 are used in air mass factor calculation for partially cloudy pixels. There is an indication that the
143 cloud algorithm is likely conservatively masking out good NO_2 retrievals according to a
144 validation study conducted by Judd et al. (2020). Though Judd et al (2020) used data with
145 quality flag equals to unity, we used the quality flag value (0.75) recommended by the NO_2
146 algorithm theoretical basis document (van Geffen et al., 2019). Only data with quality flag >
147 0.75 were used as this quality flag setting ensures that cloudy retrievals or retrievals with
148 snow/ice covered pixels are screened out. The TROPOMI Level 2 product file consists of pixel
149 level (3.5 km x 5.6 km) NO_2 tropospheric column amount which we used in this study. The NO_2
150 algorithm retrieves total column NO_2 and separates the stratosphere from troposphere using
151 chemical transport model predicted stratospheric NO_2 analysis fields (van Geffen et al., 2019).
152 The expected accuracy of the tropospheric NO_2 column for polluted regions with high NO_2
153 values is ~25% and independent validation efforts using ground-based spectrometers such as
154 Pandora have confirmed that tropNO_2 is generally under-estimated, especially in polluted regions
155 and that significant sources of errors come from coarser resolution a priori profiles used in the
156 retrieval algorithm (Chan et al., 2020). Comparisons of TROPOMI tropNO_2 column with
157 Pandora ground station retrievals of tropospheric NO_2 in Helsinki showed that mean relative
158 difference is $-28.2\% \pm 4.8\%$ (Ialongo et al., 2020). Similar comparisons between Pandora
159 ground station retrievals and tropNO_2 in Canada for urban (Toronto) and rural (Egbert) stations
160 show that tropNO_2 has a -23% to -25% bias for polluted regions and a 7% to 11% high bias in
161 rural region (Zhao et al., 2020). Sources of error in tropNO_2 include altitude dependent air mass
162 factors, stratosphere-troposphere separation of NO_2, a priori NO_2 profile and shape, surface
163 albedo climatology, and calibration errors as a function of view angle (van Geffen et al., 2019;
164 Judd et al., 2020; Ialongo et al., 20; Zhao et al., 2020; Chan et al., 2020). Judd et al. (2020)

showed that the TROPOMI NO_2 validation carried out during the Long Island Sound Tropospheric Ozone Study (LISTOS) experiment showed that the TROPOMI tropNO_2 column retrievals have a bias of -33% and -19% versus Pandora and airborne spectrometer retrievals respectively. The biases improve to -19% and -7% when the TROPOMI NO_2 algorithm is run with a priori profiles from a regional air quality model indicating that retrievals are very sensitive to a priori profile. One aspect that is not fully explored by Judd et al. (2020) is the influence of aerosols on air mass factor calculations. Research on aerosol impact on air mass factors indicates that the effect of aerosols on NO_2 retrieval can vary depending on aerosol type (absorbing or scattering), amount, and vertical location (is aerosol mixed in with NO_2 in the boundary layer or is the layer detached from NO_2 layer) in the atmospheric column (Tack et al., 2019; Judd et al., 2019; Liu et al., 2020; Lin et al., 2014).

The Level 2 TROPOMI NO_2 data were downloaded from the European Space Agency datahub (https://s5phub.copernicus.eu/dhus/#/home).

The data for January to February 2020 is considered Business as Usual (BAU), the data for 15 March to 30 April 2020 is considered the lockdown period, and the data for 1 May to November 2020 is considered as representing the post lockdown period.

The TROPOMI data are available only from mid-2018 to the present. We removed the seasonality in tropNO_2 data in two simple ways: by simply taking the difference between 2019 and 2020 for the same month so the sun-satellite geometries and weather conditions are similar barring any unusual inter-annual variabilities, and by doing double differencing as described in section 3.1.

2.2. On-road NOx Emissions

188 The on-road emissions are obtained using the Fuel-based Inventory of Vehicle Emissions
189 (FIVE) where vehicular activity is estimated using taxable fuel sales for gasoline and diesel fuel
190 reported at a state-level and downscaled to the urban scale using light- and heavy-duty vehicle
191 traffic count data (McDonald et al., 2014). Once the fuel use is mapped, NO_x emissions are
192 estimated using fuel-based emission factors (in g/kg fuel) based on roadside measurements or
193 tunnel studies (Hassler et al., 2016; McDonald et al., 2012; McDonald et al., 2018). The emission
194 factors are calculated separately for light-duty gasoline vehicles and heavy-duty diesel trucks.
195 The FIVE methodology was developed to derive traffic emissions to study their impact on air
196 quality (Kim et al., 2016; McDonald et al., 2018), but in the case of 2020, the fuel-based
197 methods provide evidence for quantifying the impact of reduced human activity during the
198 lockdown period on air pollutant emissions (e.g., NO_x).

199 Here, we downscale on-road gasoline and diesel fuel sales following McDonald et al. (2014)
200 for our 2019 base year, which is treated as the BAU case. We have chosen to focus on four US
201 urban areas where real-time traffic counting data are publicly available, including the South
202 Coast air basin (Los Angeles county, Orange county, and portions of Riverside and San
203 Bernardino counties), San Francisco Bay Area (Marin, Sonoma, Napa, Solano, Contra Costa,
204 Alameda, Santa Clara, San Mateo, and San Francisco counties), New York City (Richmond,
205 New York, Kings, Queens, and Bronx counties), and the Atlanta metropolitan region (Cherokee,
206 Clayton, Cobb, Coweta, Dekalb, Douglas, Forsyth, Fulton, Gwinnett, Henry, Rockdale, and
207 Spalding counties). We also include one rural region for contrast, the San Joaquin Valley in
208 California (Fresno, Kern, Kings, Madera, Merced, San Joaquin, Stanislaus, and Tulare counties).
209 For the BAU case, we account for typical seasonal and day-of-week activity patterns of light-
210 and heavy-duty vehicles separately). For the COVID-19 case, we scale the January BAU

emissions case with real-time light- and heavy-duty vehicle traffic counting data for the year 2020, which are described in Harkins et al. (2020). Light-duty vehicle counts are used to project on-road gasoline emissions and heavy-duty truck counts for on-road diesel emissions during the pandemic.

To estimate NO_x emissions, the FIVE NO_x emission factors have been updated to 2019 based on the regression analyses of roadway studies (Hassler et al., 2016; McDonald et al., 2012; McDonald et al., 2018), and we use a value of running exhaust emission factors of 1.7 ± 2 g NO_x/kg fuel and 12.4 ± 1.9 g NO_x/kg fuel for on-road gasoline and diesel engines, respectively. Cold-start emissions are scaled relative to the running exhaust emissions based on the US Environmental Protection Agency (EPA) MOVES2014 model (EPA, 2015). We use the 2019 NO_x emission factor for both the BAU and COVID-19 adjusted cases. Thus, the differences in the BAU and COVID-19 cases are only due to changes in traffic activity. We use the same emission factor for 2019 and 2020 because past studies have shown during the 2008 Great Recession the turnover of the vehicle fleet and corresponding reductions in emission factors are slower (Bishop and Steadman, 2014). Total on-road NO_x emissions are the sum of emission estimates for light-duty vehicles and heavy-duty trucks. The off-road mobile source emissions are not included in the dataset. In cities, on-road transportation accounts for as much as 75% of the NO_x emissions (Kim et al., 2016), and is a critical emissions sector to quantify.

Uncertainties in FIVE on-road emission estimates arise from non-taxable fuel sales associated with off-road machinery, and from mismatches where fuel is sold and where driving occurs, though diesel fuel sales reports are adjusted based on where long-haul trucking occurs (McDonald et al., 2014). However, the main source of uncertainty is the accuracy of fuel-based emissions factors used to calculate co-emitted air pollutant species (McDonald et al., 2018). The

underlying traffic counting data are available at hourly time resolution; however, here we have averaged the data to daily averages. Jiang et al. (2018) report the uncertainty in fuel sales (3%-5%) and NOx emission factors (15%-17%) for on-road transportation.

2.3. Power Plant NO_x Emissions

The daily power plant NO_x emissions were obtained from the US EPA Continuous Emissions Monitoring System (https://www.epa.gov/airmarkets) and the energy generation/consumption statistics were obtained from the Energy Information Administration (eia.gov). Unlike the traffic emissions, power plant emissions did not change much during the lockdown. Power generation from fossil fuels dropped from 38,332 Gwh in March to 29,872 Gwh in April and rebounded to pre-pandemic levels by June. The total NO_x emissions in the US from power plants dropped from 54,531 tons in March to 44,016 tons in April, a 19% decrease. This may seem like a big drop in production but the absolute values are quite small. For example, NO_x emissions from power plants within the 75 km of Los Angeles emitted only 20 tons in March 2020. For January to July, nationally, total NOx emissions from power plants were 0.8 and 0.67 million metric tons in 2019 and 2020 respectively. This is a 16% reduction compared to 50% reduction in on-road emissions, for the same months between 2019 and 2020.

In contrast, on-road emissions from vehicles in the Los Angeles area alone emitted nearly 5,367 tons of NO_x. Power plant NO_x emissions in the US have decreased substantially over the last two decades; they dropped by 86% between 1990 and 2019. This is due to the shift from fossil fuels to other alternate energy sources for power generation. For example, the use of coal as a source of electricity generation went down from 51% in 2001 to 23% in 2019 while the natural gas as a source increased from 17% in 2001 to 38% in 2019. In our analysis, comparing and contrasting NO_x emissions from on-road traffic and power plants for the six locations of

interest, we considered only the power plants within 75 km radius of the center of the city location being analyzed.

2.4. Suomi National Polar-orbiting Partnership Visible Infrared Imaging Radiometer Suite (SNPP VIIRS)

NOAA currently has two VIIRS instruments in orbit - one on SNPP launched on 28 October, 2011 and one on NOAA-20 launched on 18 November, 2017. The two VIIRS instruments continuously observe the Earth with a 50-minute time difference and provide AOD retrievals for cloud/snow-free scenes during the sunlit portion of the day. The VIIRS instruments have 22 bands with 16 of the bands in the visible to long-wave infrared at moderate resolution (750m), five bands at imager resolution (375m) covering 0.64µm, 0.865µm, 1.6µm. 3.74µm, and 11.45µm, and one broad Day-Night-Band (DNB) band centered at 0.7µm. The NOAA AOD algorithm over ocean is based on the Moderate Imaging Spectroradiometer (MODIS) heritage and for over land, the algorithm derives AOD for both dark targets as well as bright surfaces (Levy et al., 2007; Laszlo and Liu, 2016; Zhang et al., 2016; Huang et al., 2016). For this study, we used the SNPP VIIRS AOD because SNPP flies in formation with S5P TROPOMI with a local equator crossing time of 1:30 PM and less than three minutes difference in overpass time. The SNPP VIIRS AOD product has been extensively validated by comparing it to Aerosol Robotic Network (AERONET) AODs and the VIIRS 550nm AOD is shown to have a global bias of -0.046±0.097 for AODs over land less than 0.1 and for AODs between 0.1 and 0.8, the bias is -0.194±0.322. In the US., for VIIRS AODs ranging between 0.1 and 0.8, the bias is -0.008±0.089 and for AODs greater than 0.8, the bias is about 0.068±0.552 (Zhang and Kondragunta, 2021). For the analysis of AOD data in this study, we remapped the high quality (Quality Flag equals 0) 750m resolution AOD retrievals to 0.05 ^{o} x 0.05^{o} resolution with a

criterion that for a grid to have a mean AOD value, there should be a minimum of 20% 750m pixels with high quality AODs.

2.5. Unemployment Rate

The civilian labor force and unemployment estimates for metropolitan areas were obtained through the Local Area Unemployment Statistics (LAUS) provided by the Bureau of Labor Statistics (bls.gov). The LAUS program is a federal-state cooperative effort in which monthly estimates of total employment and unemployment are prepared for over 7,500 areas including metropolitan areas. The seasonal adjustments are carried out by the Current Employment Statistics State and Area program (CES) using the statistical technique Signal Extraction in Auto Regressive Integrated Moving Average Time Series (SEATS). These datasets are smoothed using a Reproducing Kernel Hilbert Space (RKHS) filter after seasonal adjustment. The details of the data collection, processing and release can be found at https://www.bls.gov/lau/laumthd.htm. The data for January to November 2020 are used in this study. To compare the NO_2 variation in metropolitan areas, the TROPOMI tropNO_2 column amounts were averaged inside each metropolitan area. The 1:500,000 polygon shape files were used to test if a TROPOMI pixel is inside or outside a metropolitan area. The shape files are from United States Census Bureau (https://www.census.gov/geographies/mapping-files/time-series/geo/cartographic-boundary.html).

2.6. Matchup Criteria

The NO_2 data were matched to the on-road mobile emissions data for statistical and trend analysis with certain criteria. Prior to generating the matchups, rotated wind analysis was carried out on the original pixel level data. It is important to do this when sampling the satellite data

because NO_2 concentrations accumulate in the cities when wind speed is low and disperse away from the city when wind speed is high. The satellite data are observed once a day in the mid-afternoon whereas on-road mobile emissions represent daily values. To have representative sampling, it is common to rotate the satellite pixel-level data in the direction of the wind (Fioletov et al., 2015; Lorente et al., 2019; Goldberg et al., 2019; Zhao et al., 2020). We used the European Center for Medium range Weather Forecast (ECMWF) Re-Analysis (ERA5) 30-km resolution global wind fields (Hersbach et al., 2020). To do the wind rotation, each TROPOMI pixel was collocated to ERA5 with tri-linear interpolation method in both temporal and horizontal directions. The wind profiles were merged to the location of the TROPOMI pixel center. The east-west (U) and north-south (V) wind speed components were averaged through the vertical distribution within the bottom 100 hPa, approximated to be within the boundary layer. Then, each TROPOMI pixel was rotated and aligned with the average wind direction from the city center. The rotated pixels are gridded with 5 km x 5 km resolution to generate monthly mean values for correlation analysis with on-road NOx emissions.

Once the pixels are rotated, they are sampled for 100 km in the downwind direction, 50 km in the upwind direction, and the cross-wind direction. This way, the elevated concentrations of NO_2 moving away from the city in the downwind direction are captured. Figure 1a shows an example of the TROPOMI NO_2 tropospheric column amount with Los Angeles as the focus. The NO_2 data shown are monthly mean values for January 2020 remapped to a fixed grid. The black rectangle shows the area of interest over Los Angeles that we want to compare with on-road emissions. The ERA5 wind vectors are plotted on the NO_2 map to show wind direction. To do the wind rotation, daily NO_2 pixel level data are first remapped to a 5 km x 5 km fixed grid resolution. The grids are then rotated to align with the wind direction with downwind direction

pointing North (Figure 1b). The daily rotated grid values of NO_2 in 5 km x 5 km are averaged over a month to generate a monthly mean. The monthly mean values can vary quite a bit depending on missing data due to screening for the high quality data as well as cloud cover. In a given month, the number of pixels with valid retrievals for a particular city can vary from 2% to 100% depending on cloud and snow cover; the mean values vary depending on the location of the missing values, if they are in the center of the city where NO_2 is usually high or on the edges of the city where NO_2 values can be low depending on wind speed and direction. In our analysis for this study, prior to computing the monthly mean, the criterion we employed is that on a given day, there should be a minimum of 25% of pixels in a region selected for matchups of satellite data should have valid retrievals. The 25% threshold is a reasonable compromise because any value higher than that will reduce the sample size (number of days included in the monthly mean).

3. Results

3.1. Deseasonalizing tropNO_2 data

As already shown by many research studies, the global tropNO_2 column amounts dropped in coincidence with partial or complete lockdowns during the height of the COVID-19 pandemic in different parts of the world and in the US. In order to remove the seasonality from the signal, researchers in these studies have adopted different approaches including the use of numerical models to simulate the seasonality (e.g., Goldberg et al., 2020; Silver et al., 2020; Liu et al., 2020). Seasonality should be accounted for because in the northern hemisphere winter months, NO_2 amounts are higher than in summer months; as a result, during the transition from winter to summer, NO_2 amounts are higher in February than in March. In our study, we used a double differencing technique to account for seasonality. Consistent with Goldberg et al. (2020), we

used 1 January to 29 February 2020 as pre-lockdown period and 15 March to 30 April as the lockdown period. The difference in mean tropNO$_2$ between lockdown and pre-lockdown is referred to as 2020ΔNO$_2$. For the same two corresponding periods in 2019, the difference in mean tropNO2 is referred to as 2019ΔNO$_2$. Then, the difference of 2019ΔNO$_2$ and 2020ΔNO$_2$ was computed to tease out the changes in NO$_2$ due to reductions in emissions during the lockdown (ΔtropNO$_2$). It should be noted though that the double differencing only removes the seasonality and does not fully account for differences in meteorological events such as precipitation or anomalously cold or hot conditions in one year versus the other but on a monthly time scale they are minimized.

Figure 2a-b shows 2019ΔNO$_2$ and 2020ΔNO$_2$ which includes changes due to seasonality and any changes due to emissions either from natural sources such as fires or from anthropogenic urban/industrial sources. Figure 2c shows ΔtropNO$_2$ for the CONUS due to just changes in emissions between the pre-lockdown and lockdown periods in 2020 with the seasonality removed. Comparing Figure 2a and 2b, one can deduce that reductions in tropNO$_2$ between pre-lockdown and lockdown are much stronger in 2020 compared to 2019. However, the double difference plot in Figure 2c shows how much of that reduction seen in 2020ΔNO$_2$ (Figure 2b) is due to changes in emissions. The tropNO$_2$ changes are smaller in Figure 2c than in Figure 2b, both in magnitude as well as spatial extent of the reductions.

The lockdown measures in most states in the US began in the middle of March 2020. The first state to institute stay-at-home measures was California on 19 March and the last state was Missouri on 6 April. The cities/regions with worse traffic related ozone pollution levels based on the monitoring data from 2016-2018 compiled by the American Lung Association and the duration for which they were in a lockdown are shown in Table 1. For regions that fall into

different states (e.g., Washington-Baltimore-Arlington), the dates for the state that had the longest duration of lockdown are listed in the table. Most states were in a lockdown mode only for one to two months and given the varying nature of the lockdown in different parts of the country, we treated 15 March and 30 April as lockdown months. As shown in Figure 2a, 2019ΔNO_2 is positive in some areas and negative in some areas whereas in 2020 (Figure 2b), large negative values (reductions) are observed in most of the CONUS except in the Great Plains region and the Pacific North West. These reduced tropNO_2 amounts are attributed to reduced emissions due to lockdowns. Changes in the rural areas (either positive or negative) of the US could be due to changes to natural sources such as soil and lightning NO_x emissions or due to meteorological differences that the double differencing technique did not account for.

Fei Liu et al. (2021) used NASA global photochemical model simulations to study how long the tropNO_2 data need to be averaged to minimize the influence of meteorological variability. They simulated January 2019 to December 2020 by keeping the NOx emissions the same between the two years. and found that averaging the data over 31 days for the US leads to differences in tropNO_2 between 2019 and 2020 less than 10%. Our double differencing was done with tropNO_2 data averaged over 1.5 months which should substantially minimize the differences in meteorology.

To confirm our results, we also repeated the analysis for a longer period and found that our conclusions did not change. Setting the pre-lockdown period as 1 January to 15 March and the lockdown period as 16 March to 30 May, and we found that tropNO_2 decreases are consistent with those shown in Figure 2a-c (Figure S1a-c). We also applied scaling factors to account for seasonality and meteorological variability developed by Goldberg et al. (GRL, 2020). These scaling factors normalize tropNO_2 data to conditions of a typical week day based on TROPOMI

398 tropNO$_2$ data from 2018-2019, based on sun angle, wind speed, wind-direction, and day-of-
399 week. Figure S2 shows this analysis using the normalized tropNO2 to investigate NOx trends; it
400 shows reductions in tropNO2 for different cities during the lockdown period that are consistent
401 with the double differencing analysis.

402 ### 3.2. On-road NO$_x$ emissions and tropNO$_2$
403

404 Focusing on the regions of interest with on-road NOx emissions available for this study, we
405 calculated reductions in tropNO$_2$ for Los Angeles, Atlanta, San Francisco, San Joaquin Valley,
406 and New York City. As shown in Table 2, the largest reductions in tropNO$_2$ were observed for
407 New York City (-28%) and the smallest reductions were observed for San Joaquin Valley (-
408 17%). The largest reductions in NOx emissions were also for New York City but the smallest
409 reductions were Atlanta followed by San Joaquin Valley. The 22% reductions in tropNO2
410 observed for Los Angeles is due to nearly 50% reductions in on-road NOx emissions. Without
411 accounting for the seasonality/meteorological differences between 2020 and 2019, the tropNO2
412 reductions are 60%. This elucidates the need to account for differences in seasonality and
413 meteorology when analyzing the data for trends.

414 Goldberg et al (2020) reported tropNO$_2$ reductions of 20.2%, 18%, and 39% for Atlanta,
415 New York, and Los Angeles respectively and their analysis is also for a lockdown period
416 spanning 15 March to 30 April, 2020 . Our analysis shows that tropNO$_2$ reductions for these
417 three cities are 21%, 17%, and 22%. Though the methodology used to remove the seasonality is
418 different, the reductions in tropNO$_2$ from our analysis and that of Goldberg et al. (2020) are
419 similar, with Los Angeles showing the biggest drop in tropNO$_2$ due to lockdown measures.

420

Figure 3 shows the time series of on-road mobile (cars and trucks combined) and power plant NO_x emissions for the five different cities/regions in the US from January to November 2020; the exception is New York City for which the time series ends on 31 August due to the non-availability of traffic data. For Los Angeles, daily NO_x emissions are near 200 tons/day prior to lockdown with values slightly lower on weekends (~150 tons/day). The Los Angeles basin is home to 17 million people with 11.3 million cars; cars, trucks, and other off-road machinery contributing to 80% of the observed NO_x in a typical year according to the 2019 emissions report by South Coast Air Quality Management District (http://www.aqmd.gov/docs/default-source/annual-reports/2019-annual-report.pdf?sfvrsn=9). Due to the lockdown and stay at home orders, people stopped driving and NO_x emissions quickly began dropping on 19 March 2020; the NOx emissions begin to increase on 16 April 2020, even before the lockdown was lifted on 4 May. The lowest weekday NO_x emissions, 141.3 tons/day, occurred on 6 April. Even though the NOx emissions began to recover in the post lockdown period, they were still lower than the pre-lockdown values. Compared to on-road emissions, power plant emissions are negligible for the Los Angeles area. Power plants in the vicinity of Los Angeles (~75 km radius) emit only ~0.8 tons per day on average compared to 200 tons per day emitted by on-road vehicles during the pre-lockdown period on weekdays. On weekends, on-road emissions are lower (~150 to 175 tons/per day depending on whether it is a Saturday or Sunday) due to lower truck traffic (Marr and Harley, 2002), whereas power plant emissions do not have any weekday/weekend differences.

The NO_x emissions for the New York area encompass an area covering about 1,213 square kilometers. The city is home to 8.34 million people but there are only 1.9 million vehicles (230 cars per 1000 people) because of the reliance on public transportation, a factor of three lower

444 than for Los Angeles, which has 660 cars per 1000 people. Similar to Los Angeles, the NO_x
445 emissions dropped in New York on 21 March when lockdown measures began. The pre-
446 lockdown levels of NOx emissions are on average ~125 tons/day. It should be noted that New
447 York City is in the downwind region of NOx emissions from New Jersey and Pennsylvania and
448 it is the recipient of regionally transported pollution (Tong et al., 2008). Unlike in the Los
449 Angeles metro area, the power plant emissions are higher but showed no trend similar to on-road
450 emissions. It is noteworthy that there was a jump in power plant emissions towards the end of
451 June which coincided with the opening of retail establishments on 22 June; the power plant
452 emissions in the New York City are higher in the summer than in winter, associated with
453 increased demand for air conditioning.

454 The NO_x emissions for the metro Atlanta area are similar to New York City but with a weak
455 weekday/weekend cycle. The Atlanta region encompassing Cherokee, Clayton, Cobb, Coweta,
456 Dekalb, Douglas, Forsyth, Fulton, Gwinett, Henry, Rockdale, and Spalding counties is about
457 3,695 square kilometers and is home to nearly five million people. The pre-lockdown levels of
458 NOx emissions were on average ~125 tons/day. The metro Atlanta region is three times larger
459 than the area of New York City but the NOx emissions are similar in magnitude. The state of
460 Georgia where Atlanta is located never went into a prolonged lockdown. Though the mayor of
461 Atlanta ordered people not to gather in large groups beginning 15 March and the Governor of
462 Georgia ordered bars and clubs to close on 24 March, schools were not closed until 1 April;
463 shelter in place was implemented on 8 April but was lifted immediately with no real lockdown
464 until 1 May-23 May. Consistent with these policies, the on-road NO_x emissions were lowest on
465 23 March (88.5 tons/day) and 26 May (74.5 tons/day) and returned to pre-lockdown levels at the
466 start of 1 June. The lowest on-road NOx emission value, 74.5 tons, was observed on 26 May,

467 towards the end of the shelter in place orders. By 1 June, NO_x emissions values returned to pre-
468 lockdown levels in Atlanta.

469 For the pre-lockdown period, the weekday/weekend difference in NO_x emissions is larger in
470 New York City than in Los Angles and Atlanta areas, due to commuter travel. The mean
471 difference in NO_x emissions between weekdays and Sundays (emissions are the lowest on
472 Sundays of each week) prior to the lockdown in the Los Angeles, New York, and Atlanta are
473 54.4 tons/day (26%), 65.4 tons/day (51%), and 41.1 tons/day (33%) respectively.

474 The San Joaquin valley is a 60,000 km^2 area that includes the population centers of
475 Bakersfield and Fresno as well as major freeway corridors, including I-5 and CA-99. Due to the
476 large geographic size of the San Joaquin Valley, the emissions magnitude is comparable to urban
477 centers. The San Joaquin Valley NO_x emissions remained consistent at ~55 tons/day throughout
478 the year with a very weak weekday/weekend cycle. Similar to Los Angeles, power plant
479 emissions are insignificant.

480 For the San Francisco Bay area, the on-road NO_x emissions are higher than the San Joaquin
481 Valley region but lower than in Los Angeles. The daily average NO_x emissions prior to the
482 lockdown were ~90 tons/day and there was a small drop in emissions (-33.2 tons/day) on 6 April
483 with a trend to return to normal by mid-April. The post lockdown NOx emissions were lower
484 than pre-lockdown values for San Francisco as well.

485 ### 3.3. Correlation between on-road NO_x emissions and tropNO_2
486

487 Given the knowledge of changes in on-road emissions in the five cities due to lockdown, we
488 wanted to examine if tropNO_2 shows similar behavior by exhibiting a linear relationship, and if
489 so demonstrate that the period for which the lowest NO_x emissions were observed in traffic data

also corresponds to the lowest observed tropNO$_2$ data. Additionally, we wanted to check if the post lockdown recovery in traffic emissions is reflected in tropNO$_2$ data. We first examined the direct relationship between daily tropNO$_2$ and daily on-road NO$_x$ emissions for the five locations; but only the analysis for Los Angeles is shown in Figure 4 for illustration purpose; data from other cities showed similar behavior. The tropNO$_2$ and NO$_x$ emissions for January and February 2020, representing the BAU, and for March through November 2020 are shown in Figure 4a and Figure 4b respectively. The coincident observations of tropNO$_2$ amount sampled in the predominant wind direction are linearly correlated with on-road NOx emissions but the correlation is weak (r=0.39). The traffic emissions fall into three clusters corresponding to emissions on Sundays (~150 tons/day), Saturdays (~180 tons/day), and weekdays (~199 tons/day) with minimal variability in each cluster whereas tropNO$_2$ amount varies between 50 and 225 μmoles/m^2.

The variability in tropNO$_2$ can be attributed due to different reasons. First, the day to day variability in cloud cover can lead to gaps in data. We used the recommended quality flag threshold of 0.75 to screen out the data that has potential contamination from clouds but this strict screening reduces the number of retrievals for a given location. Second, there is also variability in the background NO$_2$ contribution to the tropospheric NO$_2$ column due to which column NO$_2$ does not correlate well with NO$_x$ emissions from sources on the ground. We analyzed the background NO$_2$ signal in the tropospheric column amount for TROPOMI for 2019 and 2020 using Silvern et al. (2019) method and found it to be higher due to the longer winter-time lifetime (lower temperature, weak photolysis, stronger wind dispersion, and less wet scavenging) and lower in the summer with monthly mean values ranging between 15 and 20 μmoles/m^2 (Figure S3). Sources of background NO$_2$ are soil emissions of NO$_x$ which are

amplified after precipitation events, lightning produced NO_x, and chemical decomposition of peroxyacetyl and alkyl nitrates. Transport of NO_2 from rural areas can also enhance tropNO_2 values that may not correlate well with NO_x emissions from sources on the ground. Third, wind speed and direction influence the mean tropospheric NO_2 computed for the Los Angeles basin because if the wind speed is high, NO_2 is dispersed and transported away from the city and if wind speed is low, NO_2 is accumulates in the city. Any variability associated with background NO_2 is detected by TROPOMI and accounted for in the column NO_2 amount, but this has no relation to the NO_x emissions from on-road sources on the ground. We did account for the effects of wind in our matchups by sampling the data in the downwind direction but higher wind speeds dilute the NO_2 concentrations observed by TROPOMI (Figure S4). Outlier values of tropNO_2 values are between 20 and 30 μmoles/m^2 even when on-road emissions are high indicating TROPOMI retrievals that are either sampled after pollutants are washed out of the atmosphere due to rain or on days when wind speeds are unusually high. Retrievals can also be noisy and have errors associated with air mass factors and a priori profiles. Parker et al. (2020) report that the Los Angeles basin was unusually wet in 2020, especially during the late March and early April 2020. Other researchers who correlated daily surface observations of NO_2 and TROPOMI tropNO_2 for 35 different stations in Europe reported similar findings and they found that correlation improved after averaging the data to monthly time scales (Ialongo et al., 2020; Cersosimo et al., 2020; Goldberg et al., 2020).

The comparison for the lockdown and post lockdown period of March through November is shown in Figure 4b; the correlation remains the same ($r = 0.39$) but the one interesting feature is that the tropNO_2 and on-road emissions are very small during the lockdown compared to the pre-lockdown. Daily NOx emissions on many days are between 100 and 150 tons after 14 March;

prior to that, the region was not under stay-at-home orders. The $tropNO_2$ never goes above 200 μmoles/m^2 for this period. Compared to the pre-lockdown period, the on-road NO_x emissions and $tropNO_2$ values shifted to lower values within each cluster (shown in blue for weekdays, green for Saturdays, and red for Sundays). During the lockdown, one would anticipate that there would not be any difference between weekday and weekend emissions but the difference is stark and is reflected in $tropNO_2$ data as well.

In order to correlate the changes in on-road NOx emissions with changes in $tropNO_2$ between 2019 and 2020 for each of the five regions in this study, we averaged daily NOx emissions values and $tropNO_2$ values for each month (January to November) and created an average value of all the five regions combined for each month. Figure 5a shows the monthly mean trend plot ΔNO_x and $\Delta tropNO_2$ for January to November; on-road emissions and tropNO2 dropped steadily and hit the lowest values in March and April, consistent with the lockdown measures. The recovery began in May and continued to November for on-road emissions but did not completely recover to the pre-lockdown levels. However, the $\Delta tropNO_2$ trend plot shows recovery up to August and then begins to show a decline from September to November. This decline in $tropNO_2$ is attributed to Los Angeles and San Francisco. Figure 5b shows the correlation of on-road NOx emissions changes (ΔNO_x) between 2020 and 2019 with the difference in $tropNO_2$ amounts between 2020 and 2019 (ΔtropNO2). The NO_x emissions were lower in 2020 compared to 2019 for all the months and all the cities. The positive linear correlation ($r = 0.68$) suggests that TROPOMI $tropNO_2$ observations captured the changes in on-road emissions and can be used to study the changes in NOx emissions due to traffic elsewhere in the US where there are no observations from the ground.

Even though traffic emissions are the dominant source for NOx, there are power plants in the vicinity of the cities emitting NOx continuously and unlike traffic emissions they do not exhibit a weekday/weekend cycle. Figure 6 shows a map of tropNO$_2$ for the second quarter in 2020 (April/May/June) with on-road emissions and power plant emission for each of the five analysis cities as stacks. The locations of power plants in other parts of the country are circled in pink, indicating that these power plants emit greater than 1500 tons in a given quarter; power plants with lower monthly NOx emissions (< 1500) tons are not shown on the map. It is difficult to isolate the NO$_2$ plumes from power plants in urban areas in the TROPOMI tropNO$_2$ map as the NO$_x$ emitted from the power plants mixes and becomes indistinguishable from on-road emissions. Consistent with this analysis, changes in NO$_x$ emissions between 2020 and 2019 for power plants within 75 km of each of the five analysis cities correlated weakly with changes in tropNO$_2$ (Pearson correlation coefficient = 0.35); power plant NO$_x$ emissions can explain only 12% of the variability seen in tropNO$_2$ (Figure 7). Also as can be seen in Figure 7, the daily average changes in power plant emissions between 2020 and 2019 were positive for some plants and negative for some but mostly varied between ±20 tons/day.

3.4. Correlation between tropNO$_2$ and AOD

The premise for the impact of NO$_x$ emissions reductions on improved air quality due to reduced human activity during the lockdown period depends on how the photochemical processes changed compared to the BAU scenario. The photochemical production of ozone and surface PM$_{2.5}$ (particulate mass of particles smaller than 2.5 μm in median diameter) depends not only on NOx emissions but also on VOCs and their ratio (Baider et al., 2015; Parker et al., 2020: McDonald et al., 2018; Qin et al., 2021). Most analysis of the impact of COVID-19 lockdowns

582 on air quality using satellite data have focused on TROPOMI NO_2 and attributed the reductions
583 of NO_x emissions to improved air quality; the reductions in VOC emissions are largely unknown,
584 especially from non-vehicular sources. Atmospheric formation of nitrate and organic aerosols is
585 driven by NO_x, VOCs, and ammonia emissions and if the photochemical processes are in a NO_x
586 limited or VOC limited regime. To analyze the AOD data for indications of reduced aerosol
587 formation due to reduced NOx emissions, one complicated factor is the transport of smoke
588 aerosols from upwind regions and how the transported signal can be removed from the AOD
589 data. To address this issue, we tested the hypothesis that the AOD/NO_2 ratio is small when
590 pollution sources are local and high when non-local sources bring transported aerosols into the
591 domain. We calculated the weekly correlation between AOD and NO_2 and obtained the slope for
592 each week over one year in 2019 and 2020, to document the changes in slope as a function of
593 time during the year (Figure 8a-c); In Figure 8a-b, we show an example of how slopes are
594 derived using the scatter plot between VIIRS AOD and TROPOMI tropNO2 for one week in
595 September 2019 and in 2020. For 2019, when the fire season was not a major contributing factor
596 to aerosol concentrations, the slopes are small in the winter months and slowly increase towards
597 the summer (Figure 8c). This is consistent with the knowledge that ammonium nitrate formation
598 peaks in the summer due to the availability of ammonia from increased agricultural activity and
599 higher volatility associated with higher temperatures (Schiferl et al., 2014).

600 The weekly scatter plots of AOD and tropNO_2 for September 2019 and 2020 in Figure 8a-b show
601 that the tropNO_2 values in both years ranged between 30 and 120 μmoles/m^2 whereas AOD
602 values in 2020 were much higher (between 0.2 and 0.9) compared to values in 2019 (between 0.1
603 and 0.2). The AOD values in the US typically range between 0 and 1, with higher AODs
604 typically observed in the presence of biomass burning smoke or dust storms. Given this

knowledge that slopes are higher when transported aerosol is involved, we were able to filter the AOD data. The filtered data will be used in a future study to analyze trends in AOD due to NOx emissions reductions.

3.5. Correlation of tropNO2 and Unemployment Rate

Because of the lockdown measures and work from home policies for majority of the workplaces in the US, the service industry has suffered and the unemployment rate has risen. The US unemployment rate increased from about 4.4% in March to 14.7% in April during the first phase of lockdowns. The unemployment rate nationwide improved as the progressed but certain parts of the country continued to experience a very high unemployment rate throughout 2020 (Figure 9). Amongst the employed, 28% of employees continued to work from home as of November indicating that below normal NO_x emissions data are to be expected. The correlation between unemployment rate and tropNO_2 for metropolitan areas with a pre-pandemic civilian labor force greater than two million is negative for the second and third quarters (the regression line shown in Figure 9 is for second quarter data). The unemployment rate combined with telework policies have contributed to reduced NO_x emissions and thus lower tropNO_2 values across the US. This is similar to the positive correlation between Gross Domestic Product (GDP) and tropNO_2 reported by Keller et al. (2020). For reasons un-known, cities such as Phoenix, AZ, Minneapolis, MN, Dallas and Houston, TX, and Chicago, IL showed no change or a slight increase in tropNO_2 in 2020 compared to 2019 though unemployment rate in 2020 was much higher compared to 2019. Keller et al. (2020) do not report these outliers because their analysis is for all developing countries around the world and is not granular at the city level like our analysis.

4. Discussion

The TROPOMI tropNO$_2$ data captures the day to day variability in tropospheric NO$_2$ concentrations but due to cloud cover and uncertainties associated with assumptions such as a priori profile and lower sensitivity to near surface NO$_2$, on certain days the tropNO$_2$ retrievals do not adequately represent the changes in near surface NO$_2$ (Ialongo et al., 2020; Cersosimo et al., 2020; Goldberg et al., 2020). The tropospheric NO$_2$ variability is very well captured, however, on monthly scales and even on weekly scales, to the extent that weekday/weekend cycles are noticeable. When using the TROPOMI tropNO$_2$ data, we wanted to establish that it not only shows the reductions/drop in tropNO$_2$ due to reductions in on-road NOx emissions but that the trend during the post-lockdown recovery phase can be detected as well.

The spatial and temporal analysis, relating indicators of human activity during and prior to the COVID-19 lockdown to air quality conditions, shows that while power plant emissions changes were not drastic compared to on-road emissions, the on-road emissions in the five analysis cities dropped coinciding with the start date and the duration of the lockdown. The changes in on-road NOx emissions correlated with tropNO$_2$ changes for these five locations, giving confidence in use of tropNO$_2$ data in other parts of the CONUS, and to draw conclusions about relating changes in tropNO$_2$ to economic activity changes. We found that the weekday-weekend differences were pronounced in on-road emissions and tropNO$_2$ data, and the lowest values of on-road NOx occurred on weekends even during the lockdown periods. The unemployment rate and its increase during the lockdown and post lockdown period appears to also be a good proxy for economic activity and is correlated well with the decrease in tropNO$_2$. At the height of the lockdown in the second quarter of 2020, the unemployment rate increase was

as high as 17% in populated metropolitan areas; even at the end of the third quarter of 2020, the unemployment rate increase was ~10%. The first quarter unemployment rate was constant at ~5% and did not vary; it showed no relationship to tropNO$_2$ as expected because the impacts due to the lockdown did not affect unemployment rate until the second quarter

The satellite data must be analyzed by considering various quality flags and understanding the limitations of the algorithm. It is likely using the quality flag > 0.75 for TROPOMI tropNO$_2$ was conservative, but the extremely low daily tropNO$_2$ values on certain days even when on-road NO$_x$ emissions were high is indicative that the TROPOMI data are more interpretable when averaged to weekly or monthly time scales. For tropNO$_2$ retrievals that have quality flags between 0.5 and 0.75, suggesting cloud contamination, in future work, we will look at the coincident high resolution (750m) VIIRS cloud mask product to analyze TROPOMI flags for cloud contamination. This analysis will help improve our analysis using the daily tropNO$_2$ retrievals by either including more retrievals or removing some retrievals from the matching with on-road emissions data.

5. Conclusions

It has already been established by numerous research studies that reduced traffic (on-road) and industrial emissions led to improved air quality during the COVID-19 lockdown measures implemented by various countries across the globe. However, most studies used mobility data as a proxy for reduced human activity to interpret satellite observations of tropNO$_2$ but did not directly relate the reduced on-road emissions with reduced air quality observations. Here, for the first time we directly correlate on-road NO$_x$ emissions data to TROPOMI tropNO$_2$ in four urban and one rural area in the US. For this, we used TROPOMI tropNO$_2$, VIIRS AOD,

674 on-road NOx emissions, and unemployment rates to develop a comprehensive analysis for 2019
675 and 2020. Where needed, we conducted rotated wind analyses to sample correctly and match the
676 on-road NOx emissions with tropNO$_2$ data. We also developed a novel way of deseasonalizing
677 tropNO$_2$ data, and used changes in unemployment rate data as an indicator for economic activity.

678 Our analysis of reductions in on-road NO$_x$ emissions from light and heavy-duty vehicles
679 derived from fuel sales data showed a reduction from 9% to 19% between February and March
680 2020. When lockdown measures were the most stringent, at the onset of the lockdown period in
681 the middle of March 2020 in most of the US and between March and April 2020, the on-road
682 NO$_x$ emissions dropped further by 8% to 31%. These precipitous drops in NO$_x$ emissions
683 correlated well with tropNO$_2$. Furthermore, the changes in tropNO$_2$ across the continental US
684 between 2020 and 2019 correlated well with changes in the on-road NO$_x$ emissions (Pearson
685 correlation coefficient of 0.68) but correlated weakly with changes in emissions from power
686 plants (Pearson correlation coefficient of 0.35). These findings confirm the known fact that
687 power plants are no longer a major source of NO$_2$ in urban areas of the US. As the US entered
688 into a post-pandemic phase between May and November 2020, the increased mobility resulted in
689 increased NO$_x$ emissions nearly returning to the pre-lockdown phase but not entirely back to
690 100%. Though the lockdown in most of the US ended by May, the on-road NOx emissions did
691 not bounce back to near normal values until August; for Los Angeles and San Francisco, the on-
692 road NOx emissions continued to be 20% below normal even in November. These changes are
693 reflected in the tropNO$_2$ data, with the exception that Los Angeles and San Francisco, where the
694 tropNO$_2$ diverged from on-road NO$_x$ emissions trends, which needs further inquiry. The positive
695 linear correlation between on-road NOx emissions and TROPOMI tropNO$_2$ ($r = 0.68$) suggests
696 that satellite tropospheric column observations of NO$_2$ captured the changes in on-road emissions

and can be used to study changes in NOx emissions due to traffic where ground observations are not available.

The negative correlation between changes in tropNO$_2$ and increased unemployment rate indicates that with the increased unemployment rate combined with telework policies across the US for non-essential workers, the NO$_2$ values decreased at the rate of 0.8 μmoles/m^2 per unit percentage increase in the unemployment rate.

Across the US we found positive spatial correlation between S5P TROPOMI tropNO$_2$ and SNPP VIIRS AOD measurements in urban regions indicating common source sectors for NO$_2$ and aerosols/aerosol precursors. We developed a new mechanism using the changes in AOD-tropNO2 slope to screen for fire events influencing aerosol concentrations in urban/industrial regions that can be used to analyze changes in aerosols due to emissions reductions. The COVID-19 pandemic experience has provided the scientific community an opportunity to identify scenarios that can lead to a new normal urban air quality and assess if the new normal can be sustained with novel policies such as increased telework and a shift towards driving electric cars.

Acknowledgements. This work is part of a NOAA wide COVID-19 project funded by the Joint Polar Satellite System (JPSS) and the office of Oceanic and Atmospheric Research (OAR) to investigate the impact of lockdown on aerosols and trace gases including greenhouse gases. The authors thank Mitch Goldberg (Chief Scientist of NOAA National Environmental Satellite Data and Information Services), Greg Frost (Program Manager, NOAA Climate Program Office), and Satya Kalluri (Science Advisor to the JPSS program) for securing funds for this

720 work. The authors thank the European Space Agency for the provision of the Sentinel 5
721 Precursor Tropospheric Monitoring Instrument data. The authors also thank members of NOAA
722 NESDIS JPSS aerosol calibration and validation team for the routine validation of Suomi
723 National Polar-orbiting Partnership Visible Infrared Imaging Radiometer Suite aerosol optical
724 depth product (Istvan Laszlo, Hongqing Liu, and Hai Zhang) used in our analysis. Brian
725 McDonald acknowledges the support from NOAA NRDD Project (#19533) - "COVID-19: Near
726 Real-time Emissions Adjustment for Air Quality Forecasting and Long-Term Impact
727 Analyses." Daniel Tong acknowledges the partial support of NOAA Weather Program Office
728 (NA19OAR4590082), and Daniel Goldberg acknowledges the support of NASA RRNES grant
729 #: 80NSSC20K1122. The authors acknowledge the help of Amy Huff (IM Systems Group) in
730 proof reading the manuscript.

731 **Author Contributions.** SK conceived the scope of the scientific study and formulated the
732 analysis and wrote the manuscript. ZW conducted the scientific analyses including the
733 generation of the figures used in the manuscript. BM processed and provided the on-road NO_x
734 emissions data and wrote Section 2.2. DLG and DT conducted analysis that helped interpret the
735 features observed in TROPOMI tropospheric NO_2 data shown in Figures 4 and 5 and reviewed
736 the manuscript.

737 **Disclaimer.** The scientific results and conclusions, as well as any views or opinions expressed
738 herein, are those of the author(s) and do not necessarily reflect those of NOAA or the
739 Department of Commerce.

740 **Data Statement.** The publicly available SNPP VIIRS AOD data can be obtained from NOAA
741 CLASS (https://www.avl.class.noaa.gov) and the gridded Level 3 AOD data can be obtained
742 from ftp://ftp.star.nesdis.noaa.gov/pub/smcd/VIIRS_Aerosol/npp.viirs.aerosol.data/epsaot550.

743 The Sentinel 5P TROPOMI NO_2 data can be obtained from

744 https://scihub.copernicus.eu/dhus/#/home. The on-road NOx emissions data are currently not

745 publicly available as co-author BM's team is in the process of publishing its analyses.

746

747

748

749

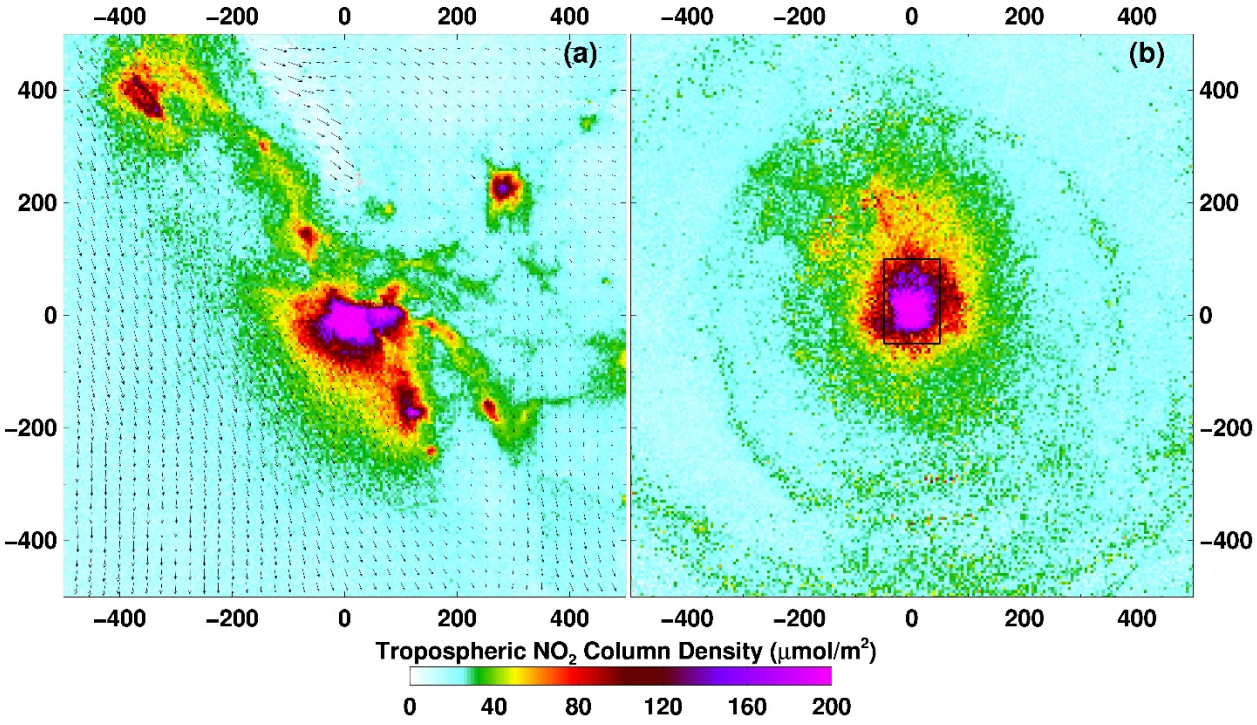

750

751 Figure 1: Sentinel 5P TROPOMI monthly mean tropNO_2 for January 2020 for Los Angeles. (a)
752 Original pixel level data remapped to 5 km x 5 km resolution and averaged for the month. The
753 monthly mean ERA5 wind vectors are overlaid on the tropNO_2 map to indicate the wind
754 direction. (b) Remapped tropNO_2 data grids rotated in the direction of the wind using ERA5
755 wind fields. The downwind direction is towards North (zero on the axis). For the monthly mean
756 to be computed, we used a criterion that at least 25% of the days in a month should have
757 retrievals. The black rectangle defines the area for which tropNO_2 data are averaged.

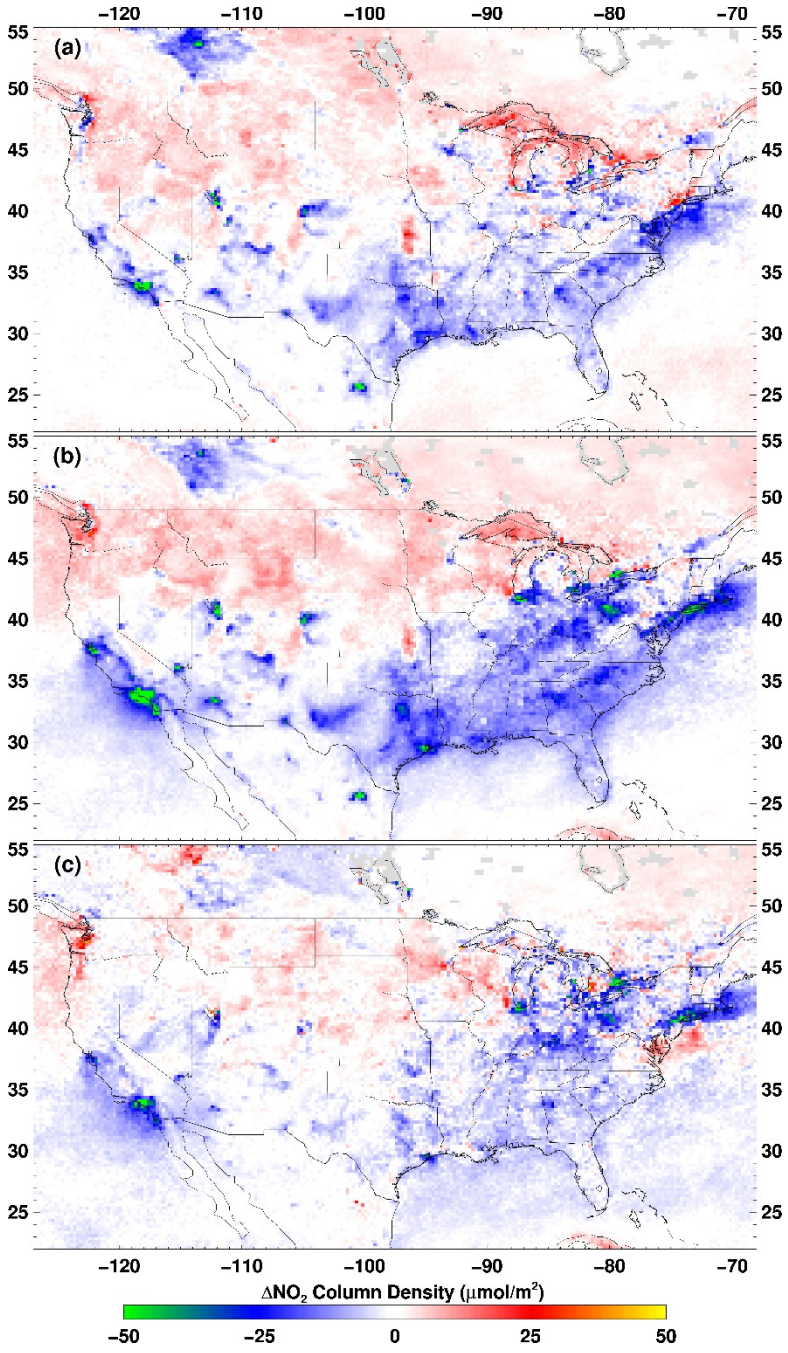

758

759 Figure 2: tropNO$_2$ changes between pre-lockdown period (January to February) and lockdown
760 period (15 March to 30 April) for (a) 2019ΔNO$_2$, (b) 2020ΔNO$_2$, and (c) the difference between
761 2020ΔNO$_2$ and 2019ΔNO$_2$. The double differencing is expected to minimize the seasonal
762 differences and provide a realistic estimate of change in tropNO$_2$ due to emissions changes.

763

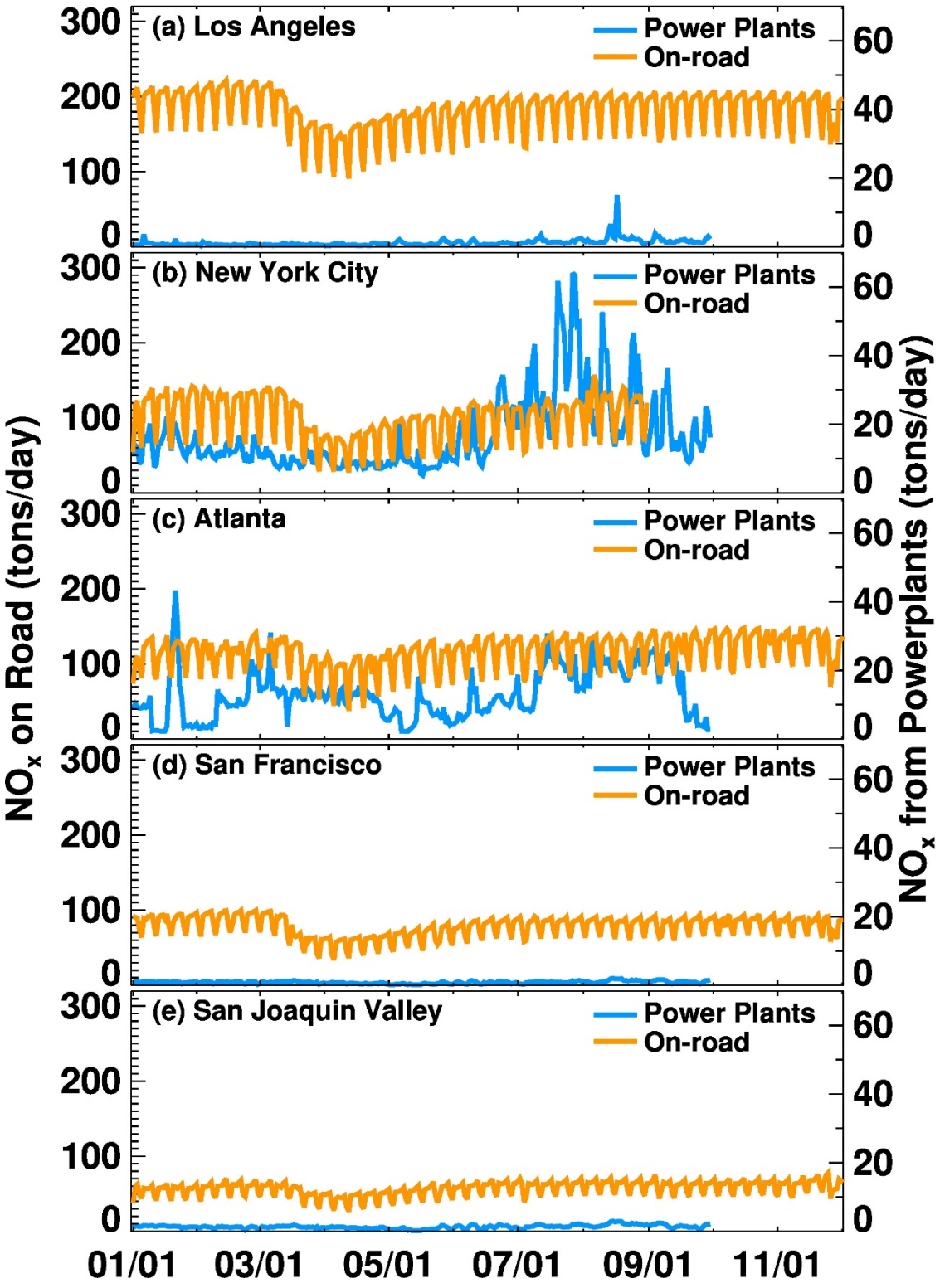

764

765 Figure 3: Time series of daily on-road and power plant NOx emissions for different cities from
766 January to November 2020. Note that the time series ends on 31 August for New York City
767 because the traffic count data are not available for September to November.

768

769

770

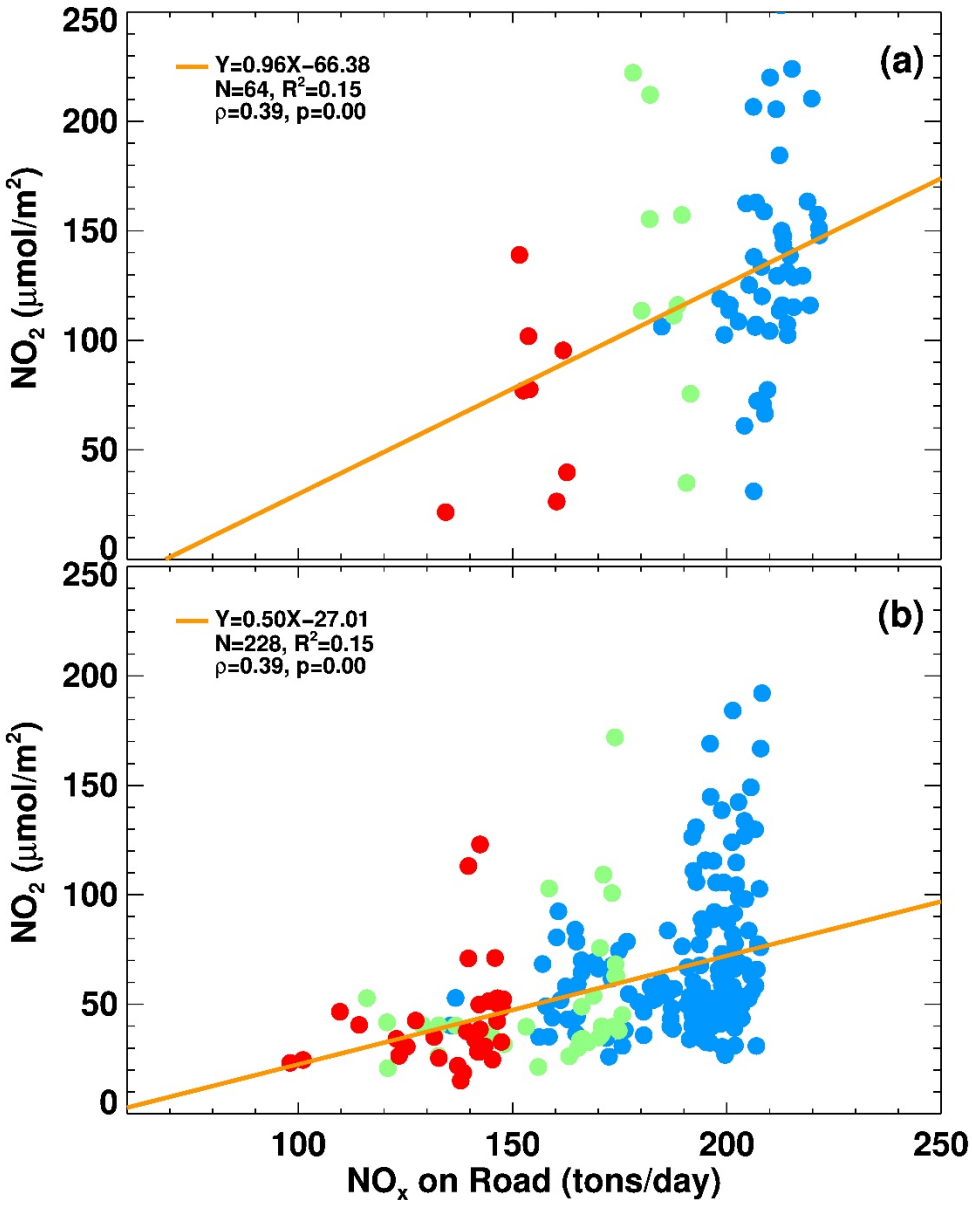

771
772

773 Figure 4: Correlation between daily tropNO_2 and daily on-road NO_x emissions for Los Angeles, CA. (a)
774 For pre-lockdown (January and February) and (b) For lockdown and post lockdown period (March
775 through end of November). Red color is for data gathered on Sundays, green color is for data gathered on
776 Saturdays, and blue color is for data gathered on weekdays.

777

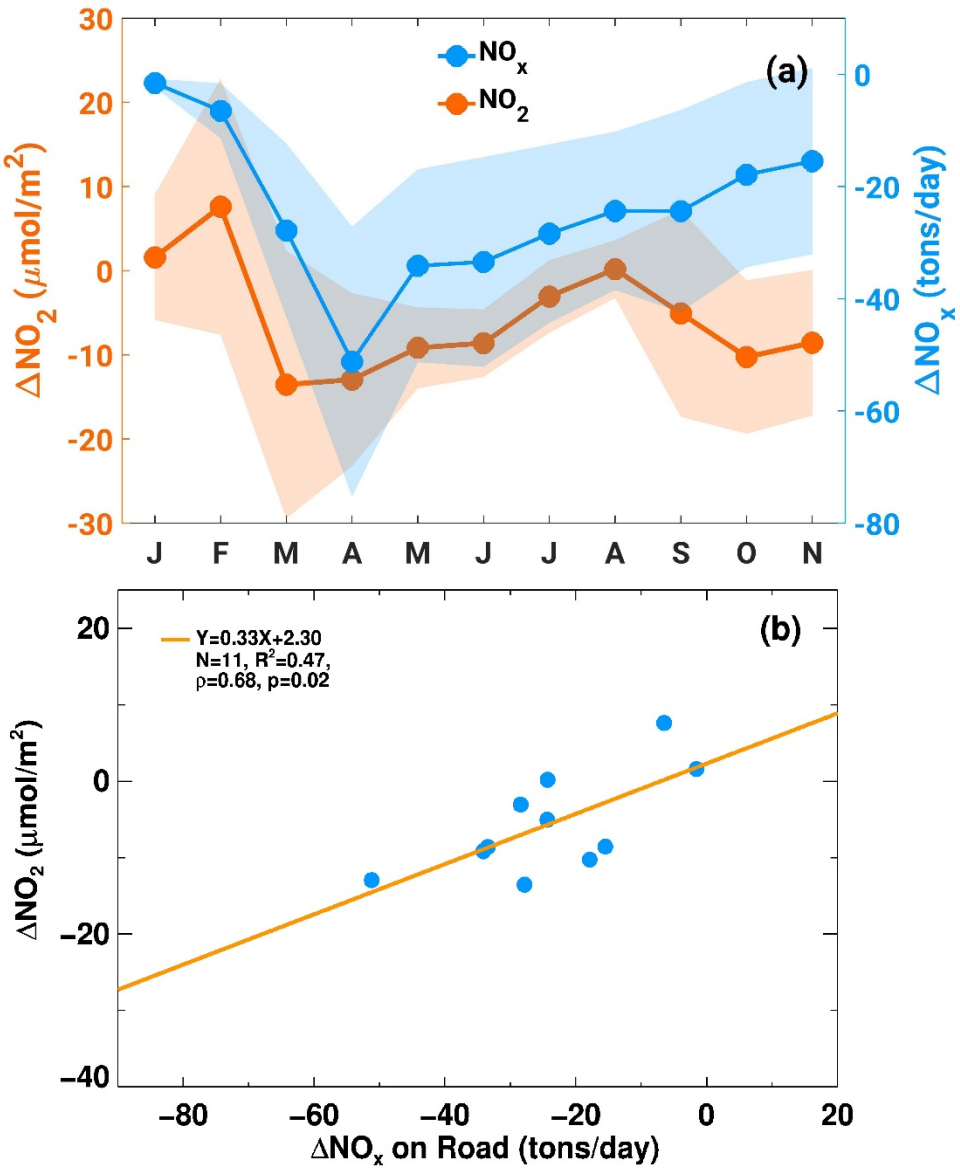

Figure 5: Trends in on-road monthly mean NOx emissions (tons/day) and tropNO_2 (μmoles/m^2) between 2019 and 2020 averaged for the five analysis cities. (a) Average monthly mean differences for the five cities from January to November. (b) Correlation between five-city average changes in on-road monthly mean NOx emissions and changes in five-city average monthly mean tropNO_2

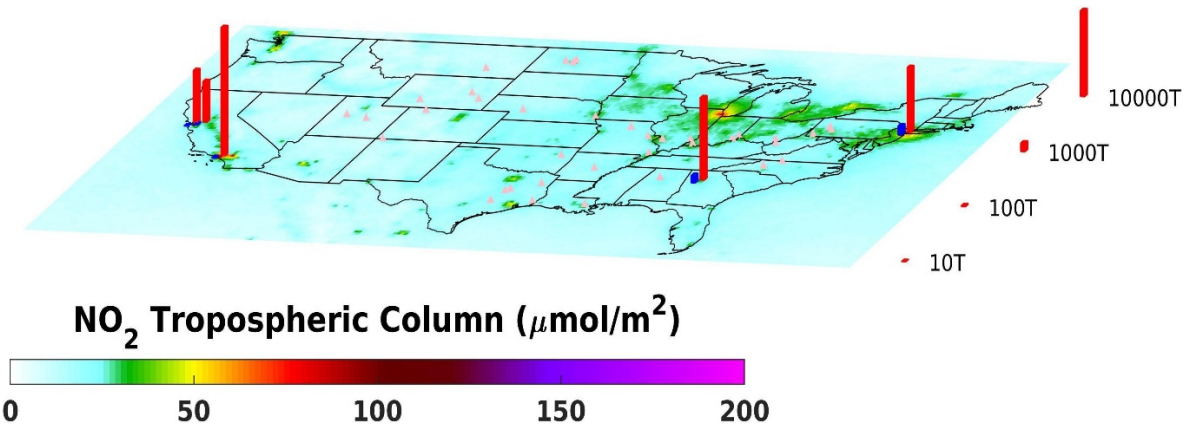

789

790 Figure 6: tropNO2 map for second quarter of 2020. The red columns show total on-road NOx
791 emissions and the blue columns show NOx emissions from power plants nearby these five cities
792 (New York, Atlanta, Los Angeles, San Francisco, and San Joaquin Valley). Power plants with
793 monthly mean NOx emissions greater than 500 tons are also shown in the map as pink dots.

794

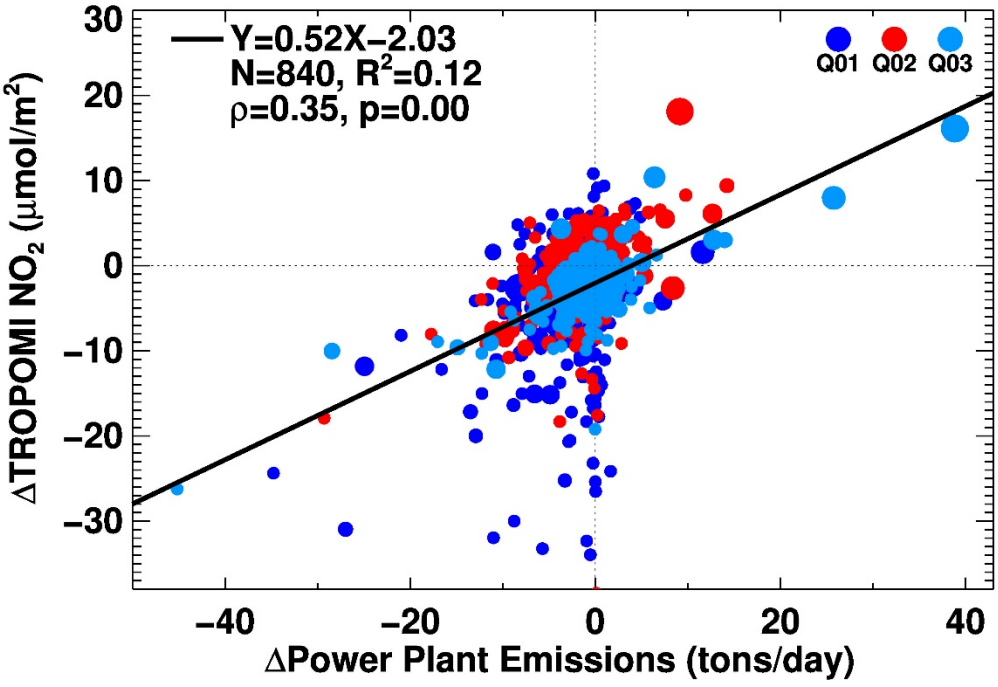

795

796 Figure 7: Correlation of monthly mean tropNO$_2$ changes between 2020 and 2019 with changes in
797 power plant monthly mean NO$_x$ emissions. The size of the circle indicates the magnitude of total
798 monthly emissions (high, medium, and low) of individual power plant. To obtain monthly
799 means, daily total NO$_x$ emissions were added and divided by the number of days in a month to
800 get average values in units of tons/day.

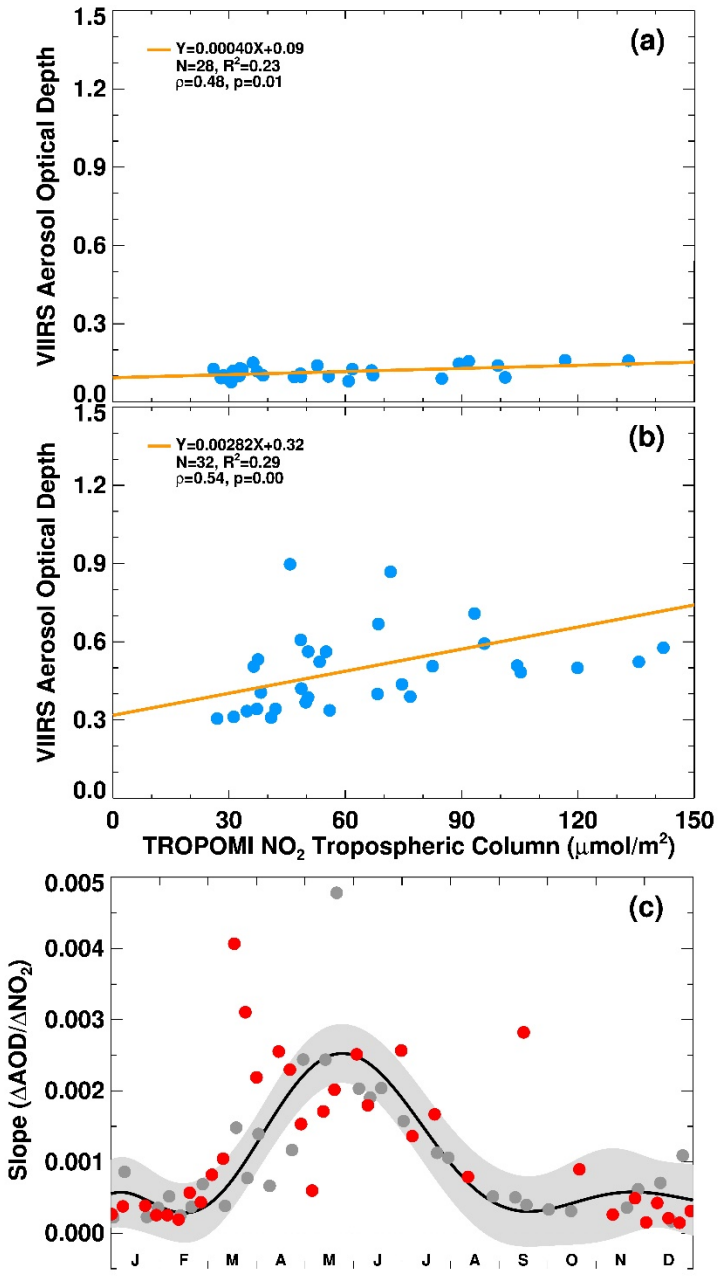

801

802

803 Figure 8: (a) Example correlation of VIIRS AOD and TROPOMI tropNO$_2$ during one week,
804 September 15-21, 2019, (b) Same for September 13-19, 2020, (c) Time series of weekly slope
805 (AOD/NO$_2$) with data for 2019 in gray color and data for 2020 in red color for Los Angeles,
806 California. The black solid line is the fit to 2019 data indicating seasonal photochemistry. Any
807 data points that depart from the shaded gray region are treated as the period when transported
808 aerosols (e.g., smoke) influenced the air mass over Los Angeles.

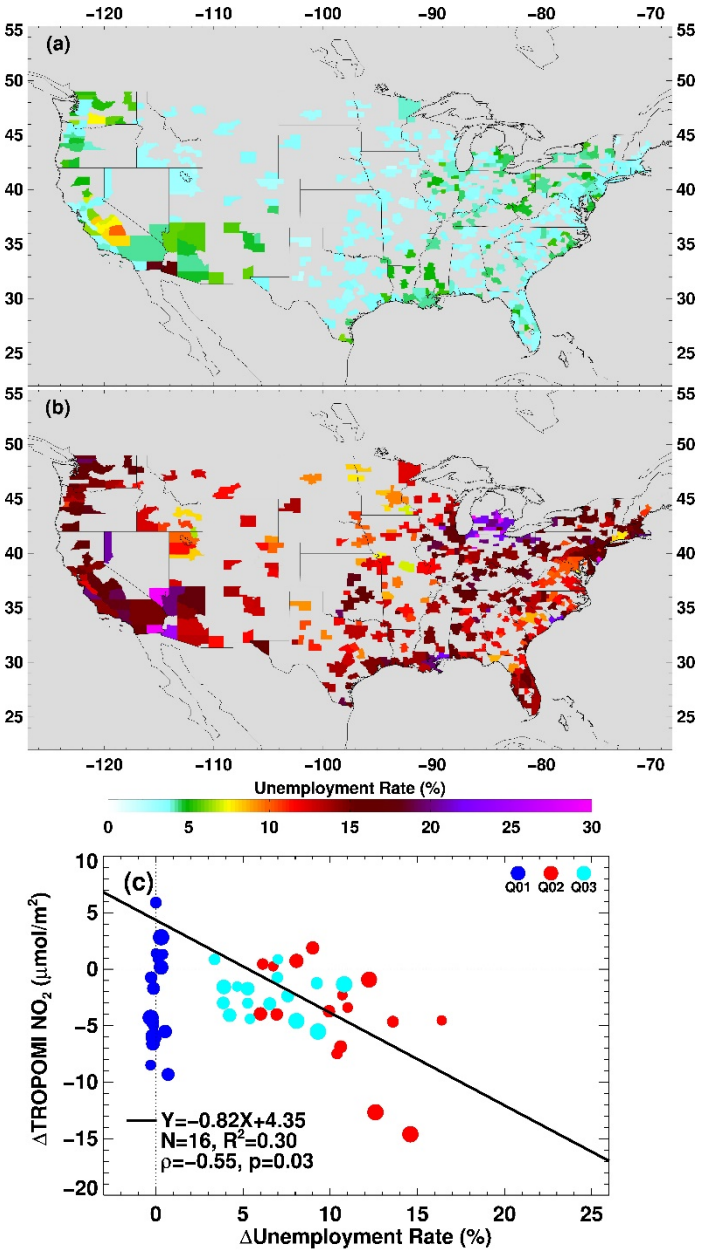

Figure 9: The impact of COVID-19 lockdown on the unemployment rate in metropolitan areas and tropNO_2. (a) Unemployment rate in April 2019, (b) Unemployment rate in April 2020, and (c) Correlation between increase in unemployment between 2020 and 2019 and tropNO_2 changes. Only data for metropolitan areas where the civilian labor force in 2019 was greater than two million are shown in the correlation plot. In the first quarter (Q01) unemployment changes are close to zero as pandemic impact did not begin until late March. Strong negative correlation is observed for the second (Q02) and third (Q03) quarters. The solid black line is the fit to the second quarter data.

Table 1: Ranking of cities for ozone pollution and their lockdown periods

City/Region	Ozone Pollution Ranking	Lockdown Start Date	Lockdown End Date
Los Angeles-Long Beach, CA	1	19-Mar	4-May
Visalia, CA	2	19-Mar	4-May
Bakersfield, CA	3	19-Mar	4-May
Fresno-Madera-Hanford, CA	4	19-Mar	4-May
Sacramento-Roseville, CA	5	19-Mar	4-May
San Diego-Chula Vista-Carlsbad, CA	6	19-Mar	4-May
Phoenix-Mesa, AZ	7	30-Mar	30-Apr
San Jose-San Francisco-Oakland, CA	8	19-Mar	4-May
Las Vegas-Henderson, NV	9	1-Apr	30-Apr
Denver-Aurora, CO	10	26-Mar	26-Apr
Salt Lake City-Provo-Orem, UT	11	30-Mar	13-Apr
New York-Newark, NY-NY-CT-PA*	12	22-Mar	15-May
Redding-Red Bluff, CA	13	19-Mar	4-May
Houston-The Woodlands, TX	14	2-Apr	20-Apr
El Centro, CA	15	19-Mar	4-May
Chicago-Naperville, IL-IN-WI*	16	23-Mar	1-May
El Paso-Las Cruces, TX-NM	17	2-Apr	15-May
Chico, CA	18	19-Mar	4-May
Fort Collins, CO	19	26-Mar	26-Apr
Washington-Baltimore-Arlington, DC-MD-VA-WV-PA*	20	30-Mar	15-May
Dallas-Fort Worth, TX-OK	21	2-Apr	20-Apr
Sheboygan, WI	22	24-Apr	26-May
Philadelphia-Reading-Camden, PA-NJ-DE-MD*	23	30-Mar	15-May
Milwaukee-Racine-Waukesha, WI	24	24-Apr	26-May
Hartford-East Hartford, CT	25	23-Mar	20-May

*Dates reflect the period that is the longest for any given state in the region

848

849

Table 2: Reductions in on-road NOx emissions and tropNO$_2$ between 15 March to 30 April and 1 January to 29 February Derived using Double Differencing Technique

City	2019ΔNOx (%)	2020ΔNOx (%)	Seasonality Removed On-road NOx Emissions Changes (%) 2020ΔNOx - 2019ΔNOx)	2019ΔNO$_2$ (%)	2020ΔNO$_2$ (%)	Seasonality Removed TropNO$_2$ Reductions (%) (2020ΔtropNO$_2$ - 2019ΔtropNO$_2$)
Atlanta	10.41	-17.70	-28.11	-22.67	-44.14	-21.47
San Francisco	10.54	-33.95	-44.49	-23.79	-48.18	-24.39
San Joaquin Valley	14.27	-18.39	-32.66	-27.30	-44.62	-17.32
New York City	11.04	-36.87	-47.91	-6.07	-34.05	-27.98
Los Angeles	10.57	-25.10	-35.67	-37.90	-59.68	-21.78

850

851

852

853

854

855

856

857

858

859

860

861

862

863

864

865

866

References

Achakulwisut, P., Brauer, M., Hystad, P., Anenberg, S. C. (2019). Global, national, and urban burdens of paediatric asthma incidence attributable to ambient NO_2 pollution: estimates from global datasets. *Lancet Planet Health*. 1-4, DOI: 10.1016/S2542-5196(19)30046-4

Baidar, S., Hardesty, R. M., Kim, S.-W., Langford, A. O., Oetjen, H., Senff, C. J., et al. (2015).Weakening of the weekend ozone effect over California's South Coast Air Basin: Weekend ozone effect over California. *Geophysical Research Letters*, *42*, 9457–9464. doi: 10.1002/2015GL066419

Bauwens, M., Compernolle, S., Stavrakou, T., Muller, J.-F., van Gent, J., Eskes, H., Levelt, P. F., Van der A. R., Veefkind, P., Vlietinck, J., Yu, H., Zehner, C. (2020). Impact of Coronavirus Outbreak on NO_2 Pollution Assessed Using TROPOMI and OMI Observations. *Geophysical Research Letters*. doi: 10.1029/2020GL087978

Bishop, G. A., and Stedman, D. H. (2014), The recession of 2008 and its impact on light-duty vehicle emissions in three western United States cities, *Environ Sci Technol*, *48*, 14822-14827, doi:10.1021/es5043518.

Cersosimo, A., Serio, C., Masiello, G. (2020). TROPOMI NO_2 Tropospheric Column Data: Regridding to 1 km Grid-Resolution and Assessment of their Consistency with In Situ Surface Observations. *Remote Sens.*, *12*, 2212. https://doi.org/10.3390/rs12142212

Chan, K. L., M. Wiegner, J. van Geffen, I. De Smedt, C. Alberti, Z. Cheng, S. Ye, and M. Wenig, MAX-DOAS measurements of tropospheric NO2 and HCHO in Munich and the comparison to OMI and TROPOMI satellite observations (2020). *Atmos. Meas. Tech., 13*, 4499–4520. https://doi.org/10.5194/amt-13-4499-2020

de Gouw, J.A., Parrish, D.D., Frost, G.J. and Trainer, M. (2014), Reduced emissions of CO_2, NOx, and SO_2 from U.S. power plants owing to switch from coal to natural gas with combined cycle technology. Earth's Future, 2: 75-82. https://doi.org/10.1002/2013EF000196

EPA (2015), MOVES2014a (Motor Vehicle Emission Simulator), Office of Transportation and Air Quality, U.S. Environmental Protection Agency.

Fioletov, V. E., McLinden, C. A., Krotkov, N., Li, C. (2015). Lifetimes and emissions of SO2 from point sources estimated from OMI. *Geophys. Res. Lett.*, *42*, 1969–1976, doi: 10.1002/2015GL063148.

Gkatzelis, G.I., J.B. Gilman, S.S. Brown, H. Eskes, A.R. Gomes, A.C. Lange, B.C. McDonald, J. Peischl, A. Petzold, C. Thompson, A. Kiendler-Scharr (2021). The Global Impacts of COVID-19

Lockdowns on Urban Air Pollution: A Review. *Elementa: Science of Anthropocene*. 9 (1): 00176. doi: https://doi.org/10.1525/elementa.2021.00176

Goldberg, D. L., Anenberg, S. C., Griffin, D., McLinden, C. A., Lu, Z., & Streets, D. G. (2020). Disentangling the impact of the COVID-19 lockdowns on urban NO_2 from natural variability. *Geophysical Research Letters*, 47, e2020GL089269. https://doi.org/10.1029/2020GL089269

Goldberg, D. L., Lu, Z., Streets, D. G., de Foy, B., Griffin, D., McLinden, C. A., Lamsal, L. N., Krotkov, N. A., Eskes, H. Enhanced capabilities of TROPOMI NO_2: Estimating NO_X from North American 2 cities and power plants. (2019). *Environ. Sci. Technol.*, 53, 21, 12594–12601 https://doi.org/10.1021/acs.est.9b04488

Harkins, C., et al. (in review). "A fuel-based method for updating mobile source emissions during the COVID-19 pandemic." Environmental Research Letters.

Hassler, B., B. C. McDonald, G. J. Frost, A. Borbon, D. C. Carslaw, K. Civerolo, C. Granier, P. S. Monks, S. Monks, D. D. Parrish, I. B. Pollack, K. H. Rosenlof, T. B. Ryerson, E. von Schneidemesser, and M. Trainer (2016), Analysis of long-term observations of NOx and CO in megacities and application to constraining emissions inventories, *Geophys Res Lett*, *43*, 9920-9930, doi:10.1002/2016gl069894.

Hersbach, H, Bell, B, Berrisford, P, et al. The ERA5 global reanalysis. *Q J R Meteorol Soc*. 2020; 146: 1999– 2049. https://doi.org/10.1002/qj.3803

Hoesly, R. M., Smith, S. J., Feng, L., Klimont, Z., Janssens-Maenhout, G., Pitkanen, T., Seibert, J. J., Vu, L., Andres, R. J., Bolt, R. M., Bond, T. C., Dawidowski, L., Kholod, N., Kurokawa, J.-I., Li, M., Liu, L., Lu, Z., Moura, M. C. P., O'Rourke, P. R., and Zhang, Q. (2018). Historical (1750–2014) anthropogenic emissions of reactive gases and aerosols from the Community Emissions Data System (CEDS). *Geosci. Model Dev.*, 11, 369–408. https://doi.org/10.5194/gmd-11-369-2018

Huang, M., et al. (2014), Changes in nitrogen oxides emissions in California during 2005–2010 indicated from top-down and bottom-up emission estimates, *J. Geophys. Res. Atmos.*, 119, 12,928– 12,952, doi:10.1002/2014JD022268.

Huang, J., Kondragunta, S., Laszlo, I., Liu, H., Remer, L. A., Zhang, H., Superczynski, S., Ciren, P., Holben, B. N., and Petrenko, M. (2016), Validation and expected error estimation of Suomi-NPP VIIRS aerosol optical thickness and Ångström exponent with AERONET, *J. Geophys. Res. Atmos.*, 121, 7139– 7160, doi:10.1002/2016JD024834.

Iolango, I., Virta, H., Eskes, H., Hovila, J., Douros, J. (2020). Comparison of TROPOMI/Sentinel 5 Precursor NO_2 observations with ground-based measurements in Helsinki, *Atmos. Meas. Tech.*, *13*, 205–218, https://doi.org/10.5194/amt-2019-329

951 Jiang, Z., B. C. McDonald, H. Worden, J. R. Worden, K. Miyazaki, Z. Qu, D. K. Henze, D. B. A.
952 Jones, A. F. Arellano, E. V. Fischer, L. Y. Zhu, and K. F. Boersma (2018), Unexpected
953 slowdown of US pollutant emission reduction in the past decade, *P Natl Acad Sci USA*, *115*,
954 5099-5104, doi:10.1073/pnas.1801191115.

955

956 Judd, L. M., Al-Saadi, J. A., Szykman, J. J., Valin, L. C., Janz, S. J., Kowalewski, M. G., Eskes,
957 H. J., Veefkind, J. P., Cede, A., Mueller, M., Gebetsberger, M., Swap, R., Pierce, R. B., Nowlan,
958 C. R., Abad, G. G., Nehrir, A., and Williams, D. (2020). Evaluating Sentinel-5P TROPOMI
959 tropospheric NO_2 column densities with airborne and Pandora spectrometers near New York
960 City and Long Island Sound, Atmos. Meas. Tech., 13, 6113–6140, https://doi.org/10.5194/amt-
961 13-6113-2020

962 Keller, C. A., Evans, M. J., Knowland, K. E., Hasenkopf, C. A., Modekurty, S., Lucchesi, R. A.,
963 Oda, T., Franca, B. B., Mandarino, F. C., Díaz Suárez, M. V., Ryan, R. G., Fakes, L. H., and
964 Pawson, S. (2020). Global Impact of COVID-19 Restrictions on the Surface Concentrations of
965 Nitrogen Dioxide and Ozone, Atmos. Chem. Phys. Discuss. [preprint],
966 https://doi.org/10.5194/acp-2020-685, in review.
967

968 Kim, S.-W., McDonald, B. C., Baidar, S., Brown, S. S., Dube, B., Ferrare, R. A., Frost, G.
969 J., Harley, R. A., Holloway, J. S., Lee, H.-J., et al. (2016), Modeling the weekly cycle of
970 NO_x and CO emissions and their impacts on O_3 in the Los Angeles-South Coast Air Basin during
971 the CalNex 2010 field campaign, *J. Geophys. Res. Atmos.*, 121, 1340– 1360,
972 doi:10.1002/2015JD024292.
973

974 Kondragunta, S., D. Crisp, and C. Zehner (2020), Disseminating scientific results in the age of
975 rapid communication, *Eos, 101,* https://doi.org/10.1029/2020EO150710. Published on 20
976 October 2020.

977

978 Kroll, J.H., Heald, C.L., Cappa, C.D. *et al.* The complex chemical effects of COVID-19
979 shutdowns on air quality. *Nat. Chem.* **12,** 777–779 (2020). https://doi.org/10.1038/s41557-020-
980 0535-z
981

982 Lamsal, N. L., Duncan, B.N., Yoshida, Y., Krotkov, N. A., Pickering, K. E., Streets, D. (2015).
983 U.S. NO_2 trends (2005–2013): EPA Air Quality System (AQS) data versus improved
984 observations from the Ozone Monitoring Instrument (OMI), *Atmospheric Environment*, *100*,
985 130-143.

986 Laszlo, I. and Liu, H., 2016. EPS Aerosol Optical Depth (AOD) Algorithm Theoretical Basis
987 Document, version 3.0.1, June 28, 2016, NOAA NESDIS.
988

989 Levy, R.C., Remer, L.A., Mattoo, S., Vermote, E.F., and Kaufman, Y.J. (2007). Second-
990 generation operational algorithm: retrieval of aerosol properties over land from inversion of

991 Moderate Resolution Imaging Spectroradiometer spectral reflectance. *J Geophys Res.*, *112*.
992 doi:10.1029/2006JD007811

993 Lin, J.-T., Martin, R. V., Boersma, K. F., Sneep, M., Stammes, P., Spurr, R., Wang, P., Van
994 Roozendael, M., Clémer, K., and Irie, H. (2014). Retrieving tropospheric nitrogen dioxide from
995 the Ozone Monitoring Instrument: effects of aerosols, surface reflectance anisotropy, and vertical
996 profile of nitrogen dioxide, *Atmos. Chem. Phys., 14*, 1441–1461. https://doi.org/10.5194/acp-14-
997 1441-2014

998 Liu, F., Page, A., Strode, S. A., Yoshida, Y., Choi, S., Zheng, B., Lamsal, L., Li, C., Krotkov, N.
999 A., Eskes, H., van der, R., Veefkind, P., Levelt, P. F., Hauser, O. P., Joiner, J. (2020). Abrupt
1000 decline in tropospheric nitrogen dioxide over China after the outbreak of COVID-19, *Science*
1001 *Advances, 6*, 28, eabc2992. DOI: 10.1126/sciadv.abc2992

1002 Liu, F. et al. (2021). Abrupt decline in tropospheric nitrogen dioxide after the outbreak of
1003 COVID-19. Paper presented at 101st virtual American Meteorological Association meeting.
1004 Liu, M., J. Lin, H. Kong, K. F. Boersma, H. Eskes, Y. Kanaya, Q. Hes, X. Tian, K. Qin, P. Xie,
1005 R. Spurr, R. Ni, Y. Yan, H. Weng, J. Wang (2020). A new TROPOMI product for tropospheric
1006 NO_2 columns over East Asia with explicit aerosol corrections. *Atmos. Meas. Tech., 13*, 4247–
1007 4259. https://doi.org/10.5194/amt-13-4247-2020

1008 Lorente, A., Boersma, K.F., Eskes, H.J. *et al.* Quantification of nitrogen oxides emissions from
1009 build-up of pollution over Paris with TROPOMI. *Sci Rep* **9,** 20033 (2019).
1010 https://doi.org/10.1038/s41598-019-56428-5

1011 Mazuuca, G. M., X. Ren, C. P. Loughner, M. Estes, J. H. Crawford, K. E. Pickering, A. J.
1012 Weinheimer, and R. R. Dickerson, Ozone production and its sensitivity to NOx and VOCs:
1013 results from the DISCOVER-AQ field experiment, Houston 2013. 2016. *Atmos. Chem. Phys.,*
1014 *16,* 14463–14474. doi: 10.5194/acp-16-14463-2016

1015 McDonald, B. C., S. A. McKeen, Y. Y. Cui, R. Ahmadov, S. W. Kim, G. J. Frost, I. B. Pollack,
1016 T. B. Ryerson, J. S. Holloway, M. Graus, C. Warneke, J. B. Gilman, J. A. de Gouw, J. Kaiser, F.
1017 N. Keutsch, T. F. Hanisco, G. M. Wolfe, and M. Trainer (2018), Modeling ozone in the Eastern
1018 U.S. using a fuel-based mobile source emissions inventory, *Environ Sci Technol*, *52*, 7360-7370,
1019 doi:10.1021/acs.est.8b00778.

1020 McDonald, B. C., T. R. Dallmann, E. W. Martin, and R. A. Harley (2012), Long-term trends in
1021 nitrogen oxide emissions from motor vehicles at national, state, and air basin scales, *J Geophys*
1022 *Res-Atmos*, *117*, D00V18, doi:10.1029/2012jd018304.

1023

1024 McDonald, B. C., Z. C. McBride, E. W. Martin, and R. A. Harley (2014), High-resolution
1025 mapping of motor vehicle carbon dioxide emissions, *J Geophys Res-Atmos*, *119*, 5283-5298,
1026 doi:10.1002/2013jd021219.

1027 McDonald, B. C., Dallmann, T. R., Martin, E. W., and Harley, R. A. (2012), Long-term trends in
1028 nitrogen oxide emissions from motor vehicles at national, state, and air basin scales, *J. Geophys.*
1029 *Res.*, 117, D00V18, doi: 10.1029/2012JD018304

1030 McDonald, B. C., et al. (2018). Volatile chemical products emerging as largest petrochemical
1031 source of urban organic emissions. *Science 359*, 760-764.

1032 Naeger, A.R. and Murphy, K. (2020). Impact of COVID-19 Containment Measures on Air
1033 Pollution in California. *Aerosol Air Qual. Res.* https://doi.org/10.4209/aaqr.2020.05.0227

1034 Parker, H. A., Hasheminassab, S., Crounse, J. D., Roehl, C. M., & Wennberg, P. O. (2020).
1035 Impacts of traffic reductions associated with COVID-19 on Southern California air quality.
1036 Geophysical Research Letters, 47, e2020GL090164. https://doi.org/10.1029/2020GL090164
1037

1038 Qin, M., Murphy, B.N., Isaacs, K.K. *et al.* (2021). Criteria pollutant impacts of volatile chemical
1039 products informed by near-field modelling. *Nat Sustain 4*, 129–137.
1040 https://doi.org/10.1038/s41893-020-00614-1

1041 Schiferl, L. D., C. L. Heald, J. B. Nowak, J. S. Holloway, J. A. Neuman, R. Bahreini, I. B.
1042 Pollack, T. B. Ryerson, C. Wiedinmyer, and J. G. Murphy (2014), An investigation of ammonia
1043 and inorganic particulate matter in California during the CalNex campaign, J. Geophys. Res.
1044 Atmos., 119, 1883–1902, doi:10.1002/2013JD020765

1045 Silver, B., X. He, S. Arnold, D. V. Spracklen, The impact of COVID-19 control measures on air
1046 quality in China. (2020). *Environ. Res. Lett. 15*, 084021. https://doi.org/10.1088/1748-
1047 9326/aba3a2

1048 Silvern, R. F., D. J. Jacob, L. J. Mickley, M. P. Sulprizio, K. R. Travis, E. A. Marais, R. C.
1049 Cohen, J. L. Laughner, S. Choi, J. Joiner, and L. N. Lamsal, Using satellite observations of
1050 tropospheric NO_2 columns to infer long-term trends in US NOx emissions: the importance of
1051 accounting for the free tropospheric NO_2 background. (2019). *Atmos. Chem. Phys., 19*, 8863–
1052 8878. https://doi.org/10.5194/acp-19-8863-2019

1053 Straka, W. III, S. Kondragunta, Z. Wei, H. Zhang, S. D. Miller, A. Watts, Examining the
1054 Economic and Environmental Impacts of COVID-19 Using Earth Observation Data. (2021).
1055 Remote Sensing. 13(1):5.

1056

1057 Tack, F., A. Merlaud, A. C. Meir, T. Vlemmix, T. Ruhtz, M-D. Iordache, X. Ge, :/ vam der War.
1058 D/ Schuettemeyer, M. Ardelean, A. Calcan, D. Constantin, A. Schonhardt, K. Meuleman, A.
1059 Richter, and M. V. Roozendae, Intercomparison of four airborne imaging DOAS systems for
1060 tropospheric NO_2 mapping – the AROMAPEX campaign. (2019). *Atmos. Meas. Tech.,12*, 211–
1061 236. https://doi.org/10.5194/amt-12-211

1062 Today in energy, https://www.eia.gov/todayinenergy/detail.php?id=37752, December 11, 2018

1063 Tong, D., L. Pan, W. Chen, L. Lamsal, P. Lee, Y. Tang, H. Kim, S. Kondragunta, I. Stajner,
1064 Impact of the 2008 Global Recession on air quality over the United States: Implications for
1065 surface ozone levels from changes in NOx emissions. (2016). *Geophys. Res. Lett.,*
1066 *10*.1002/2016GL069885

1067 Tong, D.Q., L. Lamsal, L. Pan, C. Ding, H. Kim, P. Lee, T. Chai, and K.E. Pickering, and I.
1068 Stajner, Long-term NOx trends over large cities in the United States during the 2008 Recession:
1069 Intercomparison of satellite retrievals, ground observations, and emission inventories. (2015).
1070 *Atmospheric Environment, 107*, 70-84. doi:10.1016/j.atmosenv.2015.01.035

1071
1072 van Geffen, J., H. J. Eskes, K. F. Boresma, J. D. Maasakkers, and J. P. Veefkind, TROPOMI
1073 ATBD of the total and tropospheric NO_2 data products, S5P-KNMI-L2-0005-RP, v1.4.0, 2019

1074

1075 Vadrevu, K. P., A. Eaturu, S. Biswas et al., Spatial and temporal variations of air pollution over
1076 41 cities of India during the COVID-19 lockdown period. (2020). *Sci. Rep*. 10, 16574.
1077 https://doi.org/10.1038/s41598-020-72271-5.

1078

1079 Zhang, H., Kondragunta, S., Laszlo, I., Liu, H., Remer, L. A., Huang, J., Superczynski, S.,
1080 and Ciren, P. (2016), An enhanced VIIRS aerosol optical thickness (AOT) retrieval algorithm
1081 over land using a global surface reflectance ratio database, *J. Geophys. Res.*
1082 *Atmos.*, 121, 10,717– 10,738, doi:10.1002/2016JD024859.

1083 Zhang, H., & Kondragunta, S. (2021). Daily and Hourly Surface PM2.5 Estimation from
1084 Satellite AOD. *Earth and Space Science*, 8,
1085 e2020EA001599. https://doi.org/10.1029/2020EA001599

1086

1087 Zhang, Q., Y. Pan, Y. He, W. W. Walters, Q. Ni, X. Liu, G. Xu, J. Shao, C. Jiang, Substantial
1088 nitrogen oxides emission reduction from China due to COVID-19 and its impact on surface
1089 ozone and aerosol pollution. (2021). *Science of The Total Environment, 753*.

1090 Zhao, X., D. Griffin, V. Fioletov, C. McLinden, A. Cede, M. Tiefengraber, M. Muller, K.
1091 Bognar, K. Strong, F. Boersma, H. Eskes, J. Davies, A. Ogyu, and S. C. Lee. (2020).
1092 Assessment of the quality of TROPOMI high-spatial-resolution NO_2 data products in the Greater
1093 Toronto Area, *Atmos. Meas. Tech., 13*, 2131–2159. https://doi.org/10.5194/amt-13-2131-2020

1094 Zheng, H., S. Kong, N. Chen, Y. Yan, D. Liu, B. Zhu, K. Xu, W. Cao, Q. Ding, B. Lan, Z.
1095 Zhang, M. Zheng, Z. Fan, Y. Cheng, S. Zheng, L. Yao, Y. Bai, T. Zhao, S. Qi. (2020).
1096 Significant changes in the chemical compositions and sources of PM2.5 in Wuhan since the city
1097 lockdown as COVID-19, Science of the Total Environment, 739.

1098
1099